# THREE-DIMENSIONAL FINITE ELEMENT ANALYSIS OF FLEXIBLE PAVEMENTS CONSIDERING NONLINEAR PAVEMENT FOUNDATION BEHAVIOR


BY

MINKWAN KIM

B.Eng., Inha University, 1998
M.Eng., Inha University, 2000
M.S., University of Illinois at Urbana-Champaign, 2005



DISSERTATION

Submitted in partial fulfillment of the requirements
for the degree of Doctor of Philosophy in Civil Engineering
in the Graduate College of the
University of Illinois at Urbana-Champaign, 2007

Urbana, Illinois


Doctoral Committee:

Associate Professor Erol Tutumluer, Chair
Professor Imad L. Al-Qadi
Associate Professor William G. Buttlar
Assistant Professor C. Armando Duarte
Professor Marshall R. Thompson

## ABSTRACT

With the current move towards adopting mechanistic-empirical concepts in the design of pavement structures, state-of-the-art mechanistic analysis methodologies are needed to determine accurate pavement responses, such as stress, strain, and deformation. This research has focused on the nonlinear modulus and deformation behavior of pavement foundation geomaterials, i.e., fine-grained subgrade soils and unbound aggregates used in untreated base/subbase layers, due to repeated wheel loading. This nonlinear behavior is commonly characterized by stress dependent resilient modulus material models that need to be incorporated into finite element based mechanistic pavement analysis methods to predict more accurately critical pavement responses. This dissertation describes the development of a finite element mechanistic analysis model for both the axisymmetric and three-dimensional analyses of flexible pavements. To properly characterize the resilient behavior of pavement foundations, nonlinear stress-dependent modulus models have been programmed in a User Material Subroutine (UMAT) in the general-purpose finite element program ABAQUS™. The developed UMAT is verified first with the results of a well established axisymmetric nonlinear pavement analysis finite element program, GT-PAVE. Next, the UMAT subroutine performance is also validated with the instrumented full scale pavement test section study results from the Federal Aviation Administration's National Airport Pavement Test Facility. The predicted responses at different locations in the test sections are compared with the field measured responses under different sections and load levels to indicate that proper characterizations of the nonlinear, stress-dependent geomaterials make a significant impact on accurately predicting measured pavement responses from three-dimensional pavement analyses.

Different resilient modulus models developed from conventional and true triaxial test data on unbound granular materials are also studied. When the intermediate principal stresses are taken into account in the three-dimensional modulus model development unlike in the axisymmetric models, large discrepancies are obtained in the computed pavement responses when compared to those from the axisymmetric nonlinear finite element analyses. Finally, as an important application of the developed UMAT nonlinear material subroutine in the analysis of flexible pavements subjected to multiple axle/wheel loads, load spreading and nonlinear modulus distributions of pavement layers are found to considerably impact pavement surface deflections and critical pavement responses.

## ACKNOWLEDGEMENTS

I would like to express my sincere gratitude to my advisor, Professor Erol Tutumluer, who provided me valuable advice, encouragement, and guidance on the matter of academic and personal as well. He always shared his enthusiasm and knowledge with me. I am also grateful to the member of my graduate committee, Professor Imad L. Al-Qadi, Professor William G. Buttlar, Professor Armando C. Duarte, and Professor Marshall R. Thompson for their constructive suggestions and thoughtful advices on the many aspects encountered in the completion of this study.

I want to thank my colleagues and friends at the Department of Civil and Environmental Engineering for their friendly and continuous supports during the complete this work. They will always be remembered for the wonderful times we spent together during my stay in Champaign, Illinois.

Finally, I am deeply indebted to my parents and family for their endless patience, comprehension, and love, and especially acknowledge the endless support and encouragement of my wife, Ji Young.

# Table of Contents

# List of Figures

# List of Tables

# Chapter 1 Introduction

## 1.1 Introduction

Flexible pavements with asphalt concrete (AC) surface courses are used all around the world. The various layers of the flexible pavement structure have different strength and deformation characteristics which make the layered system difficult to analyze in pavement engineering. Asphalt concrete in the surface layer is a viscous material with its behavior depending on time and temperature. On the other hand, pavement foundation geomaterials, i.e., coarse-grained unbound granular materials in untreated base/subbase course and fine-grained soils in the subgrade, exhibit stress-dependent nonlinear behavior. Most of the currently used flexible pavement structural analysis models assume linear elastic behavior. As the demand for applied wheel loads and number of load applications increases, it becomes very important to properly characterize the behavior of unbound granular material and subgrade soil layers as the foundations of the layered pavement structure.

Previous laboratory studies have shown that elastic or resilient responses of granular materials in base/subbase and subgrade soils follow a nonlinear, stress-dependent behavior under repeated traffic loading (Brown and Pappin, 1981; Thompson and Elliot, 1985). Unbound granular materials exhibit stress-hardening, whereas, fine-grained soils show stress-softening type behavior. Finite element programs that analyze pavement structures need to employ this kind of nonlinear resilient characterization to more realistically predict pavement responses. Although specific pavement structural analysis programs, such as the ILLI-PAVE (Raad and Figueroa, 1980) and GT-PAVE

(Tutumluer, 1995), take into account stress-dependent moduli, general-purpose finite element programs do not properly account for such nonlinear behavior of the pavement geomaterials. Recent work by Taciroglu (1998) and Schwartz (2002) clearly indicated the need to develop proper pavement geomaterial constitutive behavior models to use in general purpose finite element programs.

## 1.2 Statement of Research Need

Many general-purpose finite element programs, such as ABAQUS™, ANSYS™, ADINA™, etc., allow use of built-in nonlinear constitutive models. These models, however, have not been readily applicable to nonlinear pavement structural analyses. This is because these constitutive models often define material behavior as a function of strain state, which is more applicable to incremental tangent or incremental secant stiffness type nonlinear analyses. These built-in models do not properly represent deformation characteristics under the applied wheel loads.

The research proposed here focuses on employing nonlinear resilient behavior of pavement geomaterials in the general-purpose finite element model ABAQUS™ (Hibbit et al, 2005) for mechanistic pavement analysis. Both axisymmetric and three-dimensional nonlinear finite element analyses of flexible pavements will be studied. Nonlinear resilient response models will be programmed in a user material subroutine of ABAQUS™ (UMAT) to compute accurately the geomaterial moduli in the base, subbase, and subgrade layers as a function of applied stress state. Nonlinear pavement analyses will be performed to predict flexible pavement critical responses. These responses are the stresses, strains, and deformations in the pavement structure that can be directly linked to the major mechanistic pavement deterioration modes such as fatigue cracking and rutting. Mechanistic based pavement analysis and design primarily deals with these critical responses and predicts pavement performance using distress models or transfer functions.

## 1.3 Objectives of Study

The main objective of the research study proposed here is to develop user material subroutines applicable to general-purpose ABAQUS$^{TM}$ finite element program for nonlinear pavement foundation geomaterials, and evaluate the influence of the nonlinear geomaterial characterizations on the response of flexible pavements using both axisymmetric and three-dimensional ABAQUS$^{TM}$ finite element analyses. The following is the specific objectives of the proposed research:

(I) Develop nonlinear stress-dependent user material subroutine for the resilient behavior of base/subbase and subgrade layers in flexible pavement analysis using the general-purpose ABAQUS$^{TM}$ finite element program;

(II) Determine the finite element mesh domain size for the axisymmetric and three-dimensional finite element pavement models by comparing results with those of the closed form linear elastic layered solutions;

(III) Verify the developed user material model subroutine using the specific-purpose axisymmetric pavement analysis program, GT-PAVE, by generating pavement responses for the nonlinear geomaterial characterizations;

(IV) Validate the developed user material subroutine by comparing predicted pavement responses from three-dimensional finite element analyses with the measured responses of instrumented full-scale pavement test sections;

(V) Perform three-dimensional finite element analyses for predicting critical pavement responses using the developed nonlinear material subroutines to evaluate differences between axisymmetric and three-dimensional pavement analyses;

(VI) Evaluate the impacts of granular material models from both standard repeated load triaxial and true triaxial testing in the laboratory to focus on the effects of intermediate principal stress ($\sigma_2$) in modulus characterization;

(VII) Finally, conduct multiple wheel loading analyses in terms of various highway vehicle axle/wheel arrangements and aircraft gear/wheel configurations in the full three-dimensional finite element model using the developed nonlinear UMAT material subroutines and investigate the validity of superposition principle in nonlinear analysis.

## 1.4 Outline of Thesis

Previous research studies on granular materials and soils are reviewed in Chapter 2. The characterizations of unbound granular material and subgrade soil used in the pavement structure are reported for particular characteristics of these materials under repeated wheel loadings. The so-called resilient behavior is introduced. Previously proposed modulus characterization models for granular materials and soils represented by various mathematical combinations are also summarized.

In Chapter 3, numerical solutions formulated for pavement analyses are reviewed covering elastic layered solutions and finite element analysis programs. In the investigation of finite element models, both two-dimensional and three-dimensional analyses are examined. Finite element programs reviewed in this chapter consist of both pavement analysis programs and general-purpose finite element programs used for pavement analysis.

In Chapter 4, pavement domain selections for finite element analyses are studied. Two element types, i.e., regular finite sized elements and infinite elements, are examined for pavement analysis. Through case studies, the most appropriate pavement domain is selected for the most accurate finite element analysis results.

In Chapter 5, the theoretical background and characteristics of nonlinear finite element analyses of ABAQUS$^{TM}$ program are introduced. The applications of the developed material model subroutine for axisymmetric ABAQUS$^{TM}$ model are illustrated and the results from ABAQUS$^{TM}$ analyses are compared with those from the pavement finite element analysis program, GT-PAVE. Comparisons are made within axisymmetric analysis results emphasizing the importance of nonlinear geomaterial characterizations on the predicted critical pavement responses in contrast to linear elastic results.

In Chapter 6, as the ultimate goal, the research is proposed to deal with the implementation of the nonlinear solution technique in three-dimensional ABAQUS$^{TM}$ finite element analysis. Comparisons are made between axisymmetric and three-dimensional analysis results emphasizing the importance of nonlinear geomaterial characterizations on the predicted critical pavement responses in contrast to linear elastic results. The finite element analyses emphasizing the use of data from true triaxial test are also studied to evaluating the impacts of intermediate principal stresses ($\sigma_2$).

In Chapter 7, the field validation of nonlinear finite element analyses were conducted in three-dimensional finite element analyses. The resilient modulus values and other material properties can be obtained from the backcalculation studies. It is shown that the developed material subroutines embedded in ABAQUS$^{TM}$ program can be reasonably applied to the analysis of multi gear loads.

In Chapter 8, three-dimensional nonlinear finite element analysis of full multiple wheel loadings accounts for the effects of different axle/wheel configurations. For this purpose, both linear elastic and nonlinear, stress-dependent geomaterial models are employed in the analyses. Comparisons are made between the single wheel superposition and full three-dimensional loading results to emphasize the importance of nonlinear material characterizations on predicting more accurate critical pavement responses and the effects of multiple wheel load interactions.

In Chapter 9, comprehensive research findings are summarized and recommendations are made for finite element modeling of flexible pavements. Suggestions are also made for future research need areas to improve major findings presented in this thesis.

# Chapter 2 Granular Material and Subgrade Soil Characterizations

## 2.1 Introduction

Mechanistic concepts have been adopted for the analysis and design of flexible pavements in the recent years. Mechanistic analysis demands accurate material characterizations of pavement structural layers. Pavement foundation geomaterials in base/subbase and subgrade layers do not behave linear elastically under repeated wheel loads. After pavement construction, trafficking requires that applied wheel load stresses are kept small compared to the strength of material and repeated for a large number of times. The deformation under each load application becomes almost completely recoverable and proportional to the load magnitude and can be considered elastic. Thus, the elastic deformation is almost the same in all loading cycles at about the same stress state. This characteristic behavior is known as the resilient behavior. The term 'resilient' refers to that portion of the energy that is put into a material while it is being loaded, which is recovered when it is unloaded. Therefore, resilient modulus is the elastic modulus of pavement materials with certain amount of permanent deformation already accumulated in the geomaterials. This chapter will focus on the main characteristics and modeling of resilient behavior observed in pavement geomaterials, i.e., subgrade soils and unbound aggregate materials.

## 2.2 Unbound Granular Materials

Unbound granular materials are typically used in the base/subbase layer of the flexible pavement structure. Granular materials consist of aggregate particles, air voids, and water. The characterization of these types of materials deals with the behavior of the individual constituent elements and their interaction. When granular materials deform under wheel loads, consolidation, distortion, and attrition occur. Thus, mechanics of particulate medium needs to be studied to properly characterize unbound granular material behavior. Because of the macro scale of practical interest is in the broad range of pavement layered analysis, the microscopic effects of unbound granular materials can be treated as a continuum. However, since the mechanical behavior of unbound granular materials is affected by stress history, density, void ratio, water content, etc., it has been quite challenging to develop an appropriate mathematical model that includes all factors within the framework of continuum mechanics.

## 2.3 Subgrade Soils

With varying traffic and environmental conditions in a pavement structure, the most significant influence on pavement design and thickness determination is often by subgrade soils. This influence is the most pronounced at low subgrade support values, i.e., for weal soils. Factors that have a significant effect on the soil behavior can be loading condition, stress state, soil type, compaction, and soil physical states. The most important stress factor for soils is the deviator stress. Although the resilient modulus typically increases with increasing confining stress, the deviator stress has the most significant effect on resilient modulus of fine-grained subgrade soils. Therefore, constitutive relationships are primarily established between the resilient behavior and the deviator stress. In addition, the physical state is mainly represented by moisture content and dry density for compaction characteristics, Liquid Limit (LL), Plastic Limit (PL), Plasticity Index (PI), and saturation levels. Soil suction is controlled by grain size distribution, internal soil structure, and the closeness of the ground water table and has a major influence on subgrade moisture content.

## 2.4 Mechanistic Based Pavement Design Concepts

Existing pavement analysis and design methods often follow several empirical procedures developed through investigations from specific type of pavement structure with limited conditions. These empirical methods have taken a conservative approach of the relative strength properties of pavement foundation geomaterials in flexible pavements. Also, the empirical methods have limitations for changes of loadings and environmental conditions. The main limitation of empirical methods is that they cannot be confidently extrapolated beyond those conditions on which they are based. The essential need for the pavement design procedures to properly account for varying design situations has led to widespread research efforts to develop so-called mechanistic analysis and design concepts. A major aspect of mechanistic based design is the proper characterization of pavement materials for more accurate response prediction.

In the mechanistic approach, the pavement is treated as a layered structure, and the components of this structure must be properly understood as the constituent materials. For mechanistic analysis, the material resilient behavior is characterized using mathematical models. First theoretical background is needed for understanding some of the idealizations and assumptions made in developing the models. Secondly, laboratory tests must be conducted to study the material behavior under similar field conditions such as loadings, environmental conditions, and construction effects expected to apply to the pavement in service. The laboratory data must be examined to develop models that can predict measured material behavior and field response. Several unbound granular material and subgrade soil models have been developed for pavement design and evaluation. These models have involved repeated loading tests and considered the nonlinear stress-dependent material behavior (Brown and Pappin, 1981; Thompson and Elliot, 1985; Taciroglu, 1998; Schwartz, 2002).

### 2.4.1 Resilient Behavior

The resilient material behavior of unbound granular materials and subgrade soils is discussed in this section. In resilient modulus tests, both resilient and permanent deformations occur during the initial stage of load application as indicated in Figure 2-1. However as the number of load repetitions increase, the amount of permanent deformation in each load application decreases. Finally permanent deformation does not increase significantly with each load application.

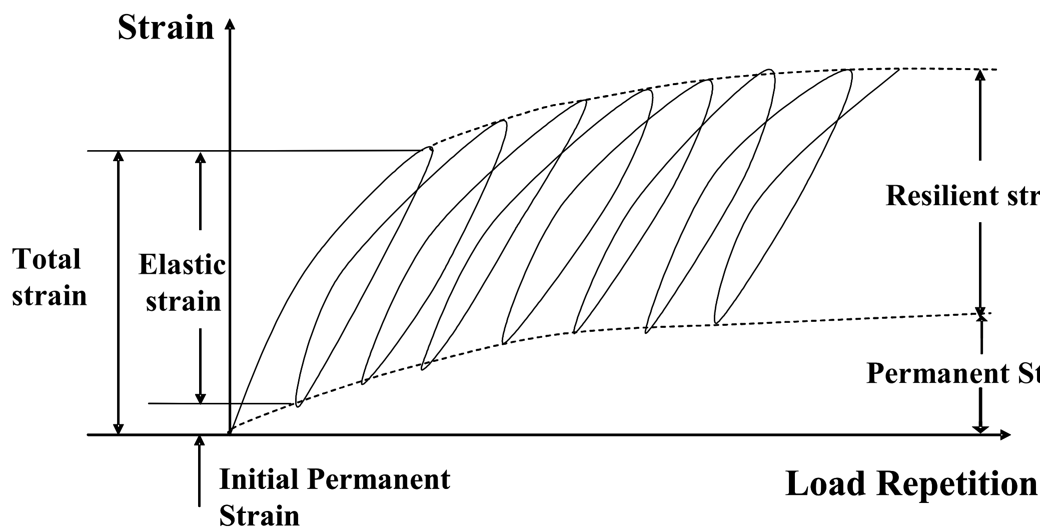


Figure 2-1 Deformation Response of a Pavement under Dynamic Loading (Huang, 1993)

The resilient material properties are one of the essential input variables to evaluate pavement structures using mechanistic concepts. The resilient modulus is defined by

$$M_R = \frac{\sigma_d}{\varepsilon_r} \tag{2-1}$$

where $M_R$ is resilient modulus, $\sigma_d$ is deviator stress = $(\sigma_1 - \sigma_3)$, and $\varepsilon_r$ is recoverable strain.

The test procedure for the determination of resilient modulus was described in AASHTO T307 (2002) protocol. A series of repeated axial stress of fixed magnitude for a load pulse duration of 0.1-sec. and cycle duration of 1.0-sec. are applied to a cylindrical test specimen. The specimen is subjected to a dynamic cyclic stress and a static confining stress by means of a triaxial pressure chamber. The total resilient axial deformation of the specimen is measured and the recoverable deformation or strain is used to calculate the resilient modulus. The test begins by applying a minimum of 500 to 1,000 load repetitions for the conditioning stage using a haversine shaped load pulse. This is followed by a sequence of loading with varying confining pressure and deviator stress pairs. The confining pressure is set constant, and the deviator stress is increased. Subsequently, the confining pressure is increased, and the deviator stress varied. The resilient modulus values are reported at a total of 15 specified deviator stress and confining pressure values. The stress sequences followed and the detailed procedure can be found in the AASHTO T307 Protocol.

### 2.4.2 Modeling Resilient Modulus of Unbound Granular Materials

Although unbound granular materials are one of the most commonly used materials in civil engineering, it is often challenging to model their deformation characteristics numerically. Granular materials constitute a discontinuous particulate medium physically and the resilient behavior is strongly influenced by the applied wheel load levels and the thicknesses of surface materials overlain. It is more appropriate to use some particulate material models under loading condition to determine the critical stresses, strains, and deformations in the materials. Accurate material characterization is defined as the selection or formulation of proper constitutive equations to represent the behavior of materials under loading.

Many parameters influence the behavior of granular materials under repeated loading. The resilient behavior of granular materials defined by resilient modulus is affected by factors such as stress level, density, grain size, aggregate type, particle shape, moisture content, and number of load applications. Resilient models of granular materials increase with increasing stress states (stress-hardening), especially with confining pressure and/or bulk stress, and slightly with deviator stress (Lekarp et al., 2000).

Modeling is needed to properly define and predict material behavior and performance. It is essential that the stress-strain relationship be modeled as accurately as possible with constitutive laws. The constitutive behavior of granular materials is characterized by a stress-dependent resilient modulus and several mathematical formulations have been suggested using different stress components. Although researchers present mathematical formulations that fit their particular data, great effort is clearly needed in developing more general models and procedures that have a sound theoretical basis and useful applicability. Since 1960, numerous research efforts have been devoted to characterizing the resilient behavior of granular materials (Seed et al., 1967; Hicks and Monismith, 1971; Uzan, 1985; Witczak and Uzan, 1988). To deal with such characteristics, repeated load triaxial test is usually used and resilient modulus can be defined as a function of stress state. The complexity of the problem has made it a very difficult task to combine soil mechanics theoretical principles with simplicity that is required for characterizing material response. Due to advanced numerical approximation techniques such as the finite element method, nonlinear stress-dependent models can be efficiently used in a mechanistic approach to properly characterize the actual behavior of granular materials. In the following sections, currently available models are discussed in detail.

#### 2.4.2.1 Confining Pressure Model

Seed et al. (1967) introduced a simple model for the resilient modulus relating it to confining stresses. They conducted repeated load triaxial tests on sands and gravels, and expressed the results in the form:

$$M_R = K_1(\sigma_3)^{K_2} \tag{2-2}$$

where $\sigma_3$ is confining pressure and $K_1$ and $K_2$ are regression analysis constants from experimental data. This model, however, did not give high correlation coefficients.

2.4.2.2 K-θ Model

One of the most popular models was developed by Hicks and Monismith (1971). This model, known as the K-θ model, has been the most widely used for modeling modulus as a function of stress state applicable to granular materials.

$$M_R = K(\theta)^n \tag{2-3}$$

where θ is bulk stress = ($\sigma_1$+2$\sigma_3$) or ($\sigma_d$+3$\sigma_3$), $\sigma_d$ is deviator stress = ($\sigma_1$-$\sigma_3$) and K, n are regression analysis constants obtained from experimental data. Table 2-1 and Figure 2-2 show K and n relations for various granular materials by Rada and Witczak (1981). Even though it is a popular model, the K-θ model has a shortcoming since it fails to adequately distinguish the effect of shear behavior.

The impact of neglecting shear stress was illustrated in Figure 2-3 by Uzan (1985) and the K-θ model predicted an increasing resilient modulus as axial strains increased in contrast to the test data that showed a decrease in resilient modulus. According to Brown et al. (1981), the K-θ model is not able to handle volumetric strains and therefore can only be applicable to a very limited stress range when confining pressure ($\sigma_3$) is less than deviator stress ($\sigma_d$). In addition, Nataatmadja (1989) reported that this model was not dimensionally satisfied as K had the same dimension with resilient modulus ($M_R$). Despite of this weakness, the K-θ model is still being used frequently for granular materials due to its simplicity.

Table 2-1 Typical K-θ Model Parameters for Various Types of Granular Materials (Rada and Witczak, 1981)

| Type of material | No. of data points | K* (MPa) | | n* | |
|---|---|---|---|---|---|
| | | Mean | Standard deviation | Mean | Standard deviation |
| Silty sands | 8 | 11.2 | 5.4 | 0.62 | 0.13 |
| Sand-gavel | 37 | 30.9 | 29.7 | 0.53 | 0.17 |
| Sand-aggregate blends | 78 | 30.0 | 18.1 | 0.59 | 0.13 |
| Crushed stone | 95 | 49.7 | 51.7 | 0.45 | 0.23 |

*: K and n are experimentally derived factors from repeated load triaxial test data.

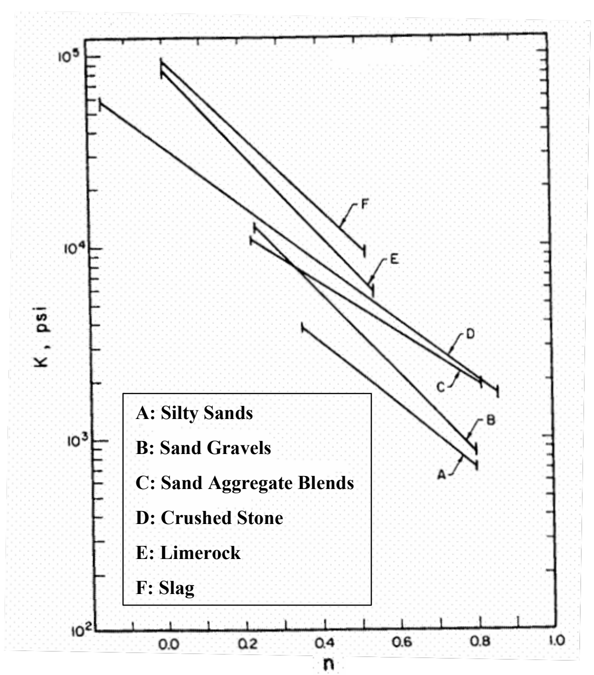


Figure 2-2 K and n Relationships for Various Types of Granular Materials (Rada and Witczak, 1981)

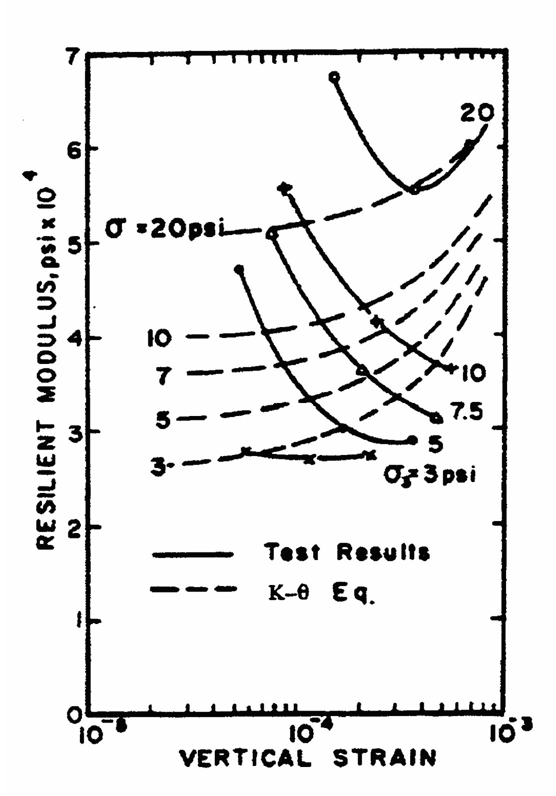


Figure 2-3 Comparison of Test Results and Predicted Behavior Using K- θ Model for a Dense Graded Material (Uzan, 1985)

### 2.4.2.3 Shackel's Model

After conducting repeated load triaxial test on a silty-clayey soil, Shackel (1973) developed the following resilient modulus model in terms of octahedral shear stress and octahedral normal stress.

$$Mr = K_1 \left[ \frac{(\tau_{oct})^{K_2}}{(\sigma_{oct})^{K_3}} \right] \qquad (2\text{-}4)$$

where $K_i$ are material regression constants obtained from triaxial test data. He proposed that his model was valid for both granular materials and cohesive soils. Since the model was defined in terms of stress invariants, it was considered to be one of the early advanced nonlinear models.

$$\sigma_{oct} = \frac{1}{3}(\sigma_1 + \sigma_2 + \sigma_3) = \frac{1}{3} I_1 \tag{2-5}$$

$$\tau_{oct} = \frac{1}{3}\left[(\sigma_1 - \sigma_2)^2 + (\sigma_2 - \sigma_3)^2 + (\sigma_1 - \sigma_3)^2\right]^{\frac{1}{2}} = \frac{\sqrt{2}}{3}\left(I_1^{\,2} - 3I_2\right)^{\frac{1}{2}} \tag{2-6}$$

where $I_1$ is the first stress invariant and $I_2$ is the second invariant.

2.4.2.4 Bulk-Shear Modulus Model

Boyce (1980) developed a nonlinear material model based on the secant bulk modulus (K) and the shear modulus (G). He found the influence of mean normal stress to resilient strain and the relationships were given as:

$$K = K_i p^{(1-n)} \tag{2-7}$$

$$G = G_i p^{(1-n)} \tag{2-8}$$

where $K_i$ is an initial value of bulk modulus, $G_i$ is an initial value of shear modulus and n is a constant less than 1. Boyce (1980) also updated his model to satisfy Maxwell's reciprocity theorem. Accordingly, the second order partial derivatives of a stress potential function are independent of the order of differentiation of volumetric and deviatoric stress components. Expressions of the moduli were given as follows:

$$K = \frac{K_i p^{(1-n)}}{1-\beta\left(\frac{q}{p}\right)^2} \tag{2-9}$$

$$G = G_i p^{(1-n)} \tag{2-10}$$

where β is $(1-n)\frac{K_i}{6G_i}$, p is mean stress, q is deviator stress. In this model, the volumetric strains and deviatoric strains are related to mean normal stress (p) and deviatoric stress (q) as follows:

$$\varepsilon_V = \left(\frac{1}{K_i}\right)p^n\left[1-\beta\left(\frac{q}{p}\right)^2\right] \tag{2-11}$$

$$\varepsilon_q = \left(\frac{1}{3}G_i\right)p^n\left(\frac{p}{q}\right) \tag{2-12}$$

where $\varepsilon_V$ and $\varepsilon_q$ are the volumetric and shear strains, respectively. This model can successfully predict measured strains from the initial bulk and shear moduli and the applied stress states.

2.4.2.5 Uzan Model

Since the K-θ model was not sufficient to describe the shear behavior of granular materials, Uzan (1985) made a modification to this model. An additional deviator stress component that includes the effect of shear behavior was shown to be in good agreement with test results.

$$M_R = K_1(\theta)^{K_2}(\sigma_d)^{K_3} \tag{2-13}$$

where $\theta$ is bulk stress = $(\sigma_1+2\sigma_3)$ or $(\sigma_d+3\sigma_3)$, $\sigma_d$ is deviator stress = $(\sigma_1-\sigma_3)$, and $K_1$, $K_2$, and $K_3$ are regression analysis constants obtained from experimental data. As shown in Figure 2-4, the results of analyses using the Uzan model appeared to be in good agreement with all aspects of granular material behavior. Considering both bulk stress and deviator stress, the Uzan model overcomes the deficiency of the K-θ model that did not include shear effects and apparently fits better with the test data than the K-θ model. This was shown to be especially important when confining stress values applied on the specimen were larger than the applied deviator stresses during testing.

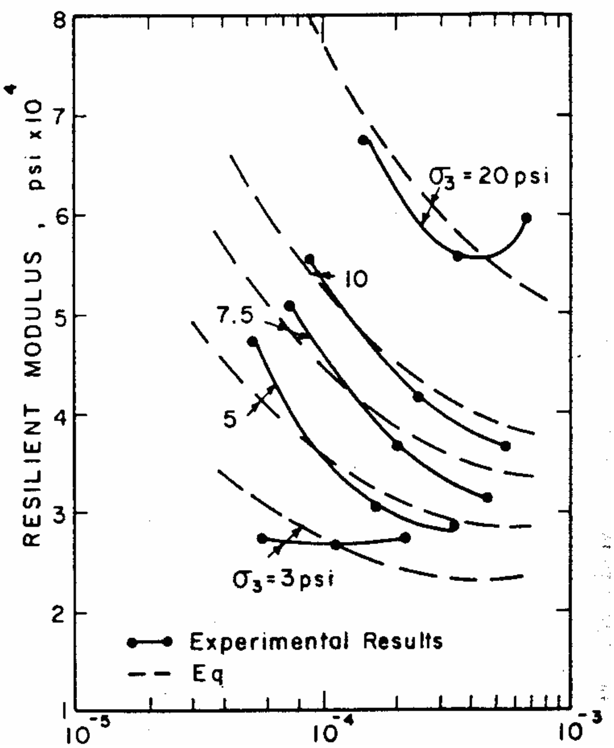


Figure 2-4 Comparison of Test Results and Predicted Behavior using the Uzan Model Equation for a Dense Graded Aggregate (Uzan, 1985)

### 2.4.2.6 Lade and Nelson Model

Lade and Nelson (1987) proposed an elastic material model based on energy conservation for closed-loop strain path. In this model, isotropic and nonlinear assumption was used in the elastic behavior of granular materials. With the assumption of energy conservation, the work during any arbitrary closed path stress cycle was written as:

$$W_{cycle} = \oint_{cycle} dW = \oint_{cycle} \left( \frac{I_1}{9K} dI_1 + \frac{dJ_2}{2G} \right) = 0 \tag{2-14}$$

where K is bulk modulus, G is shear modulus, $I_1$ is the first stress invariant, and $J_2$ is the second deviatoric invariant. The first order partial differential equation is derived from Equation 2-14 as follows:

$$\frac{I_1}{9K^2}\frac{\partial K}{\partial\sqrt{J_2}} = \frac{\sqrt{J_2}}{G^2}\frac{\partial G}{\partial I_1} \tag{2-15}$$

After substituting $K = \dfrac{E}{3(1-2\nu)}$ and $G = \dfrac{E}{2(1+\nu)}$ into Equation 2-15, the equation can be expressed in terms of E (Young's modulus).

$$\frac{1}{\sqrt{J_2}}\frac{\partial E}{\partial\sqrt{J_2}} = R\,\frac{1}{I_1}\frac{\partial E}{\partial I_1} \tag{2-16}$$

where $R = \dfrac{6(1+\nu)}{(1-2\nu)}$. The final form of the stress-dependent modulus equation was proposed by Equation 2-17.

$$E = M\,p_a\left[\left(\frac{I_1}{p_a}\right)^2 + R\frac{J_2}{p_a}\right]^{\lambda} \tag{2-17}$$

where $p_a$ is atmospheric pressure and M and $\lambda$ are material constants. This Lade and Nelson model did not give good results due to the energy conservation principles adopted in this hyperelastic material model formulation since energy dissipates when granular materials are subjected to repeated loading.

2.4.2.7 Universal Octahedral Shear Stress Model

Witczak and Uzan (1988) proposed an improvement over the Uzan (1985) model by replacing the deviator stress term with octahedral shear stress. This model also used atmospheric pressure ($p_a$) to normalize the bulk and shear stress terms to make the model parameters dimensionless.

$$M_R = K_1 p_a \left(\frac{I_1}{p_a}\right)^{K_2} \left(\frac{\tau_{oct}}{p_a}\right)^{K_3} \tag{2-18}$$

where $I_1$ is first stress invariant = ($\sigma_1+\sigma_2+\sigma_3$) or ($\sigma_1+2\sigma_3$), $\tau_{oct}$ is octahedral shear stress $=1/3\{(\sigma_1-\sigma_2)^2 + (\sigma_1-\sigma_3)^2 + (\sigma_2-\sigma_3)^2\}^{1/2} = \frac{\sqrt{2}}{3}(\sigma_1 - \sigma_3)$, $p_a$ is atmospheric pressure, and $K_1$, $K_2$, and $K_3$ are regression constants obtained from experimental data.

2.4.2.8 Itani Model

An improved correlation between the resilient modulus and various stress state variables, such as deviator stress, mean stress, confining stress, and axial strain, was obtained from multiple regression analyses. Itani (1990) proposed the material model with a high correlation coefficient ($R^2$ = 0.96) as follows:

$$M_R = K_1 p_a \left(\frac{\sigma_\theta}{p_a}\right)^{K_2} (\sigma_d)^{K_3} (\sigma_3)^{K_4} \tag{2-19}$$

where $\sigma_\theta = (\sigma_1+\sigma_2+\sigma_3) = (\sigma_1+2\sigma_3)$, $\sigma_d = \sigma_1-\sigma_3$, $\sigma_3$ is confining stress, $p_a$ is atmospheric pressure, and $K_1$, $K_2$, $K_3$ and $K_4$ are multiple regression constants obtained form triaxial tests. With the goal of developing improved models to characterize the resilient modulus, laboratory test data from different aggregate gradations were used in this study. Itani concluded that this model was useful to predict resilient modulus, although there was a slight multi-colinearity problem. This is due to the fact that two independent triaxial stress states are expressed in three stress terms in this equation.

2.4.2.9 Crockford et al. Model

Crockford et al. (1990) developed a resilient modulus model which was expressed as a function of volumetric water content, suction stress, octahedral shear stress, unit weight of material normalized by the unit weight of water, and the bulk stress. The model was proposed as follows:

$$M_R = \beta_0 \left(\theta + 3\Psi \frac{V_w}{V_t}\right)^{\beta 1} (\tau_{oct})^{\beta_2} \left(\frac{\gamma}{\gamma_w}\right)^{\beta_4} \tag{2-20}$$

where $\beta_0$, $\beta_1$, $\beta_2$, and $\beta_3$ are material constants, $\Psi$ is suction stress, $\frac{V_w}{V_t}$ is volumetric water content, $\tau_{oct}$ is octahedral shear stress, and $\frac{\gamma}{\gamma_w}$ is unit weight of material normalized by the unit weight of water. When eliminating moisture term and the normalized unit weight term, Equation 2-20 simplifies to the octahedral shear stress model of Witczak and Uzan (1988).

2.4.2.10 UT-Austin Model

UT-Austin model was developed by Pezo (1993) with a good agreement of the resilient modulus data from the repeated load triaxial test. This model predicts the response variable, axial strain, instead of the resilient modulus using the applied confining and deviator stresses. Since this model is independent of the response variables, it is very useful for any condition.

$$M_R = \frac{\sigma_D}{\varepsilon_r} = \frac{\sigma_d}{a\sigma_d^b\sigma_3^c} = \frac{1}{a}\left(\sigma_d^{1-b}\sigma_3^{-c}\right) = K_1\left(\sigma_d\right)^{K_2}\left(\sigma_3\right)^{K_3} \tag{2-21}$$

where $\sigma_d$ is deviator stress = ($\sigma_1$-$\sigma_3$), $\sigma_3$ is confining stress and $K_1$, $K_2$ and $K_3$ are regression analysis constants obtained from experimental data.

2.4.2.11 Lytton Model

Lytton (1995) proposed that the principles of unsaturated soil mechanics could be applied to the universal octahedral shear stress model (Witczak and Uzan, 1988) because unbound aggregate materials in pavements are normally unsaturated. To evaluate the effective resilient properties of unsaturated granular materials, he added a suction term to the universal octahedral shear stress model.

$$M_R = K_1 p_a \left(\frac{I_1 - 3\theta f h_m}{p_a}\right)^{K_2}\left(\frac{\tau_{oct}}{p_a}\right)^{K_3} \tag{2-22}$$

where $p_a$ is atmospheric pressure, $I_1$ is first stress invariant = $(\sigma_1+\sigma_2+\sigma_3)$, $\theta$ is volumetric water content, f is function of the volumetric water content, $h_m$ is matric suction, $\tau_{oct}$ is octahedral shear stress $=1/3\{(\sigma_1-\sigma_2)^2 + (\sigma_1-\sigma_3)^2 + (\sigma_2-\sigma_3)^2\}^{1/2}$, and $K_1$, $K_2$, and $K_3$ are multiple regression constants obtained from triaxial tests.

2.4.2.12 NCHRP 1-37A Mechanistic Empirical Pavement Design Guide (MEPDG) Model

In the MEPDG (NCHRP 1-37A, 2004), a generalized constitutive model was adopted to characterize the resilient modulus of unbound aggregates. This equation combines both the stiffening effect of bulk stress and the softening effect of shear stress. Thus, the values of $K_2$ should be positive, since increasing the bulk stress produces a stiffening of the material. However, $K_3$ should be negative to show a softening effect. To properly find the model constants, the multiple correlation coefficients determined for test results have to exceed 0.90. Note that this model is proposed for use with both unbound aggregates and fine-grained subgrade soils.

$$M_R = K_1 p_a \left(\frac{\theta}{p_a}\right)^{K_2} \left(\frac{\tau_{oct}}{p_a}+1\right)^{K_3} \tag{2-23}$$

where $\theta$ is the bulk stress = $\sigma_1+\sigma_2+\sigma_3$, $\tau_{oct}$ is octahedral shear stress $=1/3\{(\sigma_1-\sigma_2)^2 + (\sigma_1-\sigma_3)^2 + (\sigma_2-\sigma_3)^2\}^{1/2}$ , $p_a$ is atmospheric pressure, and $K_1$, $K_2$, and $K_3$ are constants obtained from experimental data.

### 2.4.3 Modeling Resilient Modulus of Subgrade Soils

Resilient modulus of subgrade soils is often predicted using a simple empirical relationship such as using the California Bearing Ratio (CBR) value. However, it is evident that the subgrade soil response is commonly nonlinear and stress-dependent. This characterization has also been demonstrated by laboratory tests. Therefore, the nonlinear stress-dependent behavior must be incorporated into the characterization of subgrade soils which typically soften with increasing stress level commonly referred to as the stress-softening nature of the resilient modulus.

#### 2.4.3.1 Empirical Relationships

The earliest attempts to incorporate subgrade resilient modulus were based on the empirical relationships between CBR (California Bearing Ratio) and resilient modulus. Several correlations were proposed in various design procedures in the form:

$$M_R = K_1 (CBR)^{K_2} \tag{2-24}$$

where $K_1$ and $K_2$ are constants proposed by various researchers [$K_1$ = 1,500 and $K_2$ = 1.0 from Heukelom and Foster (1960), $K_1$ = 2,555 and $K_2$ = 0.64 from Lister and Powell (1987), $K_1$ = 3,000 and $K_2$ = 0.65 from CSIR (the Council of Scientific and Indistrial Research), $K_1$ = 5,409 and $K_2$ = 0.711 from Green and Hall (1975)]. While these relationships came from empirical and rational characterization, linear relationship still remains a weakness. In the MEPDG (NCHRP 1-37A, 2004), $K_1$ was selected to 2,555 and $K_2$ was selected to 0.64 for the subgrade strength and stiffness correlation.

2.4.3.2 Brown and Loach Models

Brown (1979) proposed a nonlinear resilient response model for the subgrade developed from repeated load triaxial testing. The model realistically took into account the effect of mean normal stress caused by overburden in the pavement subgrade layers. Moreover, the deviator stress calculated within the subgrade was considered to be caused only by the wheel loading. This separates wheel load deviator stress from increasing overburden stress in deep subgrade layers. The model is expressed by:

$$M_R = A\left(\frac{p_0}{q_R}\right)^B \tag{2-25}$$

where $p_0$ is effective mean normal stress caused by overburden, $q_R$ is deviatoric stress caused by wheel loading, and A and B are material constants. Typical ranges of A and B are 2.9 to 29.0 and 0 to 0.5, respectively for subgrade soils. Later, Loach (1987) proposed a modified version of Brown's model in which an additional deviatoric stress term $q_R$ was included in above equation as follows:

$$M_R = C\ q_R\left(\frac{p_0}{q_R}\right)^D \tag{2-26}$$

where C and D are material constants in the range of 10 to 100, and 1 to 2, respectively. The soil used in triaxial testing was silty clay, known as Keuper Marl, which had been used extensively as the subgrade in the test facility at University of Nottingham. During testing, the effect of mean normal stress due to overburden $p_0$ in the model was simulated by the cell pressure and soil suction. Loach's model was believed to constitute an improvement to Brown's model since it was formulated after completing a comprehensive set of cyclic triaxial tests on samples more representative of soil in the ground than tests reported by Brown (1979).

#### 2.4.3.3 Semilog Model

Fredlund et al. (1977) proposed this model for a moraine glacial till and obtained the range of parameter k = 3.6 to 4.3 and n = 0.005 to 0.09 for resilient modulus and deviator stress in units of kPa.

$$\log(M_R) = k - n\,\sigma_d \qquad (2\text{-}27)$$

#### 2.4.3.4 The Bilinear or Arithmetic Response Model

For the majority of fine-grained subgrade soils, soil modulus decreases in proportion to the increasing stress levels thus exhibiting stress-softening type behavior. For this category of subgrade materials, a stress-softening response appears. As a result, the most important parameter affecting the resilient modulus becomes the vertical deviator stress on the top of subgrade due to the applied wheel load. The bilinear or arithmetic model by Thompson and Robnett (1979) was been one of the most commonly used resilient modulus models for subgrade soils expressed by the modulus-deviator stress relationship given in Figure 2-5. This bilinear soil model used in the ABAQUS$^{TM}$ finite element program user material subroutine developed in this study is expressed as follows:

$$
\begin{aligned}
M_R &= K_1 + K_3 \times (K_2 - \sigma_d) \text{ when } \sigma_d \le K_2 \\
M_R &= K_1 - K_4 \times (\sigma_d - K_2) \text{ when } \sigma_d \ge K_2
\end{aligned}
\tag{2-28}
$$

where $K_1(E_{Ri})$, $K_2(\sigma_{di})$, $K_3$, and $K_4$ are material constants obtained from repeated triaxial tests and $\sigma_d$ is the deviator stress = $(\sigma_1 – \sigma_3)$. As indicated by Thompson and Robnett (1979), the value of the resilient modulus at the breakpoint in the bilinear curve, $E_{Ri}$, (see Figure 2-5) can be used to classify fine-grained soils as being soft, medium or stiff.

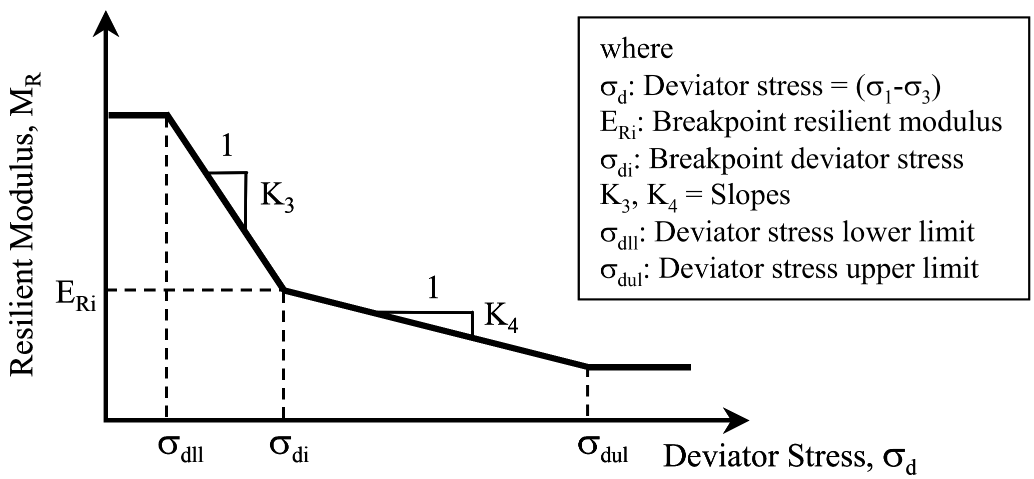


Figure 2-5 Stress-dependency of Fine-Grained Soils Characterized by the Bilinear Model (Thompson and Robnett, 1979)

2.4.3.5 Hyperbolic Model

A hyperbolic model was proposed by Boateng-Poku and Drumm (1989) in the following form:

$$M_R = \frac{g_1 + g_2\sigma_d}{\sigma_d} \tag{2-29}$$

where $g_1$ and $g_2$ are constants from statistical analysis and $\sigma_d$ is the deviator stress. Statistical analysis of laboratory test data is quite direct by recognizing that the transformed variable ($y' = M_R \times \sigma_d$) represents a linear regression equation with the constants $g_1$ being the relationship intercept and $g_2$ the slope of the transformed analysis ($y'$ versus $\sigma_d$). The practical significance of $g_2$ is that it presents the asymptotic value of the $M_R$ response as the limit of $M_R$ is taken at an infinite deviator stress ($\sigma_d$) level.

2.4.3.6 Dawson and Gomes Correia Model

Dawson and Gomes Correia (1996) developed a resilient modulus model based on the analysis of laboratory test data and recognizing the need for realistic values at low stress or strain. This model included the parameters of mean normal stress, deviator stress, and plastic limit of soil sample.

$$M_R = 49{,}200 + 950\,p_0' - 370\,q_r - 2{,}400\,w_p \tag{2-30}$$

where $p'_0$ is mean normal effective stress replaced by the soil suction, $q_r$ is repeated deviator stress, $w_p$ is the plastic limit expressed as a percentage. $p'_0$ and $q_r$ are in kPa.

## 2.5 Summary

In this chapter, resilient behavior was defined first. Then, various resilient modulus models for unbound granular base and fine-grained subgrade soils were reviewed. Factors affecting resilient behavior from laboratory repeated load test were mainly reviewed under current stress states and material variables. The models which consider confinement and shear stress effects in characterization were recommended for pavement design and analysis use. The extent of resilient modulus dependence on each of the components changes depending on the type of materials and the applied stress regimes. These recently developed resilient modulus models adequately described the behavior in terms of current material stress conditions and properly predicted the resilient behavior of both granular materials and subgrade soils. Most of these models for geomaterials were developed based on repeated load triaxial testing under axisymmetric stress condition. To develop more realistic models for the resilient behavior of pavement materials, it may be worthwhile to perform true triaxial tests with cubical specimens and three-dimensional stress states to predict more accurate resilient responses.

# Chapter 3 Structural Analysis and Finite Element Modeling of Flexible Pavements

## 3.1 Flexible Pavement Analysis

Pavement analysis has been transitioning from empirical methods to mechanistic approaches. Due to the limitations of computational capabilities, pavement designs were dominated first by empirical methods which were limited to a certain set of environmental and material conditions. If these conditions were changed, the design was no longer valid. The effectiveness of any mechanistic design method relies on the accuracy of the predicted stresses and strains and finite element analysis is one of the most commonly used mechanistic analysis tool. This chapter will review in detail the use of major mechanistic analysis approaches on the structural modeling of flexible pavements: elastic layered approach and finite element method.

## 3.2 Elastic Layered Programs for Pavement Analysis

Structural analysis of pavement systems started from the classical solutions of Boussinesq (1885) and Burmister (1943). Based on two classical approaches, many solution techniques have been developed for the numerical evaluations.

### 3.2.1 One Layer Approach

Unsurfaced pavements can be treated as elastic layered systems in the semi-infinite half-space. These are axisymmetric problems to designate radial, tangential, and vertical stress conditions (see Figure 3-1).

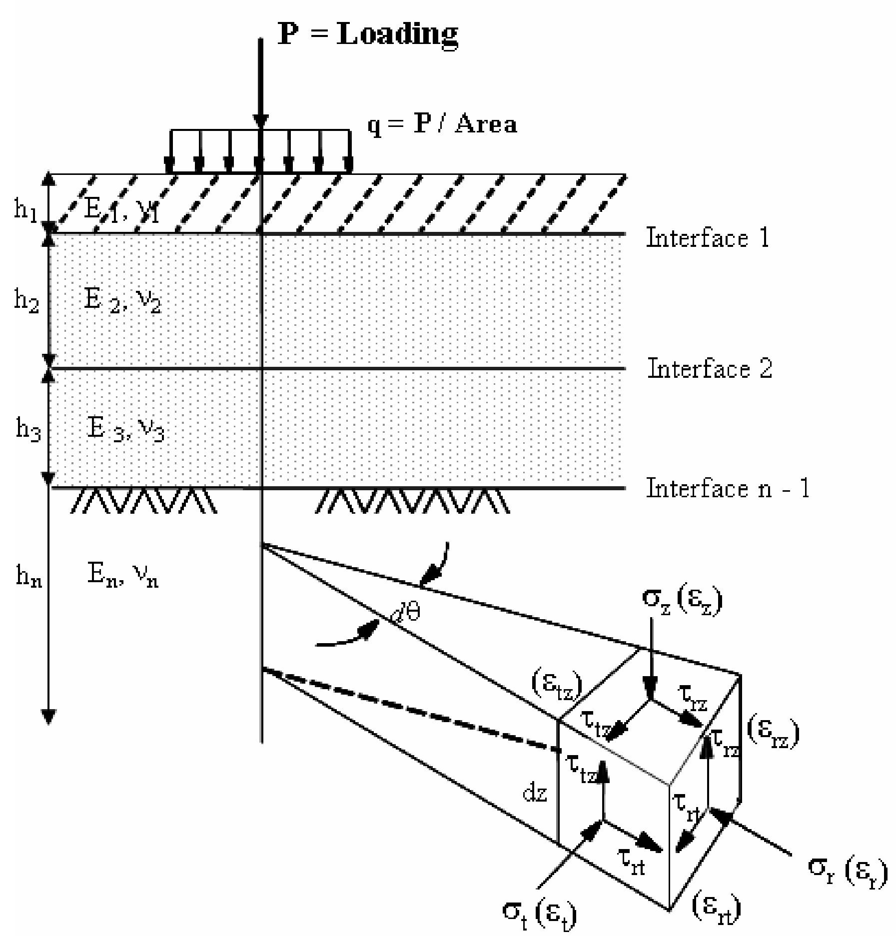


Figure 3-1 Generalized Multilayered Elastic System in Axisymmetric Condition

Boussinesq (1885) solved the problem of semi-infinite linear elastic homogeneous half-space with a concentrated loading by combining equilibrium equations with the constitutive and kinematic equations. However, the Boussinesq equations for concentrated loading did not apply directly to flexible pavement structures, since layer structures had different elastic moduli and Poisson's ratios.

Foster and Ahlvin (1958) integrated the concentrated loading of Boussinesq's study over uniformly loaded circular area for use in flexible pavement analysis. They presented charts for determining horizontal stresses, vertical stresses, and elastic strains in the semi-infinite half-space for an incompressible solid. Later, they also tabulated the pattern of stress, strain, and deflection results at a large number of points with different values of Poisson's ratio in the homogeneous half-space.

### 3.2.2 Multi Layer Theory

While Boussinesq's equations represent an elastic solution to the one layer system, Burmister (1943) developed solutions first for two-layer and later for three-layer systems, which advanced pavement analysis considerable. One advantage of this theory is that it can be used to obtain a multi layered system of large number of layers. But several assumptions were needed to use Burmister's theory.

1. Each layer is homogeneous, isotropic, and linearly elastic;
2. Weightless and infinite layers are considered;
3. Layers have a finite thickness except the bottom layer which is infinite;
4. A circular uniform pressure is applied on the surface;
5. Interface between two layers is continuous.

When compared to critical pavement responses, multi layer theory of Burmister was more accurate than one layer theory of Boussinesq. Numerous tables and charts were prepared for Burmister solutions applicable to two or three layers only.

### 3.2.3 Linear Elastic Layered Programs for Multilayered Systems

After the emergence of powerful computers, several linear elastic computer programs have been developed for pavement analysis. The prime objective of these computer programs was eliminating complex computation to obtain stresses, strains, and displacements from classical multilayer theory and obtaining mechanistic solutions.

The first one was the CHEVRON program developed by Warren and Dieckman (Chevron Research Company, 1963). Later, Hwang and Witczak (1979) modified this program to incorporate nonlinear elastic material behavior of granular base and linear elastic subgrade soil in the DAMA design program for use by the Asphalt Institute. The DAMA program could be used to analyze a multi layer elastic pavement structure under a single or dual wheel load. But, the number of layers did not exceed five.

BISAR (De Jong et al., 1973) developed by Shell researchers was introduced to calculate the response of multi layer structures with linearly elastic materials. BISAR also uses Burmister's theory and analyzes multiple loading cases. This program has various advantages that use different elastic moduli, Poisson's ratios, layer thicknesses, and interface bonding conditions specified in each layer.

The University of California, Berkeley (Kopperman et al., 1986) developed ELSYM5 that could deal with five linear elastic layers under multiple wheel loads. The principal stresses, strains, and displacements could be calculated at specified locations.

As linear elastic programs were developed, the study of nonlinear elastic material properties for unbound granular base and subgrade soil materials also started as early as late 1960's. Initial attempts were made to account for the changing moduli with stress levels at different depths in the layers, and the constant Poisson's ratio was assumed. Early work by Kasianchuk (1968) and Huang (1968) employed nonlinear analysis using the classical elastic layered solutions in which the modulus was varied with depth only. Kasianchuk divided each pavement layer into thinner sublayers to model the modulus changes. To solve for the stresses, initial estimates of moduli were inputs in the first iteration. The gravity stresses were added to these calculated stresses and new moduli were calculated using laboratory determined material characterizations for base and subgrade. The iterative process was repeated until the moduli used were compatible with the stress distribution. The major approximation used in this method was that the modulus in the radial direction of each sublayer was assumed to be constant.

Huang (1968) made a half-space of seven layers to show the effect of nonlinearity of granular materials on pavement responses and the lowest layer was considered as a rigid base with a very large modulus value. Using a similar method of successive approximations, the first modulus of each layer was assumed and then the stresses were calculated by layered theory. Using the sum of the calculated stresses and geostatic stresses, new sets of moduli were estimated from a nonlinear material model. And then, new stresses were calculated for the next iteration. Until the moduli between two consecutive processes converged to a specified tolerance, the process was continued.

The KENLAYER computer program provided the solution for an elastic multilayer system under a circular loaded area and was developed by Huang (1993) at University of Kentucky. This program handled multiple wheels, iterations for nonlinear layers, and viscoelastic layers. To deal with nonlinearity, KENLAYER divided the layers into a number of sublayers and the stresses at the mid-height were used to compute the modulus of each layer. This was assigned to layered systems under single, dual, dual tandem, or dual tridem wheels with each layer behaving differently, such as linear elastic, nonlinear elastic, and viscoelastic. Damage analysis was also performed by dividing one year into different periods.

LEDFAA (Federal Aviation Administration, 1993) was developed by the Federal Aviation Administration (FAA). This was a computer program for performing thickness design of airport pavements. It implemented an advanced design procedure based on elastic layered theory. At the same time, elastic layered design better predicted the wheel load interactions for the aircraft because the landing gear configurations and layered pavement structures could be modeled directly using the elastic layered design procedure. The modulus values of aggregate layers were calculated by WES Modulus procedure (Barker and Gonzales, 1991) included with sublayering performed automatically. The modulus values of the sublayers decreased with increasing depth of a sublayer within the aggregate layer and were also dependent on the modulus of the subgrade/subbase layer below the aggregate layer. Sometimes, unusually high moduli were predicted on the top of base layer due to doubling of the modulus in the sublayers from subgrade to the top of the base layer (Tutumluer and Thompson, 1997).

### 3.2.4 Characteristics of Elastic Layered Programs

Elastic layered analyses have been easily implemented and widely accepted. Although elastic layered programs have several advantages, they can not give accurate pavement responses. First of all, these methods assume that all layers are linear elastic but this assumption makes it difficult to analyze layered system consisting of nonlinear base/subbase and subgrade soil materials. Secondly, all wheel loads applied on top of the surface layer have to be axisymmetric, which is not true for actual wheel loads. At last, elastic layered programs assume isotropic material property that is not realistic for most geomaterials, especially not for unbound aggregate materials (Tutumluer and Thompson, 1997). Limitations like these are hard to show that realistic pavement responses can be predicted using elastic layered programs. These difficulties can be overcome by using the finite element method.

## 3.3 Finite Element Programs for Pavement Analysis

Finite element models have been applied extensively to analysis of pavement structures. In this section, the development of several nonlinear solution techniques including finite element methods currently used in pavement analysis are reviewed.

### 3.3.1 Two-dimensional or Axisymmetric Finite Element Analysis

Shifley (1967) used the finite element procedure by incorporating nonlinear material behavior in the analysis. The finite element method discretized the elastic layered system so that the resilient modulus varied both with depth and in the radial direction. Shifley used iterative procedures to account for the nonlinearity of the granular materials as characterized by nonlinear models dependent on the bulk stress and confining stress. However, the asphalt concrete and the clayey sand subgrade were considered as linear elastic. He also applied similar techniques to predict the response on several sections of a full-scale test road.

Duncan et al. (1968) proposed proper domain sizes for axisymmetric finite element modeling and incorporated nonlinear material behavior in the analysis. At first, they investigated a proper domain of axisymmetric model to obtain a reasonable comparison with elastic layered program. The results of finite element technique with a boundary at a depth of 18-times radius of loading area and at a distance of 12-times the radius of loading area were compared favorably with those determined from the Boussinesq solution. However, it was necessary to move the boundary at a depth of about

50-times the radius of loading area while maintaining the same radial constraints to get more accurate results. This study also indicated that it was feasible to approximate nonlinear material properties in the analyses. Nonlinear stress-dependent models of base and subgrade materials were incorporated. Duncan et al. analyzed the pavements for winter and summer conditions. They found that large horizontal tensile stresses developed beneath the wheel load in the granular base especially in the summer time.

Dehlen (1969) considered the nonlinearity of both modulus and Poisson's ratio with stress level for evaluating pavements with finite element techniques where an incremental loading procedure was used to account for the variations. For the first increment, the modulus and Poisson's ratio were determined from gravity stresses and the tire pressure. At each increment, the elements were checked with Poisson's ratio not being allowed to be greater than 0.5. The next load increment was then added and the process continued until the full load was applied. The results showed that the maximum surface deflection was 3 to 13% higher than for the linear analysis. The maximum vertical stress on the subgrade for the nonlinear analysis was 15 to 20% greater than the linear analysis. Little difference existed between the linear and nonlinear horizontal strains in the asphalt layer. Dehlen also indicated that accurate predictions of the stresses and displacements could be obtained with a depth to the lower boundary of 50-times the radius of loading area and a radial distance of 12-times the radius of loading area to the cylindrical boundary.

Hicks (1970) modeled a three-layer system consisting of 102-mm of asphalt concrete, 305-mm of granular base over a clay subgrade subjected to a uniformly distributed load over a circular area. This finite element method was employed to two different material models used in the characterization of granular bases. One was the model of resilient modulus by bulk stress and the other was a model of resilient modulus by the confining pressure. Using each model, the problem was solved with the wheel load applied in four equal load increments. The initial moduli were computed from the gravity stresses alone and the moduli for successive increments were computed from the stresses obtained after application of the previous increment. As compared to two different nonlinear models, the predicted surface deflections and horizontal stresses by the confining pressure-dependent model were lower than the bulk stress-dependent model, although the vertical stresses obtained by using each model were nearly the same. In all instances, the principal stress ratios ($\sigma_1/\sigma_3$) given by the confining pressure model was considerably larger than those obtained by the bulk stress model. The calculations at three different Poisson's ratios of the base showed that a change in Poisson's ratio from 0.35 to 0.5 reduced the principal stress ratio near the surface from about 10 to less than 4.

Hicks and Monismith (1971) also used a similar nonlinear finite element program which applied the wheel load in five increments. A tangent modulus and Poisson's ratio were calculated and the values of the resulting incremental strains were determined at each increment. This technique was used to predict the resilient response of a test pavement. Even though, in some cases, these predicted results deviated from measured stresses and strains, these results were consistently better than linear solutions.

Kirwan and Glynn (1969) first added horizontal compressive stresses to elements beneath the load in the finite element program to handle any tensile stresses developed in the granular base. Later, this program was modified to incorporate nonlinear material behavior by Kirwan and Snaith (1975) for nonlinear material characterization composed of a stress-dependent modulus and a set of properties for the elements within the granular layer. The load was applied and the new values were calculated for each element using the recently computed stresses. However, this program was hard to converge since it used only one step loading rather than an incremental loading scheme.

Stock et al. (1979) followed a similar approach for investigating nonlinear behavior of granular base materials using finite element analysis. To investigate the nonlinear characterizations, the granular layer was divided into four sublayers with the wheel load applied in one increment. Granular materials were characterized by the K-θ model which depends on bulk stress with a stress state failure criterion superimposed. In each sublayer, the modulus was computed followed by the stress states in the center of each sublayer underneath the load. Stock et al. concluded that the characteristics of the granular material did not have a significant effect on the vertical subgrade strain but considerably influenced the lateral tensile strain at the bottom of the asphalt layer.

Zeevaert (1980) and Barksdale et al. (1982) developed one of the most comprehensive finite element programs for the analysis of flexible pavements, the GAPPS7 program which could also analyze soil-fabric systems. Many mathematical formulations such as nonlinear soil and fabric materials, friction parameters of the fabric interface, tension stiffness of the fabric, ability to handle large displacements, no-tension conditions of the granular materials, and the yielding of plastic materials were considered. A uniaxial stress-strain curve of their research showed the nonlinear material stiffness behavior and resilient response of granular and cohesive layers were represented by using the K-θ model and the subgrade bilinear approximation model, respectively. This program used an incremental and iterative procedure like other nonlinear programs and was capable of handling geometric nonlinearities which were due to large displacements caused by the change in geometry. The piecewise incremental solutions were verified after each load increment and iterations were performed to insure equilibrium. The program was verified with several theoretical studies and laboratory measurements, especially for the complex soil-fabric behavior at interfaces.

The finite element program, SENOL was developed by Brown and Pappin (1981) for granular materials to specially apply the contour model of Pappin (1979) to flexible pavement analysis. Nonlinear bulk and shear moduli in the granular material were programmed and initial values of these moduli due to overburden stresses were initially assigned in the elements. And then, the responses of the wheel load were computed by applying the load in 10 increments and iterating until convergence of solution was satisfied. A secant modulus approach was followed in the program where the moduli were calculated at each iteration from the total accumulated response until the present load increment. The SENOL program was also developed for linear elastic layered program to compute with an equivalent Young's modulus and Poisson's ratio. The results obtained from the program showed good agreements between the measured and computed stresses and strains. However, the main advantage of using the contour model, which was adopted in this program, for the nonlinear characterization of granular bases is that the horizontal tensile stresses usually encountered in the lower part of the base using linear elastic solutions are no longer predicted.

Delft Technical University in Netherlands (Sweere et al., 1987) developed the finite element program DIANA which is similar to SENOL. Both granular materials and subgrade materials with stress-dependent resilient moduli were modeled in the program by using the simplified contour model suggested by Mayhew (1983). The nonlinear iterative and incremental procedures adopted in DIANA were also similar to SENOL program where a secant modulus was calculated using the response due to both the wheel loading and overburden stresses. As compared to the measured stresses and strains in a full-scale test pavement, predictions of DIANA, however, were not satisfactory.

Crockford (1990) developed an unusual type of nonlinear resilient response model for characterization of granular layers and pavement evaluation in conjunction with the use of a falling weight deflectometer (FWD). The model included the first stress invariant, octahedral shear stress, unit weight of aggregates and moisture content in the formulation. This model and some of the nonlinear models, such as the K-θ model and the Uzan model, were incorporated into a user-friendly finite element program named TTIPAVE. The program handled several conditions such as residual stresses, cross-anisotropic material, and slip condition at layer boundaries using interface elements. TTIPAVE analyzed as axisymmetric or plane strain layered systems using both linear and nonlinear constitutive material models. But there were several shortcomings. The nonlinear iterations used in TTIPAVE for the material characterizations were usually terminated without convergence due to some limiting values of modulus encountered in the analysis. Another shortcoming of the program a simple, coarse finite element mesh was used for all layered systems. The use of one grid creates geometric limitations and also caused important errors even for a linear elastic problem.

ILLI-PAVE is a commonly used finite element program developed at the University of Illinois (Raad and Figueroa, 1980) and the MICH-PAVE program was developed at the Michigan State University (Harichandran et al., 1989) for the analysis of flexible pavements. Both programs modeled the pavement as an axisymmetric solid of revolution and used the following resilient response models, the K-θ model for granular materials, the bilinear approximation for fine-grained subgrade soils. The principal stresses in the granular and subgrade layers did not exceed the strength of material as defined by the Mohr-Coulomb theory of failure. MICH-PAVE used a flexible boundary at a limited depth beneath the surface of the subgrade, instead of a rigid boundary placed deeper in the subgrade and then reduced run time and storage requirements. In addition, the analyses of MICH-PAVE yielded outcomes with a reduced run time and storage requirements compared to other programs.

Brunton and De Almeida (1992) developed a finite element program named FENLAP for structural analysis of pavements. The program incorporated various nonlinear stress-strain models, such as the Brown and Loach's model for subgrades and the popular K-θ model for granular materials to simulate the resilient behavior. An incremental and iterative procedure very similar to the one used in SENOL program is employed for nonlinear analysis. Modulus values are obtained for the elastic stiffnesses which calculated the average resilient modulus in the linear elastic layers to be used with falling weight deflectometer backcalculation procedures. Although the K-θ model was not appropriate for characterization of the granular layers, the model gave reasonable results in terms of vertical displacements of pavements.

GT-PAVE finite element program (Tutumluer, 1995) had also taken into account nonlinear material characterizations of granular materials and subgrade soils. The model subroutines for material nonlinearity were specifically the Uzan model and the UT-Austin model for granular materials and the bilinear model and Loach model for subgrade soils. A direct secant stiffness approach was developed for the nonlinear solution technique and successfully adopted for base/subbase and subgrade layers. As a result, a direct secant stiffness approach for nonlinear analysis was found to be a more efficient method compared to the other approaches such as the Newton-Raphson and tangent stiffness approach. A convergence criterion of a 5% maximum individual error was adopted between any two resilient moduli calculated in two subsequent nonlinear iterations and this mainly controls convergence. Tutumluer also investigated that a cross-anisotropic representation of the granular materials which was shown to reduce the horizontal tension in the granular base by up to 75%. Use of 15% of the vertical modulus in the horizontal direction was found to predict accurately the horizontal and vertical measured strains in the base layers. An iterative tension modification procedure using the modified stress transfer approach was also employed for the elimination or reduction of horizontal tension in base layer. The results from five well instrumented full-scale pavement test sections were successfully predicted using the GT-PAVE program (Tutumluer, 1995).

Thompson and Garg (1999) introduced an “Engineering Approach” to determine critical pavement responses based on the superposition of single wheel pavement responses. Both elastic layered program and axisymmetric finite element program were used to compute responses from superposition. The “Engineering Approach” used average layer modulus values obtained from nonlinear axisymmetric ILLI-PAVE finite element analysis and these values were used as inputs for elastic layered analyses. Yet, the actual modulus distributions were much different from the single modulus assignment for the entire pavement layer. Actual modulus distributions were given in accordance with stress distributions or stress bulbs in the layer.

A nonlinear finite element program that combines the nonlinear stress-dependent modulus for unbound granular base layer and Poisson's ratio for all layers was developed by Park et al. (2004). The developed program was verified by comparing the results to those obtained from the BISAR program. They modeled the stress-dependency for granular materials suitable for calculating a reduced horizontal tension in the bottom half of the unbound base layers. Unlike conventional methods for correcting horizontal tension, compressive stresses could be obtained only by the use of constitutive models.

### 3.3.2 Three-dimensional Finite Element Analysis

Chen et al. (1995) documented the effect of high inflation pressure and heavy axle load on flexible pavement performance by using a three-dimensional finite element model. All pavement structures were assumed to be homogeneous and linear elastic. Results obtained from their studies were compared to another elastic layered program, ELSYM5 (Kopperman et al., 1986), for a uniform circular pressure and had a close agreement between two models. It was found that the uniform pressure model predicted a higher percentage increase in tensile strain than the nonuniform pressure.

Helwany et al. (1998) studied three-layer flexible pavement system subjected to different types of loading. Axle loadings with different tire pressures, different configurations, and different speeds were conducted in two-dimensional (DACSAR) and three-dimensional (NIKE3D) finite element programs. Various material constitutive models such as linear elastic, nonlinear elastic, and viscoelastic were employed in these analyses. As a preliminary analysis, the analytical solutions of the one layer system, using

DASCAR and NIKE3D, agreed with the Boussinesq's solutions. This study showed that finite element modeling of pavements could be extremely useful to predict accurate pavement structure responses.

Shoukry et al. (1999) used three-dimensional finite element model to back-calculate moduli of pavement structures and compared the results with predictions of backcalculation programs such as MODCOMP, MODULUS, and EVERCALC. The measured deflections were obtained from the falling weight deflectometer tests. All pavement layers were modeled as linear layers and 8-noded solid brick elements were used. This three-dimensional finite element analysis had a fair agreement with the backcalculated layer moduli.

Wang (2001) investigated the response of flexible pavement structures with various materials, model dimensions and different loadings using three-dimensional finite element analysis. He developed an effective meshing tool for three-dimensional model incorporating multiple layers, interlayer debonding and slip, and various loadings. The effect of base material nonlinearity was studied with the stress-dependent K-θ model and the effect of spatially varying tire/pavement contact pressures on pavement surface. He concluded that spatially varying tire/pavement pressures affected the response of flexible pavement significantly.

### 3.3.3 Characteristics of Finite Element Programs for Pavement Analysis

The finite element modeling approach offers the best method of analysis for multilayered pavement systems. Three-dimensional and two-dimensional or axisymmetric finite element models have different element formulation and consider different directional components of stresses and strains. Three-dimensional finite element analysis can consider all three directional response components and should predict more accurate pavement responses.

## 3.4 General-purpose Finite Element Programs for Pavements

ABAQUS™, ANSYS™, and ADINA™ are the general-purpose finite element programs that can provide proper analyses of various engineering problems. Although pavement structural modeling has developed dramatically in recent years, pavement analysis with general-purpose programs has not been applied to flexible pavement modeling frequently. As of now, only a few researchers have investigated the nonlinear pavement responses using the general-purpose finite element programs.

Zaghloul et al. (1993) simulated the pavement responses under falling weight deflectometer loading for flexible pavements using three-dimensional analysis in the ABAQUS™. A number of material models were used to represent actual material characteristics. Asphalt concrete layers were modeled as viscoelastic materials and granular materials, which can consist of base/subbase, were modeled using the Drucker-Prager model. The Cam-Clay model was used for subgrade soils. Both static and dynamic loading analyses were conducted to predict elastic and plastic pavement responses. This capability helped explain pavement response under various loading conditions and for different material characteristics. They found that their model was capable of simulating truckloads and realistic deformation predictions were obtained.

ABAQUS™ was used for the dynamic loading response analysis by Uddin et al. (1994). They investigated the effects of dynamic loading for a cracked pavement comparing responses with static loading for a linear elastic system and the usefulness of three-dimensional finite element simulation of the pavement. They found that the corresponding static deflection under the linear elastic solution remained higher than the dynamic deflections for a cracked pavement. They also properly simulated longitudinal and transverse cracks on surface by special gap elements in ABAQUS$^{TM}$ element set.

Chen et al. (1995) have made a comprehensive study of various finite element pavement analysis programs and showed that the results from ABAQUS$^{TM}$ were comparable to those from other programs. This study included two axisymmetric finite element programs (ILLI-PAVE and MICH-PAVE), two elastic multilayered programs (DAMA and KENLAYER), and one three-dimensional finite element program (ABAQUS$^{TM}$). Of those five finite element programs, MICH-PAVE in the linear analysis and DAMA in the nonlinear analysis gave the intermediate maximum surface deflection, compressive strain at the bottom of asphalt surface, and tensile strain on the top of subgrade. An attempt of ABAQUS$^{TM}$ finite element program was made from infinite elements in the vertical direction for a linear analysis. The results from ABAQUS yielded the lowest tensile strain compared with other programs in the linear case.

Kuo et al. (1995) developed three-dimensional finite element model for concrete pavements called 3DPAVE. 3DPAVE used the ABAQUS$^{TM}$ program to overcome many of the inherent limitations of two-dimensional finite element models. They performed the feasibility study to find the most appropriate element for two-dimensional and three-dimensional model. The three-dimensional ABAQUS$^{TM}$ finite element modeling was conducted in various loading cases such as interior loading and edge loading cases with C3D27R type ABAQUS$^{TM}$ elements. To investigate the effects of separation between layers, interface friction, bonding, interface behavior, dowel bars and aggregate interlock were also modeled by ABAQUS$^{TM}$ element/material keyword library. Dense liquid foundation and elastic solid foundation solutions were modeled by FOUNDATION and BRICK elements, respectively. Comparisons between three-dimensional finite element modeling and full scale field test data proved that 3DPAVE model properly solved for the pavement behavior.

Cho et al. (1996) studied pavement modeling using various elements in ABAQUS™. The pavement structure had an asphalt concrete overlay on a Portland cement concrete pavement. Three types of models, i.e., plane strain, axisymmetric, and three-dimensional, were evaluated to facilitate the selection of an appropriate modeling and corresponding element types for simulating traffic loading effects. The plane strain model failed to calculate the accurate deflections and stress distributions. One of the severe limitations used that the plane strain approach could not reproduce actual circular or elliptical wheel loadings. The axisymmetric model with infinite elements resulted in reasonable solutions for both linear and quadratic element types. The advantage of this model was that a three-dimensional structure could be solved with a two-dimensional formulation using cylindrical coordinates. It was little more computational intensive than plane strain formulations. Although the three-dimensional model yielded reasonable pavement responses when geometry and boundary conditions were well controlled, it required more computational time and memory than two-dimensional model. Finally, they proposed that axisymmetric and three-dimensional finite element models yielded suitable results for predicting pavement responses. But all finite element solutions were based on linear elastic analyses.

Hjelmstad et al. (1996) investigated the essential aspects of modeling pavement structures with three-dimensional finite element analyses such as mesh refinement, domain extent, computational memory, and element size transitions using ABAQUS™. Due to highly localized wheel loading, the stress gradients were greatest in the vicinity of the loading. Therefore, the mesh size had to be finest in that region. The element aspect ratio and smooth transitions from one element size to another affected the accuracy of the solution and it was essential to make smooth transition. Using good aspect ratios resulted in accurate results and reduction of computation time to solve large pavement problems was important to material nonlinearity and interface condition.

ABAQUS™ program allows use of built-in nonlinear constitutive material models and several researchers analyzed pavement responses combined with nonlinear material characterizations. Taciroglu (1998) simulated the pavement responses using three-dimensional finite element analysis and adopted the K-θ model and the Uzan model as the nonlinear unbound granular material model and linear subgrade soils model. He applied the general-purpose ABAQUS™ finite element program to nonlinear flexible pavement analysis with the help of a user defined material subroutine incorporating strain-dependent type modulus models in the unbound aggregate base. This research provided an analysis of the nonlinear solution algorithms that have been used in implementing these models in a conventional nonlinear three-dimensional finite element framework. It also presented the direct secant method to converge solutions smoothly. He modeled the nonlinear resilient behavior of granular materials well and predicted that the bending stress at the bottom of the asphalt layer was approximately 25% more than that of linear elastic model. The coupled hyperelastic model was also used in combination with the no-tension model, as the latter one is applicable to any hyperelastic constitutive model. In this research, the coupled model yielded better fits to the experimental data. But the nonlinear solutions in this case often predicted high asphalt bending stresses.

Kim (2000) found that nonlinearity of unbound layers using the Drucker-Prager plasticity model was not suitable to pavement analyses. Therefore, the Uzan model was adopted for granular materials and cohesive soils for the nonlinear analysis. Mohr-Coulomb failure criterion was employed in the nonlinear finite element analysis. According to this criterion, failure occurred when the load induced stresses exceeded the material strength, which was defined based on the maximum principal stress ratio for unbound granular materials and as the maximum shear stress for subgrade soil materials. This axisymmetric model did a reasonably good job of simulating pavement behavior and gave a less stiff pavement structure in case of using the infinite elements.

Uddin et al. (2000) also implemented a viscoelastic constitutive material routine into ABAQUS™ for stiff surface soil and unpaved gravel surface soil layers subjected to static and dynamic loadings. They described a user defined material subroutine which incorporated generalized Maxwell viscoelastic model and microcracking in the three-dimensional modeling. The base and other soil layers were modeled as linear elastic materials using the backcalculated modulus values. The results showed the time-dependent viscoelastic modeling contributed to better understanding of the pavement behavior.

The ABAQUS™ program was also used for pavement analysis by Schwartz (2002) who employed the K-θ model in the base course by using the hypoelastic material model inputs in the ABAQUS™ three-dimensional modeling framework. The secant resilient modulus values could not be directly used in nonlinear solutions but were numerically converted to tangent moduli for input as a function of the first stress invariant $I_1$. A tension cut-off was also imposed by specifying a very small modulus for tensile $I_1$ values. Comparing the two-dimensional and three-dimensional finite element solutions, Schwartz reported that there were up to 25% differences between the maximum asphalt tensile stresses and strains and only 5% differences of stresses and strains on the top of subgrade. He also noted that these differences would seem acceptable for the practical design.

Erlingsson (2002) conducted three-dimensional finite element analyses of a heavy vehicle simulator used to test low volume road structures. The finite element analysis was performed using the commercial finite element package (COSMOS™). A linear elastic material model was used and the single and dual wheel configurations were given. The used elements were 8-noded hexahedron solid elements and only half of the geometry was needed as the problem considered symmetry along the wheel path. The comparison of stresses under a wheel load showed relatively good correlations in the base and subgrade. However, in the base course, deviation occured between the numerical analysis and the measurements with the measurements increasing as tire pressures increased. This was probably due to the nonlinear behavior of the base which was not taken into account in the linear elastic analysis. Surface deflection measurements under the wheel load gave lower values than the numerical analyses which did not consider nonlinear behavior. Therefore, to be able to achieve a better comparison, nonlinear analysis had to be performed.

Nesnas et al. (2002) used the ABAQUS™ solver to study three-dimensional model for the prediction of surface crack opening due to temperature variations. The

Hypermesh$^{TM}$ was used by the pre/post processor with an interface for the ABAQUS$^{TM}$ solver to perform these analyses. A mechanistic thermal model for surface cracking based on a three-dimensional finite element uncoupled formulation was used to predict the crack opening due to temperature variations. All pavement layers were assumed to be elastic and the thickness of subgrade layer was infinite. Two experimental pavement sections were built as part of a validation of the mechanistic model. Overall the surface crack opening predictions gave a relatively good agreement with results of the experimental section. In order to obtain improved predictions of the surface cracking, the monitoring of crack openings and temperatures in the neighborhood of the crack would be required.

Sukumaran (2004) presented a three-dimensional analysis model of airport flexible pavements using ABAQUS$^{TM}$. The discussed issues were construction of mesh, mesh refinement, element aspect ratios and material nonlinearities. In nonlinear material analyses, granular materials used the Mohr-Coulomb failure criterion and medium strength subgrade and Dupont clay were modeled using the von-Mises failure criterion. The model was also compared with the available failure data from the National Airport Pavement Test Facility (NAPTF) of the Federal Aviation Administration (FAA).

Perkins et al. (2004) made a proper numerical implementation of the nonlinear elastic analysis with the tension cutoff model using the ABAQUS$^{TM}$ program. Three issues were verified by creating the following material response models for the base and subgrade layers: Isotropic linear elastic without tension cutoff and with and without overlay elements, isotropic linear elastic with tension cutoff, and isotropic nonlinear elastic with tension cutoff. Overlay elements placed on top of elements having tension cutoff material behavior were used to provide numerical stability. Three models were created that used isotropic linear elastic properties with tension cutoff for the base and subgrade layers. Generally, good agreement was shown between the ABAQUS$^{TM}$ numerical and theoretical solutions for a specific set of load steps.

Saad et al. (2005) examined the dynamic response of flexible pavement structures to single wheel traffic loads using ADINA$^{TM}$ three-dimensional model. The effects of elastoplasticity of the base material and strain hardening of the subgrade material on the dynamic response were investigated. As an implicit dynamic loading, triangular wave with a peak load was adopted to have load duration of 0.1-seconds. In the material data, asphalt concrete was considered linear elastic for simplicity. The base material was modeled elastic isotropic, elastic cross-anisotropic, and a Drucker-Prager type model as a strong or weak base and the subgrade was simulated by the modified CamClay model. A sensitivity analysis of the mechanical behavior of the pavement foundation was carried out to examine its dynamic response according to the study parameters: (1) base thickness, (2) base quality, (3) subgrade quality. Several conclusions were drawn from this study. The linear elastic cross-anisotropic base behavior resulted in 4.3% increase in the fatigue strain and 2.5% increase in the vertical surface deflection. Elastoplasticity of the base material caused an increase of 46% in the rutting strain, 28% in the maximum tensile fatigue strain at the bottom of the asphalt layer, and 30% in the maximum surface deflection. The subgrade elastoplasticity had little impact on the fatigue strain which was less than 1%.

### 3.5 Summary

This chapter presented a review of numerical models of flexible pavements and recent research studies dealing with finite element modeling of flexible pavements. The literature reviewed in this chapter showed the predicted pavement responses were affected by the material properties such as asphalt concrete, base, and subgrade layer characterizations. In these studies, geomaterials used in base and subgrade layers were treated as either elastic materials or elastoplastic materials. Even when the nonlinear elasticity was considered especially in the three-dimensional finite element studies, proper stress-dependent modulus characterizations were not properly employed.

In accordance with the mechanistic-empirical design methodology, pavement analysis relies primarily on material property inputs of the individual pavement layers to determine the state of stress and predict pavement performance. When these geomaterials are used as pavement layers, the layer stiffness, or resilient modulus becomes a function of applied stress state as proven in laboratory studies. Therefore, there is a need to develop a user defined material model subroutine for the general-purpose finite element program to make it suitable for nonlinear pavement analysis. The appropriate material characterization is an essential component of flexible pavement design using mechanistic concepts.

# Chapter 4 Finite Element Meshes and Domain Selection Analysis

## 4.1 Investigation of Finite Element Mesh with Regular Elements

The first step of any finite element simulation is to discretize the actual geometry of the structure using a collection of finite elements. Each finite element represents a discrete portion of the physical structure. The finite elements are joined by the shared nodes and the collection of nodes and finite elements is called the mesh. The most cases of solid modeling with finite elements use regular elements such as linear or quadratic elements. This chapter will describe finite element mesh and domain selection for analyzing flexible pavements.

### 4.1.1 Axisymmetric Model

For the elastic half-space subjected to a uniform circular load, determination of domain size is important in that the inappropriate treatment of infinity affects the accuracy of finite element results. The layers of a pavement structure extend to infinity in the horizontal and vertical directions. According to Duncan et al. (1968), to obtain a reasonable comparison of finite element analyses, it was necessary to move the fixed bottom boundary to a depth of 50-times the radius of loading area and move the vertical roller boundary at a horizontal distance of 12-times the radius of loading area from the center of loading.

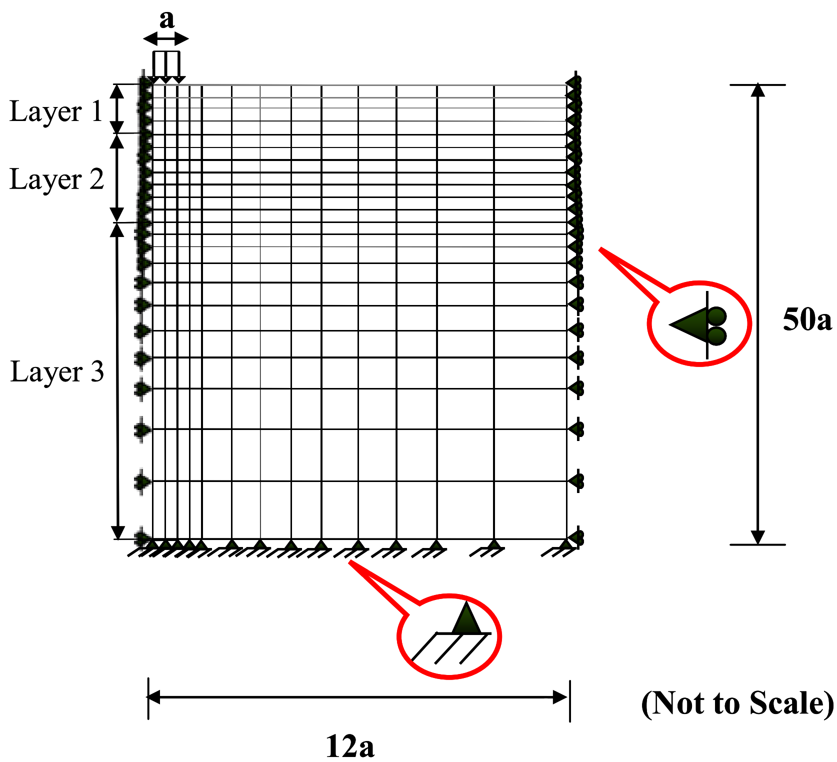


Figure 4-1 Finite Element Configuration used for Analysis by Duncan et al. (1968)

Analytically, we had two choices for infinite domain modeling in this section: (1) elastic layered program (closed-form solution), (2) modeling with finite elements truncated in far away from the area where the results are favorable with elastic layered program solutions. In this section, a proper model was investigated as the domain size was changed. At first, an investigated three-layered pavement section consisted of an axisymmetric finite element model with details shown in Table 4-1.

Table 4-1 Material Properties used in the Axisymmetric Finite Element Modeling

| Section | Element | Thickness (mm) | E (MPa) | ν | Material Properties |
|---|---|---|---|---|---|
| AC | 8-noded solid | 76 | 2,759 | 0.35 | Isotropic and Linear Elastic |
| Base | 8-noded solid | 305 | 207 | 0.40 | Isotropic and Linear Elastic |
| Subgrade | 8-noded solid | 20,955 | 41 | 0.45 | Isotropic and Linear Elastic |

The load was applied as a uniform pressure of 0.55-MPa over a circular area of 152.4-mm radius. The linear elastic solution was then obtained using both ABAQUS™ finite element program and KENLAYER (Huang, 1993) program, which is a closed form integral solution. Boundary truncation of finite element mesh was examined with two different common boundary conditions, namely the roller and fixed conditions. The bottom parts of the pavement section used fixed boundary conditions and the others used roller boundary conditions. After completing these analyses, it was found that the influence of boundary truncation was negligible for domains larger than 20-times the radius of loading area in the horizontal direction. All domain extents in the vertical direction were found to be 140-times the radius of loading area. The critical responses of pavement sections resulting from ABAQUS™ in the domain extent of 20-times the radius in the horizontal and 140-times the radius in the vertical with regular elements were identical to the results obtained from the KENLAYER program listed in Table 4-2. However, there may not be a need to go down to 140-times the radius in the vertical direction especially when the surface deflection is not evaluated as a critical pavement response. The negative sign (-) indicates compression in the tables.

Table 4-2 Predicted Critical Pavement Responses from the Domain Extent Study with 20R in the Horizontal and 140R in the Vertical Direction

| | Linear Elastic Axisymmetric Analysis | |
|---|---|---|
| Pavement response | KENLAYER | ABAQUS with regular elements |
| $\delta_{\text{surface}}$ (mm) | -0.927 | -0.930 |
| $\sigma_{\text{r bottom of AC}}$ (MPa) | 0.777 | 0.773 |
| $\sigma_{\text{v top of subgrade}}$ (MPa) | -0.041 | -0.041 |
| $\varepsilon_{\text{v top of subgrade}}$ ($\mu\varepsilon$) | -936 | -933 |

To investigate the domain extents, several different finite boundary truncations were also examined for artificial boundary conditions with regular finite element meshes. The examined domain sizes were varied from 10- to 35-times the radius of loading area in the horizontal direction. The depth was fixed at 140-times the radius of loading area which showed good agreements. All analyses were conducted using the various material properties and pavement geometries shown in Table 4-3.

Table 4-3 Inputs of Examined Pavement Sections using Axisymmetric Analyses

| | Pavement Case 1 | | Pavement Case 2 | | Pavement Case 3 | |
|---|---|---|---|---|---|---|
| Sections | Thickness (mm) | Modulus (MPa) | Thickness (mm) | Modulus (MPa) | Thickness (mm) | Modulus (MPa) |
| AC | 76 | 2,759 | 102 | 2,069 | 76 | 2,759 |
| Base | 305 | 207 | 254 | 124 | 457 | 207 |
| Subgrade | 20,955 | 41 | 20,980 | 28 | 20,803 | 41 |

The complete analysis results show differences in the predicted pavement responses and these can be seen in Table 4-4 where 'R' stands for radius of uniform circular tire pressure. Figure 4-2 shows the surface displacements to decrease as the domain extent increases. For the these pavement case studies, domain extent of 20-times the radius of loading area in the horizontal direction and 140-times the radius of loading area in the vertical direction with regular elements compared the most favorable with the elastic layered solutions. These results also showed that the influence of boundary truncation was negligible for domains larger than finite element mesh domain of 140-times the radius of loading area in the vertical direction and 20-times the radius of loading area in the horizontal direction. Since the variation of surface deflection was less than 0.025mm (1mil) with this domain, the difference was considered negligible.

Table 4-4 Predicted Critical Pavement Responses from Different Domain Extent Studies

| | Pavement Case 1 | | | | |
|---|---|---|---|---|---|
| Pavement response | KENLAYER | 15R X 140R* | 20R X 140R | 25R X 140R | 30R X 140R |
| $\delta_{\text{surface}}$ (mm) | -0.927 | -1.02 | -0.930 | -0.897 | -0.884 |
| $\sigma_{\text{r bottom of AC}}$ (MPa) | 0.777 | 0.775 | 0.773 | 0.772 | 0.7720 |
| $\sigma_{\text{v top of subgrade}}$ (MPa) | -0.040 | -0.041 | -0.040 | -0.040 | -0.040 |
| $\varepsilon_{\text{v top of subgrade}}$ ($\mu\varepsilon$) | -936 | -927 | -932 | -933 | -933 |
| | Pavement Case 2 | | | | |
| $\delta_{\text{surface}}$ (mm) | -1.24 | -1.38 | -1.25 | -1.20 | -1.18 |
| $\sigma_{\text{r bottom of AC}}$ (MPa) | 0.903 | 0.903 | 0.900 | 0.899 | 0.898 |
| $\sigma_{\text{v top of subgrade}}$ (MPa) | -0.025 | -0.025 | -0.025 | -0.025 | -0.025 |
| $\varepsilon_{\text{v top of subgrade}}$ ($\mu\varepsilon$) | -879 | -858 | -871 | -874 | -874 |
| | Pavement Case 3 | | | | |
| $\delta_{\text{surface}}$ (mm) | -0.803 | -0.899 | -0.808 | -0.775 | -0.762 |
| $\sigma_{\text{r bottom of AC}}$ (MPa) | 0.737 | 0.739 | 0.734 | 0.733 | 0.732 |
| $\sigma_{\text{v top of subgrade}}$ (MPa) | -0.024 | -0.024 | -0.024 | -0.024 | -0.024 |
| $\varepsilon_{\text{v top of subgrade}}$ ($\mu\varepsilon$) | -565 | -551 | -559 | -562 | -562 |

*: 15R X 140R means the horizontal direction X the vertical direction.

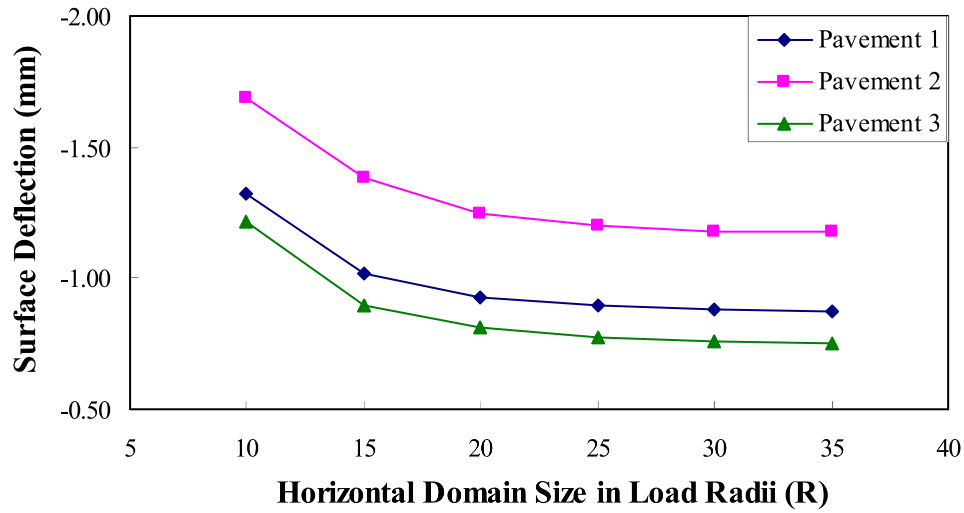


Figure 4-2 Variations of Predicted Surface Deflections with Horizontal Domain Size

### 4.1.2 Three-dimensional Model

The introduction of robust finite element modeling provided a new solution technique for three-dimensional structural analysis and design problems. The finite element modeling was initially formulated based on linear elasticity assumed in the structural elements. More recently, it has found wide applications to consider various nonlinear constitutive models and continuum solid elements. While the proposed two-dimensional or axisymmetric model has been adequate for the study of nonlinear analysis, a three-dimensional finite element model is believed to solve for more accurate pavement responses. Axisymmetric stress analysis was known to be limited in its capacity especially for modeling different geometries, such as for a pavement with a geosynthetic layer having anisotropic properties on the horizontal plane and loading conditions, and multiple wheel/gear loading cases, which do not fit with the assumptions of axial symmetry. Three-dimensional finite element analysis has been viewed as the best approach to eliminate such limitations and shortcomings with the consideration all three-directional components, i.e., x, y, and z-directions. However, the accuracy of three-dimensional finite element analysis is dependent on the mesh refinement and mesh construction dealing with certain element aspect ratios. Smooth transitioning of elements is also an important factor. Particularly, the mesh generation of three-dimensional finite element pavement models has some difficulties because the applied wheel load is localized and each layer is relatively thin compared with the infinite horizontal domain. Therefore, neatly and well constructed meshes are necessary for proper three-dimensional finite element pavement analyses.

The setups of the domain size of pavement structure and traffic load simulation are the most important factors along with mesh refinement as a first step. A fine mesh is required in the vicinity of wheel loads to capture the steep stress and strain gradients. Smaller elements can prevent the discrepancy of stress and strain distribution at the sampling points of each element and the use of more sampling points help to represent much smoother variation or approximation of the geometry.

#### 4.1.2.1 The Geometry and the Loading

The study from axisymmetric modeling showed that the domain which has 20-times the load radius in the horizontal direction and 140-times the load radius in the vertical direction had a reasonable agreement with the closed form linear elastic solutions. Based on this finding, three-dimensional finite element models were constructed as shown in Figure 4-3 to 4-5. A constructed three-dimensional finite element mesh consisted of 15,168 20-noded hexahedron elements and 67,265 nodes. Owing to the symmetry of the model and applied load, the pavement geometry was considered only quarter part.

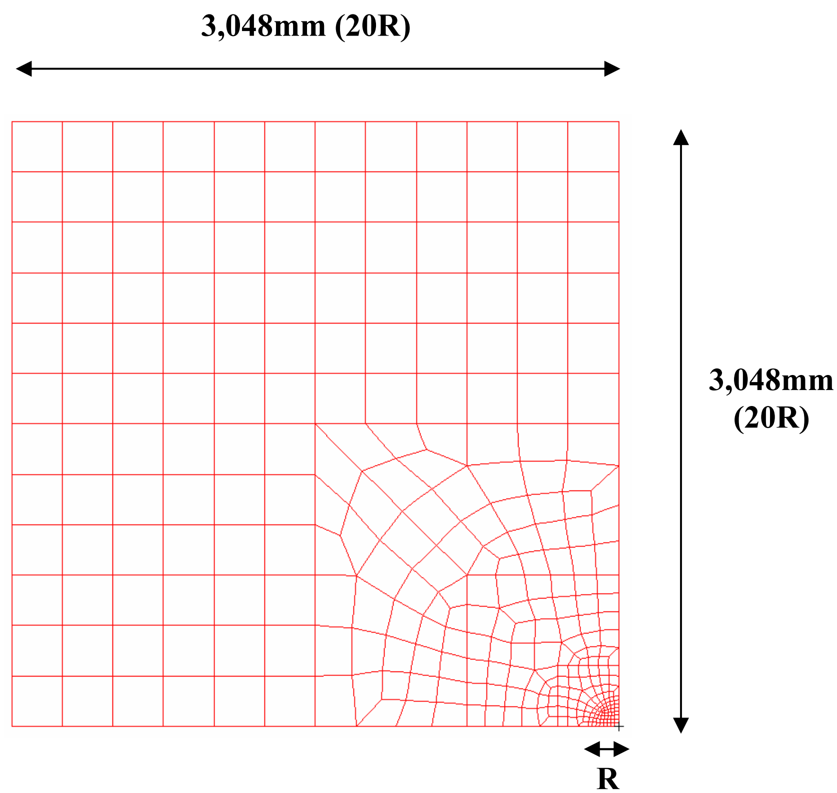


Figure 4-3 Radially Graded Transition Mesh

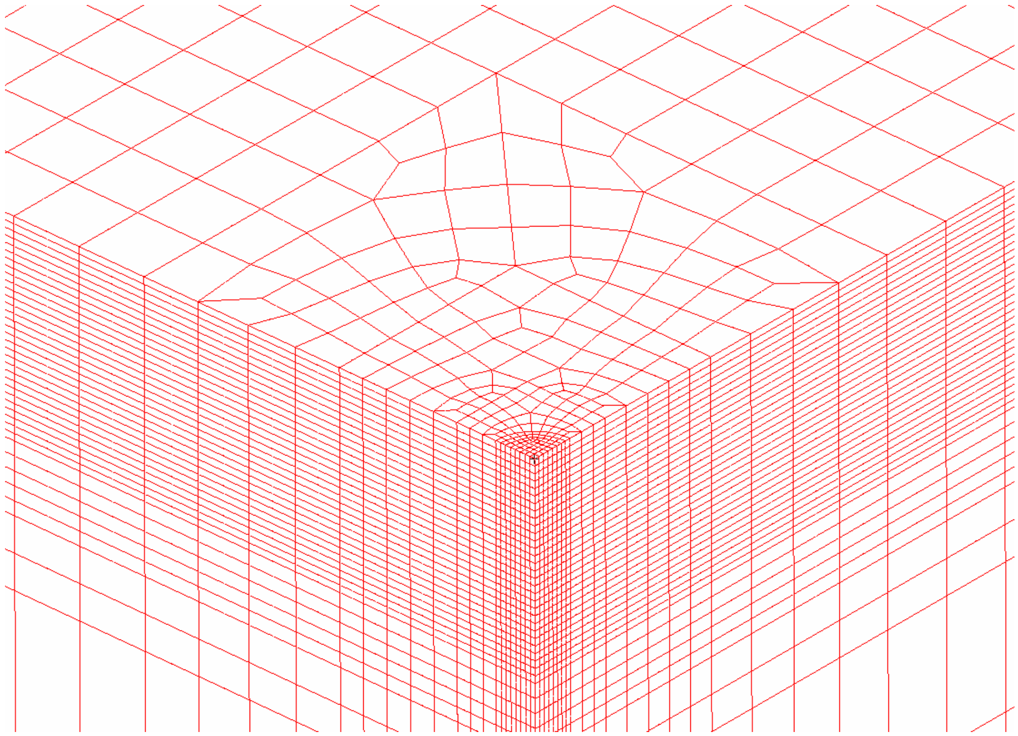

Figure 4-4 Loading Area in Three-dimensional Finite Element Mesh

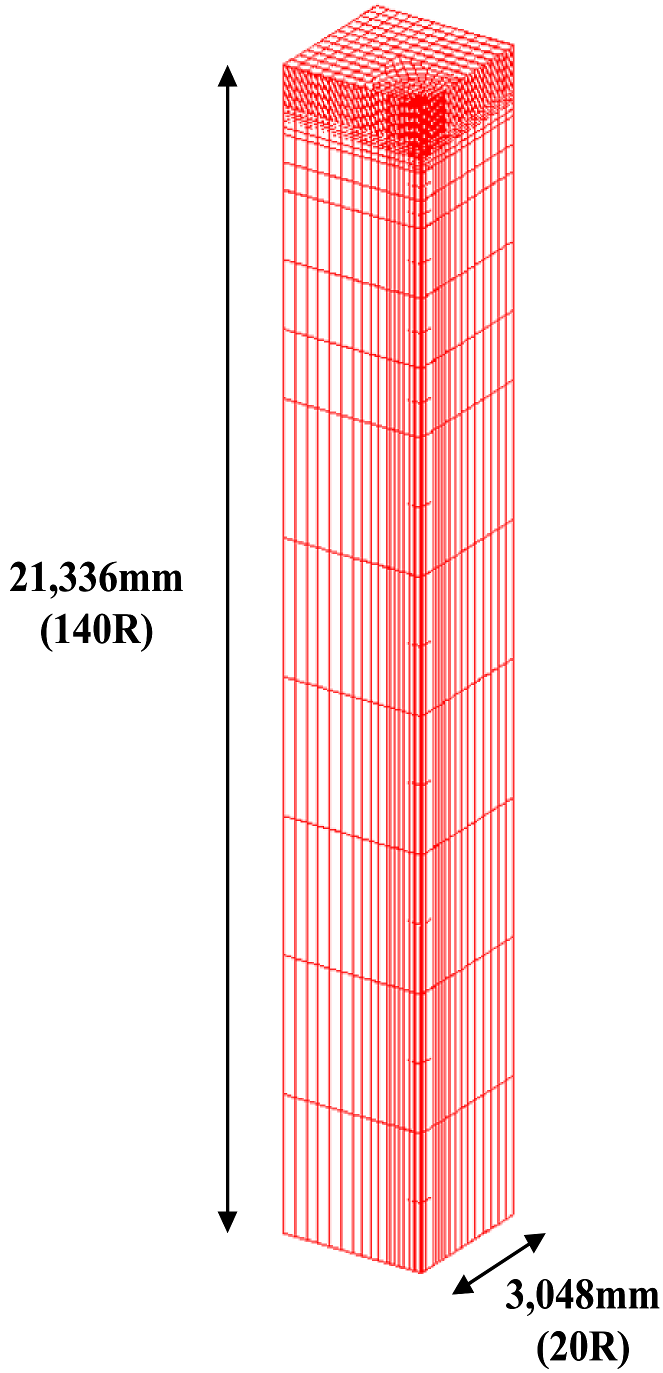


Figure 4-5 Generated Three-dimensional Finite Element Mesh

The linear elastic solutions were compared from the ABAQUS™ axisymmetric and three-dimensional models to evaluate differences between the two pavement models.

Figure 4-6 and Table 4-5 show the constructed finite element models and analysis inputs for comparison, respectively. Note that the three-dimensional model only considers one fourth of the problem to be solved due to symmetry. The wheel load, approximated as a uniform pressure of 0.55-MPa over a 152.4-mm radius of circular area, was applied over one quarter of the circular area with a fine mesh shown in the three-dimensional model.

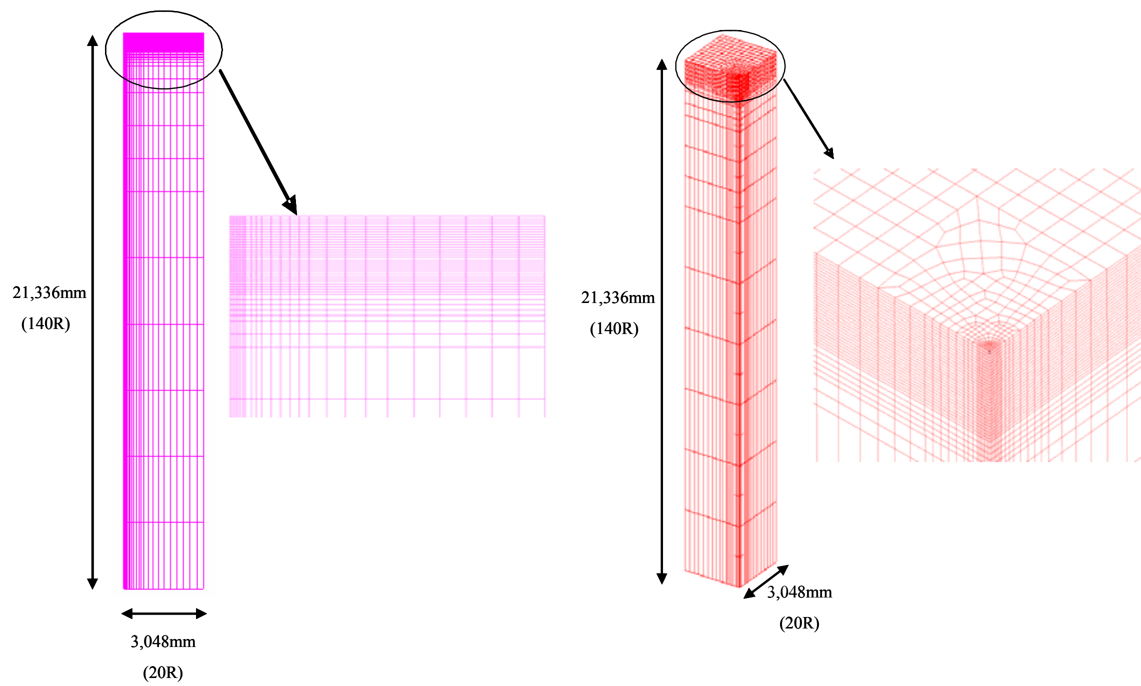


(a) Axisymmetric model (b) Three-dimensional model

Figure 4-6 Axisymmetric and Three-dimensional Finite Element Models

Table 4-5 Material Properties used in the Three-dimensional Finite Element Modeling

| Section | Element | Thickness (mm) | E (MPa) | $\nu$ | Material Properties |
|---|---|---|---|---|---|
| AC | 20-noded solid | 76 | 2,759 | 0.35 | Isotropic and Linear Elastic |
| Base | 20-noded solid | 305 | 207 | 0.40 | Isotropic and Linear Elastic |
| Subgrade | 20-noded solid | 20,955 | 41 | 0.45 | Isotropic and Linear Elastic |

As shown in Table 4-6, results of axisymmetric and three-dimensional analyses are not much different from each other. The biggest difference in pavement responses is that of the surface deflections, but still not more than 3%. The other responses, such as tensile stresses at the bottom of asphalt concrete and vertical stresses on the top of subgrade, have differences less than 1%. At this point, the issue in developing three-dimensional model is how three-dimensional results compare with axisymmetric results. They are not expected to match in all cases because some responses of the pavement structure are neglected in the axisymmetric model formulation. A very good agreement of the axisymmetric and three-dimensional models can only be expected when the restrictions of the axisymmetric model are released. Nevertheless, the closely matching results indicate that mesh construction related modeling approximations were minimized the differences between the axisymmetric and three-dimensional analyses to enable reliable comparisons.

Table 4-6 Predicted Critical Pavement Responses from Axisymmetric and Three-dimensional Linear Elastic Analyses

| | ABAQUS Linear Elastic Analysis | |
|---|---|---|
| Pavement response | Axisymmetric | Three-dimensional |
| $\delta_{\text{surface}}$ (mm) | -0.930 | -0.909 |
| $\sigma_{\text{r bottom of AC}}$ (MPa) | 0.773 | 0.770 |
| $\sigma_{\text{v top of subgrade}}$ (MPa) | -0.041 | -0.040 |
| $\varepsilon_{\text{v top of subgrade}}$ ($\mu\varepsilon$) | -933 | -930 |
| Number of nodes | 3,893 | 67,265 |
| Number of elements | 1,248 | 15,168 |

## 4.2 Investigation of Finite Element Mesh with Infinite Elements

Infinite elements provide a good treatment for solving infinite domain problems because they can represent infinity without any restrictions. Bettess (1977) and Ungless (1977) developed infinite elements and successfully applied to soil interaction and foundation problems. Infinite elements are used in boundary value problems defined in unbounded domains or problems where the region of interest is small compared to the overall structure. Infinite elements are designed to model the far field and should be placed far enough away from the area of where deformation takes place. They do not capture deformation, particularly shear deformation, very well. So, it is not easy to use nonlinear material behavior such as plasticity or creep. These elements can have only linear behavior and provide stiffness in the static analyses. Because the decay of stresses and strains is relatively insensitive to local effects associated with load transfer under the wheel loads in the far field, it is favorable to use infinite elements in these regions. The behavior of infinite element is the same as that of the regular finite element in terms of formulating the element stiffness matrix, parametric mapping, and connection with regular finite elements. Above all, the best advantage of using infinite elements is the ability to replace a high number of regular finite elements with the compatible results. The infinite elements also do not need specific boundary conditions.

The node numbering and positioning for infinite elements are important to represent accurate solutions. Their nodes should be located away from the adjacent finite element mesh. The node numbering for infinite elements must be defined such that the first face of infinite elements is connected to regular finite element mesh. The basis of the formulation of these elements is that the far-field solution along each element edge that stretches to infinite is centered about an origin. It is called pole and can be the center of loading. The second node along the infinite direction must be positioned such that it is twice as far from the pole as the node on the same edge at the boundary between the finite and infinite elements. In addition to this consideration, the second node must be located in the infinite direction such that the element edges in the infinite direction do not cross over (see Figure 4-7)

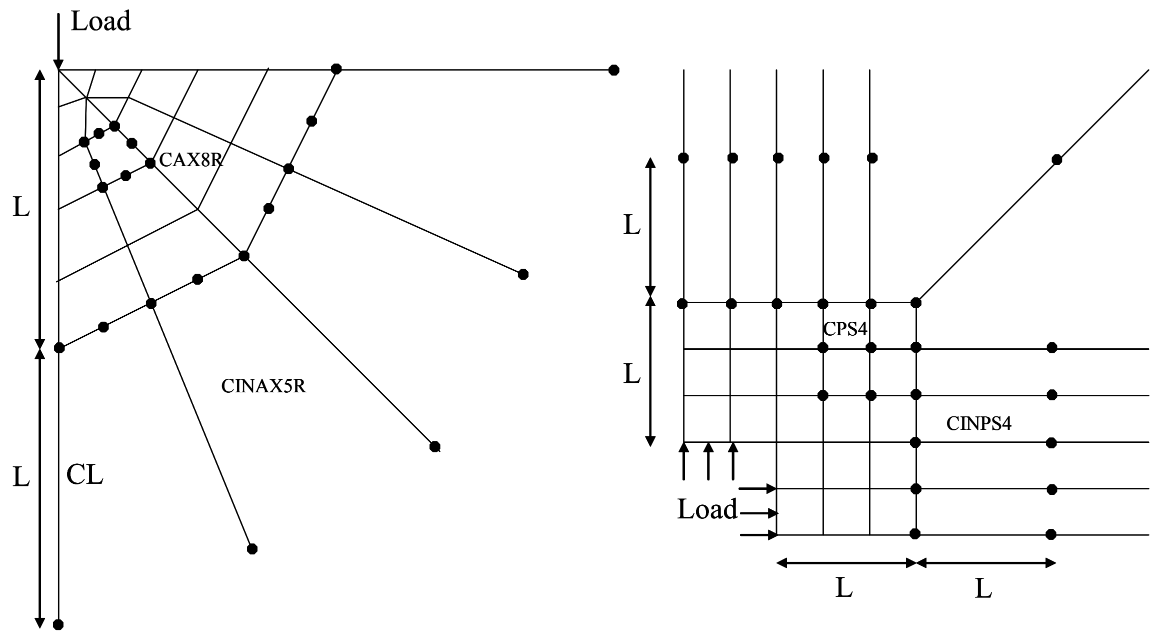


(a) Axisymmetric Element (b) Plane Stress Element

Figure 4-7 Examples of Two-dimensional Infinite Elements (Hibbit et al, 2005)

### 4.2.1 Formulation of Infinite Elements

The static behavior of the infinite elements is based on modeling the basic solution variable u, which is a displacement component with respect to spatial distance x measured from pole of the solution, so that $u \rightarrow 0$ as $x \rightarrow \infty$, and $u \rightarrow \infty$ as $x \rightarrow 0$. The formulation of three-noded one-dimensional infinite element is shown in Figure 4-8. As shown in Figure 4-8, the distance $x = a$ at node 1 is the parametric coordinate $\xi = -1$ in the parent element, $x = 2a$ at node 2 is $\xi = 0$, $x = \infty$ at node 3 of infinity is $\xi = 1$. We can obtain two-dimensional and three-dimensional models of domains that reach to infinity by combining this interpolation in the $\xi$-direction in a product form with standard linear or quadratic interpolation in orthogonal directions of the mapped space (Hibbit et al, 2005).

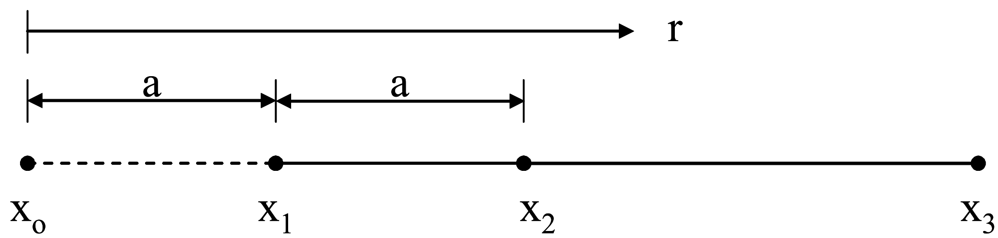


(a) Mapped Elements

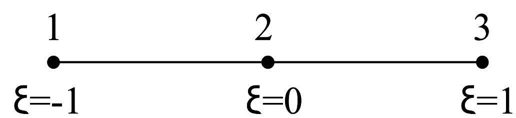


(b) Parent Elements

Figure 4-8 Mapping of One-dimensional Infinite Elements

The x(ξ) which is coordinate mapping between parametric coordinate and the physical coordinate is obtained as

$$x(\xi) = -\frac{2\xi}{1-\xi}x_1 + \frac{1+\xi}{1-\xi}x_2 \tag{4-1}$$

where $x_1$, $x_2$, and $\xi$ are shown in Figure 4-8. The terms of $-\frac{2\xi}{1-\xi}$ and $\frac{1+\xi}{1-\xi}$ are shape functions for coordinate. The inverse mapping of Equation 4-1 is chosen by solving for ξ in terms of x.

$$\xi = \frac{x - x_2}{x - 2x_1 + x_2} \tag{4-2}$$

If node 2 is twice as node 1, Equation 4-2 can be

$$\xi = 1 - \frac{2x_1}{x} \tag{4-3}$$

Thus, the displacement field, u, is given by the following expression.

$$u(\xi) = \frac{1}{2}\,\xi\,(\xi - 1)\,u_1 + (1 - \xi^2)\,u_2 \tag{4-4}$$

where $u_1$ and $u_2$ are the displacements at nodes 1 and 2, respectively.

### 4.2.2 Axisymmetric Model

Although using infinite elements can eliminate the use of many regular elements in infinite domain, one still needs to know where infinite elements should start. Thus, an investigation of different domain extents was needed and results from elastic layered program had to be evaluated.

The depth of examined pavement section was fixed to 60-times the radius of loading area due to accurate subgrade responses and the investigated length of horizontal direction was varied from 9 to 20-times the loading radius. The starting locations of infinite elements were the same with this depth and length of examined section. This investigation was conducted by using material properties and pavement geometry given in Table 4-7. The load was applied as a uniform pressure of 0.55-MPa over a circular area of 152.4-mm radius.

Table 4-7 Material Properties, Pavement Geometry, and Element Types used in the Infinite Element Axisymmetric Analyses

| Section | Regular Element | Infinite Element | Thickness (mm) | E (MPa) | $\nu$ | Material Properties |
|---|---|---|---|---|---|---|
| AC | 8-noded solid | 5-noded solid | 76 | 2759 | 0.35 | Isotropic and Linear Elastic |
| Base | 8-noded solid | 5-noded solid | 305 | 207 | 0.40 | Isotropic and Linear Elastic |
| Subgrade | 8-noded solid | 5-noded solid | 20,955 | 41 | 0.45 | Isotropic and Linear Elastic |

As shown in Table 4-8, to achieve the similar level of accuracy in the axisymmetric finite element results, the domain extent needs to be approximately 10-times the radius of loading area in the horizontal direction when the infinite elements are included. If the same level of accuracy is needed without infinite elements, the domain should be much larger than that with infinite elements. The reduction in total nodes and elements achieved by using infinite elements results in reduced memory and running time for analysis. From these examples, regular elements can show more accurate results than infinite elements and one might conclude that constructed domain with regular elements can provide more accurate results in the future three-dimensional finite element analysis. In addition, the starting locations of infinite elements are very important to obtain accurate solutions in finite element analyses (see Table 4-8). The larger domain does not always guarantee better matching results with KENLAYER elastic layered program solutions.

Table 4-8 Predicted Critical Pavement Responses with Infinite Elements compared to KENLAYER Solutions

| Pavement response | KENLAYER | ABAQUS – Infinite Elements | | | |
|---|---|---|---|---|---|
| | | 54 X 360 (9R X 60R) | 60 X 360 (10R X 60R) | 90 X 360 (15R X 60R) | 120 X 360 (20R X 60R) |
| $\delta_{surface}$ (mm) | -0.927 | -0.922 | -0.935 | -0.965 | -0.975 |
| $\sigma_{r\ bottom\ of\ AC}$ (MPa) | 0.777 | 0.770 | 0.770 | 0.769 | 0.770 |
| $\sigma_{v\ top\ of\ subgrade}$ (MPa) | -0.040 | -0.040 | -0.040 | -0.040 | -0.040 |
| $\varepsilon_{v\ top\ of\ subgrade}$ ($\mu\varepsilon$) | -936 | -931 | -932 | -934 | -934 |

The cases of infinite elements used only in the horizontal direction or vertical direction were also examined. The region in which infinite elements were not used was large enough to represent accurate pavement responses. As shown in Table 4-9 and Table 4-10, although each case shows identical results obtained by the KENLAYER elastic layered program, they do not present much advantage to reduce number of nodes and elements.

Table 4-9 Predicted Pavement Responses with Infinite Elements used in the Horizontal Direction

| Pavement response | KENLAYER | ABAQUS – Horizontal Infinite Elements | | | |
|---|---|---|---|---|---|
| | | 60 X 330 (10R X 55R) | 60 X 360 (10R X 60R) | 120 X 360 (20R X 60R) | 150 X 360 (25R X 60R) |
| $\delta_{\text{surface}}$ (mm) | -0.927 | -0.927 | -0.919 | -0.904 | -0.892 |
| $\sigma_{r\ \text{bottom of AC}}$ (MPa) | 0.777 | 0.771 | 0.771 | 0.774 | 0.774 |
| $\sigma_{v\ \text{top of subgrade}}$ (MPa) | -0.040 | -0.040 | -0.040 | -0.040 | -0.040 |
| $\varepsilon_{v\ \text{top of subgrade}}$ (με) | -936 | -932 | -933 | -935 | -935 |

Table 4-10 Predicted Pavement Responses with Infinite Elements used in the Vertical Direction

| Pavement response | KENLAYER | ABAQUS – Vertical Infinite Elements | | | |
|---|---|---|---|---|---|
| | | 360 X 120 (60R X 20R) | 420 X 120 (70R X 20R) | 450 X 120 (75R X 20R) | 480 X 120 (80R X 20R) |
| $\delta_{\text{surface}}$ (mm) | -0.927 | -0.978 | -0.940 | -0.925 | -0.914 |
| $\sigma_{r\ \text{bottom of AC}}$ (MPa) | 0.777 | 0.773 | 0.774 | 0.774 | 0.775 |
| $\sigma_{v\ \text{top of subgrade}}$ (MPa) | -0.040 | -0.040 | -0.040 | -0.040 | -0.040 |
| $\varepsilon_{v\ \text{top of subgrade}}$ (με) | -936 | -932 | -932 | -932 | -932 |

To have consistent finite element models, the domain extents with the same horizontal and vertical distances were preferred in pavement analyses. The results of these analyses were close to the results of KENLAYER solutions. Table 4-11 also shows the results from the square mesh pavement geometry using the same horizontal and vertical analysis extents.

Table 4-11 Predicted Pavement Responses with Infinite Elements from Square Pavement Geometry

| Pavement response | KENLAYER | ABAQUS | | | |
|---|---|---|---|---|---|
| | | 120 X 120 (20R X 20R) | 180 X 180 (30R X 30R) | 240 X 240 (40R X 40R) | 360 X 360 (60R X 60R) |
| $\delta_{\text{surface}}$ (mm) | -0.927 | -0.914 | -0.917 | -0.912 | -0.899 |
| $\sigma_{r\text{ bottom of AC}}$ (MPa) | 0.777 | 0.773 | 0.774 | 0.774 | 0.775 |
| $\sigma_{v\text{ top of subgrade}}$ (MPa) | -0.040 | -0.040 | -0.040 | -0.040 | -0.040 |
| $\varepsilon_{v\text{ top of subgrade}}$ ($\mu\varepsilon$) | -936 | -934 | -934 | -933 | -932 |

### 4.2.3 Three-dimensional Model

The study of the axisymmetric modeling case showed that the domain which had 10-times the load radius in the horizontal direction and 60-times the load radius in the vertical direction had reasonably close results. Based on this finding, three-dimensional modeling was conducted. The pavement section investigated consisted of three layers with the geometries and material properties listed in Table 4-12.

Table 4-12 Pavement Geometry and Material Properties used in the Three-dimensional Finite Element Modeling

| Sections | Regular Element | Infinite Element | Thickness (mm) | E (MPa) | $\nu$ | Material Properties |
|---|---|---|---|---|---|---|
| AC | 20-noded solid | 12-noded solid | 76 | 2,759 | 0.35 | Isotropic and Linear Elastic |
| Base | 20-noded solid | 12-noded solid | 305 | 207 | 0.40 | Isotropic and Linear Elastic |
| Subgrade | 20-noded solid | 12-noded solid | 20,955 | 41 | 0.45 | Isotropic and Linear Elastic |

As shown in Table 4-13, results of the axisymmetric and the three-dimensional analyses are different from each other. All these differences between the axisymmetric and the three-dimensional model were, however, rather small and almost negligible.

Table 4-13 Comparisons of Predicted Pavement Responses with Infinite Elements from Axisymmetric and Three-dimensional Finite Element Models

| Pavement response | ABAQUS - Infinite Element | |
|---|---|---|
| | Axisymmetric | Three-dimensional |
| $\delta_{\text{surface}}$ (mm) | -0.902 | -0.922 |
| $\sigma_{r\text{ bottom of AC}}$ (MPa) | 0.771 | 0.772 |
| $\sigma_{v\text{ top of subgrade}}$ (MPa) | -0.040 | -0.040 |
| $\varepsilon_{v\text{ top of subgrade}}$ ($\mu\varepsilon$) | -936 | -932 |

From the investigation of infinite element modeling, several conclusions were drawn. In both the axisymmetric and the three-dimensional modeling, it was advantageous to reduce number of nodes and elements. However, it was difficult to perform nonlinear analysis using infinite elements and establish the positioning of infinite elements. Accordingly, a domain size of 20-times the radius of loading area in the horizontal direction and 140-times the radius of loading area in the vertical direction with regular elements was adopted in this study as the standard mesh size to investigate the study objectives.

## 4.3 Summary

In this chapter, an appropriate finite element mesh domain size was examined and proposed for studying the objectives. The axisymmetric finite element analysis domain of 140-times the radius of loading area in the vertical direction and 20-times the radius of loading area in the horizontal direction with regular finite elements was found to give accurate results when compared to the results of the elastic layered program, KENLAYER. To determine characteristics of finite element mesh domain size, several different finite element analyses were also performed with regular elements having artificial truncation boundaries. From the surface displacement investigation, the influence of boundary truncation was negligible for domains larger than a finite element domain of 140-times the radius of loading area in the vertical direction and 20-times the radius of loading area in the horizontal direction.

To reduce total number of nodes and elements, which affect computational time and storage, the use of infinite elements was also investigated. Although finite element models using infinite elements showed close results with those of KENLAYER, the accuracy and the consistency of the solutions were not as good as when regular solid elements were used. Thus, the finite element model having a domain size of 140-times the radius of loading area in the vertical direction and 20-times the radius of loading area in the horizontal direction with regular elements was selected for the standard analyses in this study.

# Chapter 5 Development of A Finite Element Analysis Approach for Pavement Foundation Material Nonlinearity

As mentioned in Chapter 2, both the two-dimensional and three-dimensional finite element models have been employed to analyze the structural response of flexible pavements. Although many researchers have investigated the response of flexible pavements through two-dimensional finite element programs, two-dimensional analysis is limited in its capacity and may not capture accurately the measured pavement responses. Three-dimensional finite element analysis has been increasingly viewed as the best approach to capture realistic behavior of pavement multi layered structure because it eliminates many shortcomings of the existing two-dimensional models. However, it is time consuming for mesh construction, computation time, and memory requirement.

ABAQUS$^{TM}$ is the most widely used general-purpose program to solve engineering problems based upon the finite element method applicable to linear and nonlinear solutions (Hibbit et al, 2005). Designed as a general-purpose simulation tool, ABAQUS$^{TM}$ can be used to study even more complicated problems that need various modeling skills. For example, problems with multiple components can be modeled by associating the specific option blocks defining each component with the appropriate material models. However, some limitations still exist in representing various types of complex material behavior which is not defined. For this reason, ABAQUS$^{TM}$ offers an interface to implement any specific material model with a user material subroutine (UMAT).

## 5.1 ABAQUS$^{TM}$ Nonlinear Finite Element Program

Linear analysis is a simple approximation for design and analysis purpose. It is obviously inadequate to make realistic structural simulations. Since the stiffness is changed with stress states in pavement foundation structures, linear approximation is a major problem when solving for the actual flexible pavement structural behavior. In a nonlinear analysis, the stiffness matrix of the structure has to be assembled and inverted many times during the analysis, making it much more expensive to solve than a linear analysis. It is not possible to create solutions using superposition, since the response of a nonlinear system depends on an incremental loading scheme.

There are three types of nonlinearities in structural mechanics simulations: (1) material nonlinearity, (2) boundary nonlinearity, and (3) geometric nonlinearity. Material nonlinearity is the most familiar nonlinear characterization. Many engineering materials have a fairly linear stress-strain relationship at low stain values, but the response becomes nonlinear and irreversible beyond higher stresses and strains that material yields. Material nonlinearity can be affected by various factors than strain. Boundary nonlinearity appears when the boundary conditions change during the analysis. Boundary nonlinearities are extremely discontinuous and large changes occur in the response of the structure. Geometric nonlinearity occurs whenever the magnitude of the displacements affects the response of the structure. Geometric nonlinearity may be due to large deflections, snap through, or initial stresses.

### 5.1.1 The Governing Equation and Finite Element Implementation

The objective of a finite element analysis is to predict the displacements, stresses, and strains of a body subjected to arbitrary loadings. The solution from finite element analysis requires the equilibrium and compatibility at every point in the body and the deformation and stress fields should be connected through material constitutive model. The material constitutive model represents an attempt to describe the material behavior in relation to a computationally tractable form. Rather than solving the exact governing equation, the finite element method uses an assemblage of independent and local approximation to the stress and displacement fields. As finite element uses the interpolations as shape functions, the deformation field within an element is described in terms of the displacements of the nodal points and the stress fields are represented as forces on the nodes. Therefore, the continuum solid is represented in terms of a discrete number of nodal degrees of freedom and the governing equation can be solved either implicitly or explicitly. Especially, the implicit Lagrangian finite element program used here, i.e. ABAQUS™/Standard, embeds equilibrium states using the principle of virtual work as the weak form of the momentum equation.

In the following sections, a brief review of ABAQUS™/Standard theories related to this analysis is presented. Let V denote a volume occupied by a part of the body in the current configuration, and S be the boundary of the current material volume. Let the surface traction at any point be **t**, which is force per unit of current area, and let the body force at any point within the volume of material under consideration be **b**. Thus force equilibrium for the volume is

$$\int_S \mathbf{t}\ dS + \int_V \mathbf{b}\ dV = 0 \tag{5-1}$$

The Cauchy stress, **σ**, at a point of S is defined by

$$t = n \cdot \sigma \tag{5-2}$$

where **n** is the unit outward normal to S at the point. Using this definition, the Equation 5-1 becomes

$$\int_S \mathbf{n} \cdot \boldsymbol{\sigma}\ dS + \int_V \mathbf{b}\ dV = 0 \tag{5-3}$$

Applying the Gauss theorem to the surface integral in the equilibrium equation gives

$$\int_S n \cdot \sigma\ \ dS = \int_V \left( \frac{\partial}{\partial x} \right) \cdot \sigma\ dV \tag{5-4}$$

where **x** is the spatial position of a material particle. Because the volume is arbitrary, this equation has to apply pointwise in the body. Thus, the differential equation of translational equilibrium is as follows:

$$\frac{\partial}{\partial x} \cdot \sigma + b = 0 \tag{5-5}$$

Here the test function can be imagined to be a virtual velocity field ($\delta v$) which is completely arbitrary except that it must obey any prescribed kinematic constraints and have sufficient continuity. The virtual work rate is

$$\int_V \left( \frac{\partial}{\partial x} \cdot \sigma + b \right) \cdot \delta v \, dV = 0 \tag{5-6}$$

$$\int_V \left( \frac{\partial}{\partial x} \cdot \sigma \right) \cdot \delta v \, dV = \int_V \left[ \left( \frac{\partial}{\partial x} \right) \cdot (\sigma \cdot \delta v) - \sigma \cdot \left( \frac{\partial \delta v}{\partial x} \right) \right] dV \tag{5-7}$$

$$\int_V \left( \frac{\partial}{\partial x} \cdot \sigma \right) \cdot \delta v \, dV = \int_S n \cdot \sigma \ \delta v \, dS - \int_V \left[ \sigma \cdot \left( \frac{\partial \delta v}{\partial x} \right) \right] dV = \int_S t \cdot \delta v \, dS - \int_V \left[ \sigma \cdot \left( \frac{\partial \delta v}{\partial x} \right) \right] dV \tag{5-8}$$

The virtual work statement can then be written as

$$\int_S t \cdot \delta v \, dS + \int_V b \cdot \delta v \, dV = \int_V \sigma \cdot \left( \frac{\partial \delta v}{\partial x} \right) dV \tag{5-9}$$

The virtual velocity gradient in the current configuration is defined as

$$\frac{\partial \delta v}{\partial x} = \delta L \tag{5-10}$$

The gradient, $\delta L$, can be decomposed to a symmetric and an anti-symmetric part.

$$\delta L = \delta D + \delta \Omega \tag{5-11}$$

where $\delta D = \mathrm{sym}(\delta D) = \frac{1}{2}(\delta L + \delta L^T)$ , $\delta \Omega = \mathrm{sym}(\delta D) = \frac{1}{2}(\delta L - \delta L^T)$ . Since $\sigma$ is symmetric,

$$\sigma \cdot \delta \Omega = 0 \tag{5-12}$$

The basis of the standard displacement based finite element analysis is the principle of virtual work. This principle states that the total internal virtual work is equal to the total external work.

$$\int_V \sigma \cdot \delta D \, dV = \int_S t \cdot \delta v \, dS + \int_V b \cdot \delta v \, dV \tag{5-13}$$

where $\delta D = \frac{1}{2}\left(\frac{\partial \delta v}{\partial x} + \left(\frac{\partial \delta v}{\partial x}\right)^T\right)$. The Cauchy stress ($\sigma$), traction vector (**t**), and body force (**b**) in Equation 5-13 are all equilibrium fields, while $\delta D$ and $\delta v$ are virtual fields. Using a finite element interpolation for the unknown nodal variables and for the virtual fields, the principle of virtual work defines a set of nonlinear equations which is solved to determine the current state of the material.

The equilibrium equations given by the principle of virtual work are satisfied at the beginning of the loading increment, and the objective is to compute nodal displacements as the equilibrium is satisfied at the end of the time (loading) step.

Denoting the variation by $\delta$, the principle of virtual work is changed to:

$$\int_V \partial\sigma\cdot\delta D\,dV + \int_V \sigma\cdot\left(\partial\delta D - \frac{\partial J}{J}\delta D\right)dV - \int_S\left(\partial t\cdot\delta v - t\cdot\delta v\frac{\partial A_r}{A_r}\right)dS$$
$$-\int_V\left(\partial b\cdot\delta v - b\cdot\delta v\frac{\partial J}{J}\right)dV = -\left(\int_V \sigma\cdot\delta D\;dV - \int_S t\cdot\delta v\;dS - \int_V b\cdot\delta v\,dV\right) \tag{5-14}$$

where $\partial D = d\partial u/dx$, $\partial u$ is the displacement change, the volume change between the reference and current configuration occupied by the material is given by $J = \left|dV/dV^0\right|$, and the surface area ratio between the reference and the current configuration is given by $A_r = \left|dS/dS^0\right|$. The first term in Equation 5-14 shows the stress gradient ($\partial\sigma$) which is assumed to be linearly related to $\partial D$ through the material constitutive relation. The second integral term on left hand side explains configuration changes which are called the geometric stiffness. The remaining integral terms on left hand side are about traction and body forces. The terms of the right hand side accounts for the residual, which is the weak form of the equilibrium equation. The displacements and other unknown parameters are updated after each iteration and analysis is not completed until the residual and displacement corrections are reached below the specific criteria of tolerance. If the body is driven to equilibrium, the right hand side is zero and Equation 5-14 also yields zeros for the corrections to the displacement increments. For each iteration of the finite element solution, the stress is integrated from its value at the beginning of the time (loading) step using the current estimate of the strain increment to advance the solution. Integrating from the beginning of the time (loading) increment ensures that errors in the approximate solutions provided during the finite element iteration process do not affect the path dependent integration of the material model.

The user defined material model subroutine supplies the material Jacobian matrix of constitutive model between $\partial\sigma$ and $\partial D$ so that finite element stiffness can be built according to Equation 5-14. This consistent Jacobian (**C**) is defined as

$$C = d(\Delta\sigma)/d(\Delta\varepsilon) \tag{5-15}$$

where $d(\Delta\sigma)$ is stress gradients and $d(\Delta\varepsilon)$ is strain gradients. It is typically computed at the end of the time (loading) increment. **C** is not easy to calculate thus it is calculated through particular method such as numerical differentiation, approximation with slow convergence. The function of the user defined material model subroutine must integrate the constitutive equations over a time (loading) increment and also update all material history variables, i.e. stress, strain, stiffness, and provide material stiffness relating the change in strain increment to the change in stress increment. This stiffness is used in ABAQUS™ to compute the element stiffness matrix relating nodal forces and displacements. In the equilibrium and virtual work equation, the internal virtual work rate term is replaced with the integral over the reference volume of the virtual work rate per reference volume, the equation is written as follows:

$$\int_V \tau^c \cdot \delta\varepsilon \, dV^0 = \int_S t^T \cdot \delta v \, dS + \int_V b^T \cdot \delta v \, dV \tag{5-16}$$

where $dV^0$ is the natural reference volume, $\tau^c$ and $\varepsilon$ are any conjugate pairing of material stress and strain measures, and the superscript **T** means transpose.

The finite element interpolator can be written in general as

$$u = N_N \, \delta v^N \tag{5-17}$$

where $\mathbf{N_N}$ are interpolation functions that depend on some material coordinate system, **u** are nodal variables. The virtual field ( $\delta v$ ) must be compatible with all kinematic constraints. Equation 5-17 can be represented as

$$\delta v = N_N \, \delta v^N \tag{5-18}$$

Now $\delta\varepsilon$ is the virtual rate of material strain associated with $\delta v$. Hence, the interpolation assumption gives

$$\delta\varepsilon = \beta_N \, \delta v^N \tag{5-19}$$

where $\beta_N = \beta_N(x, N_N)$ which is matrix. The equilibrium equation is approximated as

$$\delta v^{N} \int_{V^0} \beta_B \cdot \tau^c \, dV^0 = \delta v^{N} \left[ \int_S N_N^T \cdot t \, dS + \int_V N_N^T \cdot b \, dV \right] \tag{5-20}$$

Since $\delta v^N$ is an independent variable, a system of nonlinear equilibrium equations can be written as:

$$\int_{V^0} \beta_B \cdot \tau^c \, dV^0 = \left[ \int_S N_N^T \cdot t \, dS + \int_V N_N^T \cdot b \, dV \right] \tag{5-21}$$

By taking the variation of the equilibrium, equations can be written

$$\begin{aligned} &\int_{V^0} \left( d\tau^c \cdot \delta\varepsilon + \tau^c \cdot d\delta\varepsilon \right) dV^0 - \int_S dt^T \cdot \delta v \, dS - \int_S t^T \cdot \delta v \, dA_r \left( \frac{1}{A_r} \right) - \int_V b^T \cdot \delta v \, dV \\ &- \int_V b^T \cdot \delta v \left( \frac{1}{J} \right) dV = 0 \end{aligned} \tag{5-22}$$

Using the constitutive theory, $\delta\tau^c$ can represent following form.

$$\delta\tau^c = H \cdot \delta\varepsilon + g \tag{5-23}$$

where **H** and **g** are variables defined in terms of the current state.

The complete Jacobian matrix is obtained as following:

$$K_{MN} = \int_{V^0} \beta_M \cdot H \cdot \beta_N dV^0 + \int_{V^0} \tau^c \cdot \partial_N \beta_M dV^0 - \int_S N_M^T \cdot Q_N^S \, dS - \int_V N_M^T \cdot Q_N^S \, dV \qquad (5\text{-}24)$$

where $\partial_N = \partial/\partial u^N$ , $\partial_N \varepsilon = \partial\varepsilon/\partial u^N = \beta_N$ , $\partial_N t + t\frac{1}{A_r}\partial_N J = Q_N^S$ , $\partial_N b + b\frac{1}{J}\partial_N J = Q_N^V$ .

Figure 5-1 shows the flow diagram of nonlinear ABAQUS™ analysis using the UMAT.

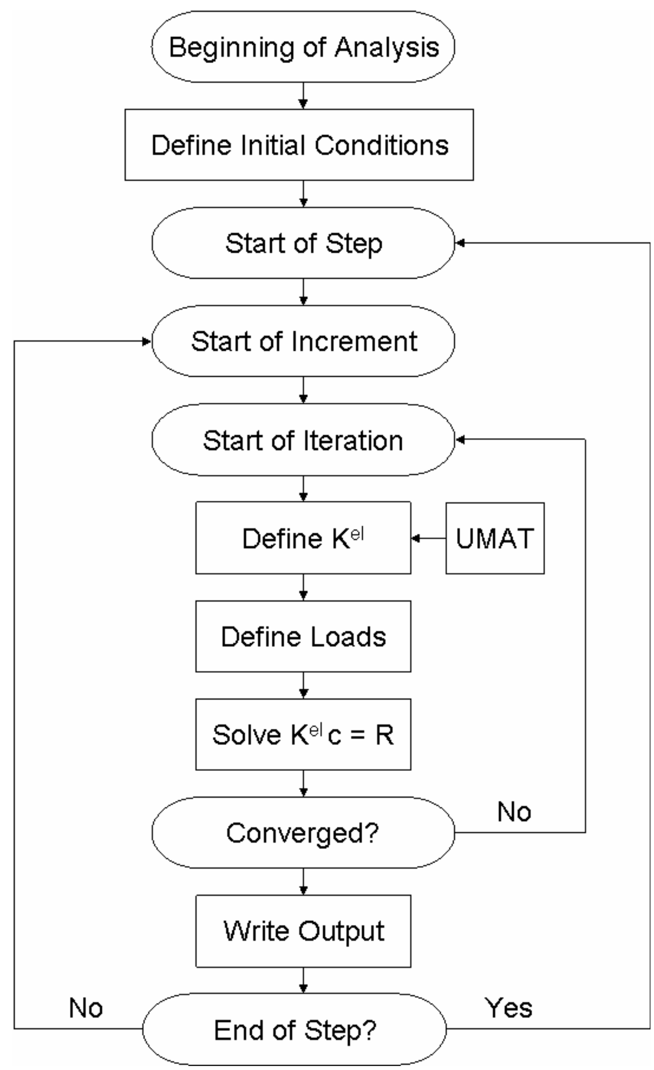


Figure 5-1 Flow Diagram of Nonlinear ABAQUS™ Analysis (Hibbit et al, 2005)

### 5.1.2 Development of User Material Subroutines in ABAQUS™

ABAQUS™ already has interfaces that allow the user to implement general constitutive model equations through material library for several materials, such as concrete, rock, soil, plastic, etc. It can also define any complex constitutive models for materials when none of the existing material models are included in the ABAQUS™ material library. There exist much improved interfaces for specifying user defined material models via the user defined material model subroutine. These interfaces make it possible to define any constitutive model of arbitrary complexity with all types of ABAQUS™ structural elements. Multiple user materials can be implemented in a single user defined material model subroutine and can be used together. This subroutine facilitates incorporating of different models without affecting the main code of the program.

To transform the constitutive rate equation into an incremental equation, UMAT must use an implicit integration of backward Euler as a suitable integration procedure. Implementation of a material model requires the compiling of the material law subroutine using the FORTRAN code. The subroutine is called at every material integration point for every iteration. ABAQUS™ passes in stresses, strains, and state variables at the beginning of each time increment along with the current strain increment. The user defined material model subroutine then updates the stresses and state variables to the values at the end of the time increment and provides the material stiffness called Jacobian. The calculation of the consistent Jacobian is required for ABAQUS™/Standard user defined material model subroutine. The exact definition of the Jacobian, which is already mentioned, is given as follows:

$$C = \frac{\partial \Delta \sigma}{\partial \Delta \varepsilon} \tag{5-25}$$

This matrix may be either symmetric or nonsymmetric dependent on the constitutive equation or integration procedure. Figure 5-2 shows the flow diagram of implementation of user material subroutine in nonlinear ABAQUS™ Analysis.

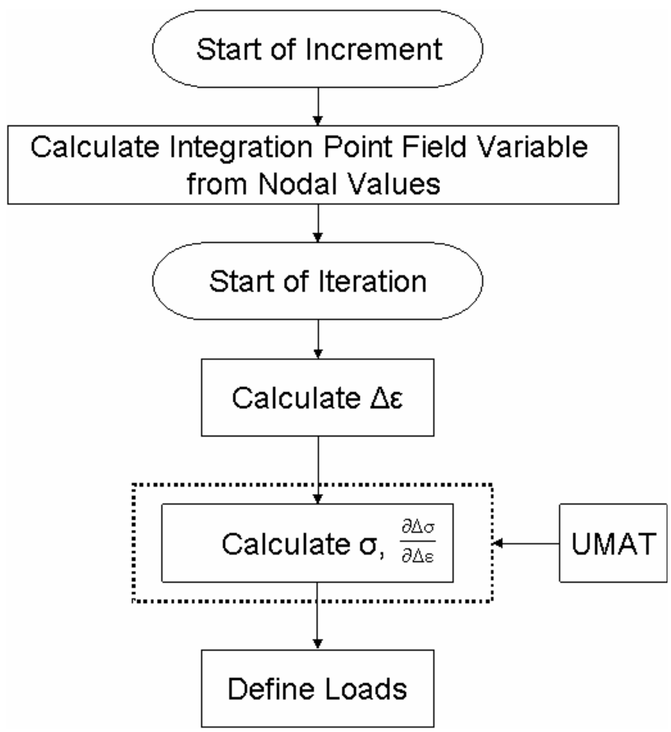


Figure 5-2 Flow Diagram of Implementation of User Material Subroutine (UMAT) in ABAQUS™ Analysis (Hibbit et al, 2005)

5.1.3 Isotropic Elastic Stress-strain Relationships

The resilient modulus approach used extensively in the material modeling of this study relies on the observed behavior of pavement materials from triaxial testing after a certain number of loading cycles. The behavior of the material in the resilient state is considered to be a quasi-elastic behavior. Thus material behavior is governed elastically and the stress-strain relations for elastic materials are given in the following section.

For linear elastic isotropic materials, two material constants are needed to define the stress-strain relations. The Lame constants, $\lambda$ and $\mu$, are used in the following stress-strain relation.

$$\sigma_{ij} = \lambda \varepsilon_{kk} \delta_{ij} + 2\mu\varepsilon_{ij} \tag{5-26}$$

where $\sigma_{ij}$ is stress tensor, $\varepsilon_{kk}$ is hydrostatic strain or volumetric strain, $\delta_{ij}$ is called the Kronecker delta, and $\varepsilon_{ij}$ is strain tensor. The Lame constants are related to Young's modulus (E) and Poisson's ratio ($\nu$) through the following equations.

$$\lambda = \frac{\nu E}{(1+\nu)(1-2\nu)} \tag{5-27}$$

$$\mu = \frac{E}{2(1+\nu)} = G \tag{5-28}$$

It is noted that $\mu$ is the same as the shear modulus (G). From the shear stress and strain relationship, $\tau_{ij} = G\gamma_{ij}$, the shear strain ($\gamma_{ij}$) is twice the strain tensor component $\varepsilon_{ij}$. From Equations 5-27 and 5-28, the strain can be derived from the general Hooke's law for isotropic elastic material expressed as

$$\varepsilon_{ij} = \frac{1+\nu}{E}\sigma_{ij} - \frac{\nu}{E}\sigma_{kk}\delta_{ij} \tag{5-29}$$

$$\varepsilon_{kk} = \frac{1+\nu}{E}\sigma_{kk} - \frac{3\nu}{E}\sigma_{kk} = \frac{1-\nu}{E}\sigma_{kk} \tag{5-30}$$

Then, the generalized Hooke's law can be written as follow:

$$\sigma_{ij} = \frac{E}{1+\nu}\varepsilon_{ij} + \frac{\nu}{1+\nu}\sigma_{kk}\delta_{ij} = \frac{\nu E}{(1+\nu)(1-2\nu)}\varepsilon_{kk}\delta_{ij} + \frac{E}{1+\nu}\varepsilon_{ij} \tag{5-31}$$

For finite element implementations, the stresses and strains can be written in vector form instead of original tensorial form. Thus, the stresses and strains are given by a constitutive relation.

$$\begin{Bmatrix} \sigma_{xx} \\ \sigma_{yy} \\ \sigma_{zz} \\ \sigma_{xy} \\ \sigma_{yz} \\ \sigma_{xz} \end{Bmatrix} = \begin{bmatrix} \lambda+2\mu & \lambda & \lambda & 0 & 0 & 0 \\ \lambda & \lambda+2\mu & \lambda & 0 & 0 & 0 \\ \lambda & \lambda & \lambda+2\mu & 0 & 0 & 0 \\ 0 & 0 & 0 & 2\mu & 0 & 0 \\ 0 & 0 & 0 & 0 & 2\mu & 0 \\ 0 & 0 & 0 & 0 & 0 & 2\mu \end{bmatrix} \begin{Bmatrix} \varepsilon_{xx} \\ \varepsilon_{yy} \\ \varepsilon_{zz} \\ \varepsilon_{xy} \\ \varepsilon_{yz} \\ \varepsilon_{xz} \end{Bmatrix} \tag{5-32}$$

The generalized Hooke's law in Equation 5-31 is also represented by Equation 5-33.

$$\mathbf{S} = \frac{E}{1+\nu}(\alpha\varepsilon I + E) \tag{5-33}$$

where **S** represents the stress tensor field, $\alpha(\nu) = \dfrac{\nu}{1-2\nu}$ is a parameter that depends on Poisson's ratio, ε is an invariant of the strain tensor, **I** is the identity tensor, and **E** is the strain tensor. The material stiffness which can be calculated by $\dfrac{\partial S}{\partial E}$ is obtained from Equation 5-33 as follows:

$$\frac{\partial S}{\partial E} = \frac{E}{1+\nu}(1 + \alpha I \otimes I) + (\alpha\varepsilon I + E) \otimes \nabla_E\left(\frac{E}{1+\nu}\right) \tag{5-34}$$

With these definitions, one can rewrite stress-strain relationship as

$$\nabla_E\left(\frac{E}{1+\nu}\right) = \nabla_E \hat{C}(E) = \frac{\partial \hat{C}}{\partial \rho}\frac{\partial \rho}{\partial E} + \frac{\partial \hat{C}}{\partial \gamma}\frac{\partial \gamma}{\partial E} = \mu\hat{C}\left(\frac{n}{\varepsilon}I + \frac{m}{3\gamma^2}\overline{E}\right) \tag{5-35}$$

where $\rho = |\varepsilon|$, $\gamma = \sqrt{\frac{1}{3}E \cdot E}$, $\dfrac{\partial \gamma}{\partial E} = \dfrac{1}{3}\dfrac{\overline{E}}{\gamma}$, $\mu = 1/(1-n-m)$, n and m are the powers of bulk stress and deviator stress term in Uzan model (n and m are $K_2$ and $K_3$ of Equation 2-13), respectively. When we let $\mathbf{N} = \dfrac{\overline{\mathrm{E}}}{\gamma}$, the material stiffness for Uzan model (1985), for example, is found as follows:

$$\frac{\partial \Delta \mathrm{S}}{\partial \Delta \mathrm{E}} = \mathrm{M}_{\mathrm{R}}(\theta, \tau)\left[1 + (\mu n \overline{\alpha} + \alpha)\mathrm{I} \otimes \mathrm{I} + \frac{\mu m}{3}\mathbf{N} \otimes \mathbf{N} + \frac{\mu \overline{\alpha} \varepsilon m}{3\gamma}\mathrm{I} \otimes \mathbf{N} + \frac{\mu \gamma n}{\varepsilon}\mathbf{N} \otimes \mathrm{I}\right] \tag{5-36}$$

where $\mathrm{M}_{\mathrm{R}}(\theta, \tau)$ is the resilient modulus from Uzan model and $\overline{\alpha} = (1+\nu)/3(1-2\nu)$.

Likewise the bilinear subgrade model (Thompson and Robnett, 1979) can be expressed as follows:

$$\frac{\partial \Delta \mathrm{S}}{\partial \Delta \mathrm{E}} = \mathrm{M}_{\mathrm{R}}(\tau)\left[1 + \alpha\, \mathrm{I} \otimes \mathrm{I}\right] \tag{5-37}$$

where $\mathrm{M}_{\mathrm{R}}(\tau)$ is the shear stress-dependent resilient modulus from the bilinear model (Thompson and Robnett, 1979).

### 5.1.4 Implementation of Nonlinear Stress-dependent Model

The analysis of flexible pavements commonly requires the prediction of stress and strain distribution and deformation characteristics in elastic layered continua. Although a flexible pavement structure consists of various materials such as bound materials like asphalt concrete and unbound materials like granular materials, all materials are commonly represented by the continuum. In a general three-dimensional continuum, the equilibrium of an element can be written as follows (Timoshenko and Goodier, 1970):

$$
\begin{aligned}
&\frac{\partial \sigma_{xx}}{\partial x} + \frac{\partial \tau_{xy}}{\partial y} + \frac{\partial \tau_{xz}}{\partial z} = 0 \\
&\frac{\partial \tau_{yx}}{\partial x} + \frac{\partial \sigma_{yy}}{\partial y} + \frac{\partial \tau_{yz}}{\partial z} = 0 \\
&\frac{\partial \tau_{zx}}{\partial x} + \frac{\partial \tau_{zy}}{\partial y} + \frac{\partial \sigma_{zz}}{\partial z} = 0
\end{aligned}
\tag{5-38}
$$

Generally, when performing a material nonlinear finite element analysis, constitutive properties are updated at the integration points within each element. When implementing a material nonlinear model using this approach, at each iteration we must update the element stiffness matrix, $K^e$, governed by

$$K^e = \int B^T D\, B\, dv \tag{5-39}$$

where B is called the strain-displacement matrix and D is the constitutive relation matrix defined as follows:

$$D = \frac{E}{(1+\nu)(1-2\nu)} \begin{bmatrix} 1-\nu & \nu & \nu & 0 & 0 & 0 \\ \nu & 1-\nu & \nu & 0 & 0 & 0 \\ \nu & \nu & 1-\nu & 0 & 0 & 0 \\ 0 & 0 & 0 & \frac{1-2\nu}{2} & 0 & 0 \\ 0 & 0 & 0 & 0 & \frac{1-2\nu}{2} & 0 \\ 0 & 0 & 0 & 0 & 0 & \frac{1-2\nu}{2} \end{bmatrix} \tag{5-40}$$

In addition to the constitutive equations, a three-dimensional continuum solution also requires the following six compatibility equations.

$$\begin{aligned} &\varepsilon_{xx} = \frac{\partial u}{\partial x}, \ \varepsilon_{yy} = \frac{\partial v}{\partial y}, \varepsilon_{zz} = \frac{\partial w}{\partial y} \\ &\gamma_{xy} = \frac{\partial u}{\partial y} + \frac{\partial v}{\partial x}, \ \gamma_{xz} = \frac{\partial u}{\partial z} + \frac{\partial w}{\partial x}, \gamma_{yz} = \frac{\partial v}{\partial z} + \frac{\partial w}{\partial y} \end{aligned} \tag{5-41}$$

where ε are normal strains, γ are shear strains, u, v, and w are the displacement components in x, y, and z directions, respectively. To imply two material nonlinearities, the Uzan model (Uzan, 1985) for unbound granular material in the base/subbase layer and bilinear model (Thompson and Robnett, 1979) for subgrade soil, matrix D can be varied throughout the element in accordance with Young's modulus (E). In this implementation, resilient modulus ($M_R$) can be substituted for Young's modulus. Therefore, matrix D can be given as follows:

$$D = \frac{M_R}{(1+\nu)(1-2\nu)} \begin{bmatrix} 1-\nu & \nu & \nu & 0 & 0 & 0 \\ \nu & 1-\nu & \nu & 0 & 0 & 0 \\ \nu & \nu & 1-\nu & 0 & 0 & 0 \\ 0 & 0 & 0 & \frac{1-2\nu}{2} & 0 & 0 \\ 0 & 0 & 0 & 0 & \frac{1-2\nu}{2} & 0 \\ 0 & 0 & 0 & 0 & 0 & \frac{1-2\nu}{2} \end{bmatrix} \tag{5-42}$$

Through this implementation, the stress-dependent $M_R$ behavior of unbound aggregate base and subgrade soils can be incorporated into the solution. As a result, $M_R$ properties varying with both depth and horizontal distance in a geomaterial layer can be predicted as a function of stress states and the material nonlinearity observed in the pavement geomaterials for base and subgrade can be considered in the ABAQUS™ finite element program through the use of the $M_R$ characterization models. The user defined material model UMAT subroutine calculates the resilient modulus of granular base and subgrade from the stress state at each integration point in each element.

Due to the nature of the material models used, which are all functions of the total stresses, an iterative procedure which considers a secant stiffness approach, is found to be necessary in the analysis with an incremental loading scheme. In each load increment, the nonlinear iterations are performed using the appropriate resilient modulus models to calculate the correct vertical resilient modulus corresponding to the total stress state. The direct secant method involves the solution of the nonlinear load displacement behavior by updating the secant stiffness in each iteration until convergence is reached for the load increment.

The Poisson's ratio is often assigned a constant value below 0.5 based on the assumption of elastic and isotropic pavement material. The stress dependency of Poisson's ratio is in general not as significant as the stress dependency of the modulus. For most pavement materials, therefore, a constant Poisson's ratio is used and these values typically lie within the range of 0.1 to 0.49.

### 5.1.5 Nonlinear Solution Technique

Several nonlinear solution techniques have been investigated for the known stress-dependent geomaterial behavior. Due to the nature of the stress-dependent resilient modulus models, an incremental tangent stiffness nonlinear solution could not be successfully implemented in the nonlinear analysis (Tutumluer, 1995). One of the particular reasons for supporting this belief is the hardening nature of the resilient behavior of unbound granular materials. Unlike many other engineering materials, the resilient modulus of granular materials increases as stresses increase. The hardening characteristics of nonlinear stress-strain behavior can be exhibited when two elastic spheres are pressed against each other. When the applied pressure is small, the contact surface between two spheres becomes small and the increase of pressure results in a large displacement between the centers of spheres. In contrast, when the applied pressure is high, the contact surface is large and the increase of pressure causes relatively small displacement between the centers of spheres with high stiffness of each sphere. Because of these characteristics, some nonlinear analysis schemes are hard to converge the solutions. Thus, an iterative procedure which considers a secant stiffness approach is necessary in the analysis with an incremental loading. In every load increment, the nonlinear iteration schemes are performed using the stress-dependent models to calculate the correct vertical resilient modulus corresponding to the total stress state.

A direct secant stiffness approach has been adopted for the nonlinear analysis of granular base and subgrade layers and programmed into the user defined material model subroutine of ABAQUS$^{TM}$ finite element program to generate the nonlinear load-displacement solution by updating secant stiffness in each iteration. This method is less complicated than other nonlinear solution techniques, but this is sophisticated enough to give good convergence of the iterations. The nonlinear analysis is performed using both an incremental loading scheme and an iterative solution technique for each load increment, similar to the approach used by Tutumluer (1995), as follows:

1. First necessary material property constants, number of load increments, and convergence criteria are inputs along with initially assumed material modulus properties and the wheel loading.

2. The nonlinear analysis is conducted by applying in typically 10 load increments. For each load increment, new values of the secant resilient modulus are computed at each integration point using the most recently calculated stresses in the elements.

3. The resilient moduli for the next iteration are computed using direct secant stiffness approach with the damping factor ($\lambda$) and checked for convergence. To converge smoothly for each load increment as shown in Figure 5-3, a

damping factor ($\lambda$ which has values between 0 and 1) is adopted to obtain the predicted resilient modulus for the next iteration in the following form:

$$M_R^j = (1-\lambda)M_R^{j-1} + \lambda M_{R\,\text{model}}^j \tag{5-43}$$

where $M_R^j =$ actual $M_R$ to be used at the end of iteration number j, $M_R^{j-1} = M_R$ used at the end of iteration number (j-1), $M_{R\,\text{model}}^j = M_R$ computed from the model at the end of iteration number j.

4. The convergence criteria used in this study set up (i) the 5% maximum difference between the old and new values of resilient modulus at each integration point in each element and (ii) the 0.2% maximum cumulative error ($E_c$) criterion as follows:

$$E_c = \frac{\sum_{i=1}^{n}(M_R^j - M_R^{j-1})^2}{\sum_{i=1}^{n}(M_R^j)^2} \tag{5-44}$$

where n = total number of integration points in the mesh, j = the last iteration number for each load increment. In general, the cumulative error can be easily satisfied with the criterion.

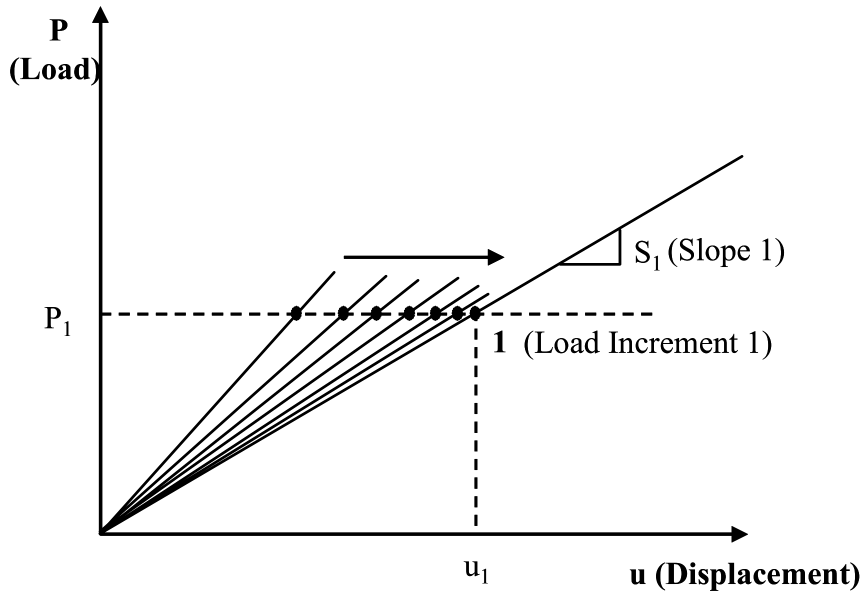


(a) Nonlinear iterations for convergence during load increment 1

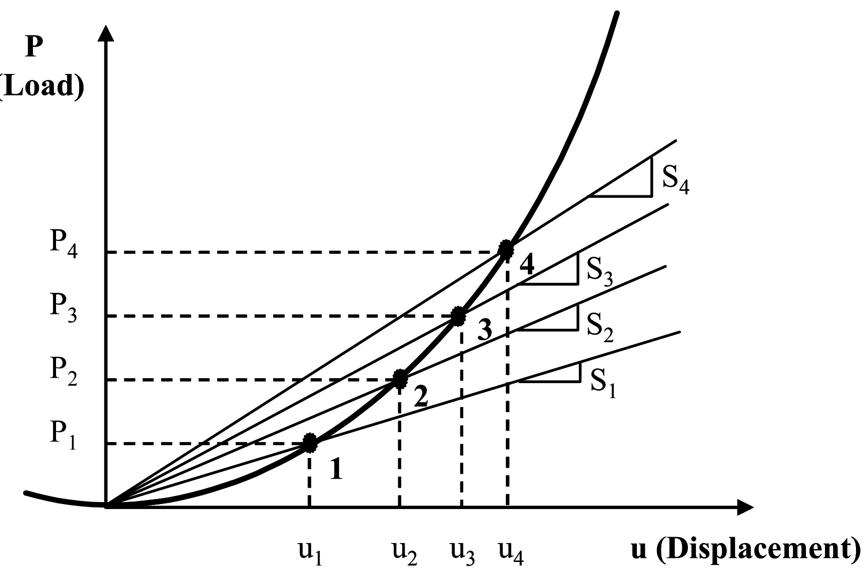


(b) Secant stiffness after 4 load increments

Figure 5-3 Resilient Modulus Search Technique Using Direct Secant Stiffness (Tutumluer, 1995)

Figure 5-4 presents a flow diagram of the user defined material model subroutine in ABAQUS$^{TM}$. The convergence of the direct secant stiffness approach can usually be controlled by assigning low damping factor ( $\lambda$ ) values. Therefore, large material property changes are avoided and the changes of the resilient moduli which can result in divergence of the solution can be prevented.

Particularly, the horizontal tension in a granular base layer has to be reduced or eliminated in the nonlinear finite element programs. This somewhat inadmissible tension condition has been dealt with in the developed UMAT subroutine which nullifies any computed horizontal tensile stresses in a granular layer. This “no tension” modification procedure, which is adopted here for the continuum assumption, eliminates any inadmissible horizontal tension in the granular base in flexible pavements.

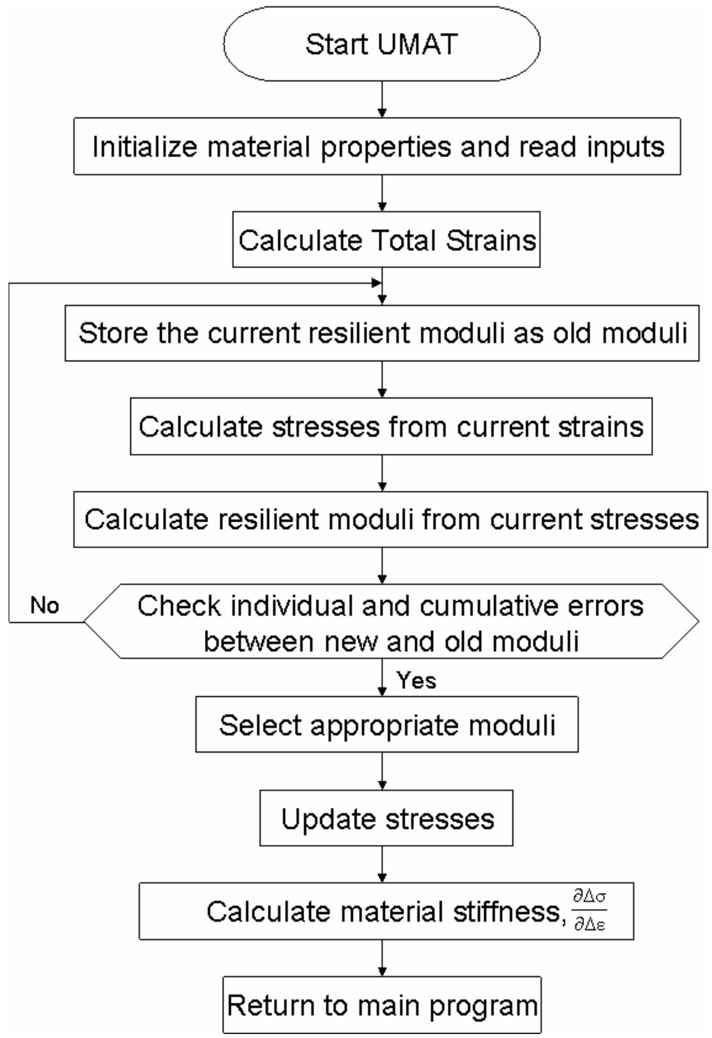


Figure 5-4 Flow Diagram of User Material Subroutine (UMAT) in ABAQUS$^{TM}$ Analysis

## 5.2 Axisymmetric Nonlinear Finite Element Analysis

To properly characterize the resilient response of unbound aggregate and subgrade soil, the Uzan type unbound aggregate model (Uzan, 1985) and the bilinear variation model of subgrade soil modulus with deviator stress (Thompson and Robnett, 1979) were both programmed in the user defined material model subroutine in the general-purpose finite element program, ABAQUS$^{TM}$. GT-PAVE axisymmetric finite element program was used to compare the solutions and verify the nonlinear analysis procedure employed in the ABAQUS$^{TM}$. Because GT-PAVE axisymmetric finite element program also considers the Uzan type unbound aggregate model and the bilinear model for subgrade soil in the nonlinear subroutine, this was an essential step to check the accuracy of the user defined material model subroutine from nonlinear axisymmetric finite element solutions.

### 5.2.1 Verification of Axisymmetric Finite Element Analysis

A conventional flexible pavement was analyzed as an axisymmetric solid consisting of linear and nonlinear elastic layers in order to employ the nonlinear response models in the ABAQUS$^{TM}$ and GT-PAVE finite element programs. To employ the nonlinear resilient material models in the finite element solutions, the Uzan base/subbase model and the bilinear subgrade model were employed for the characterization of the granular base and subgrade soil layers. These material models were introduced and discussed in detail in Chapter 2.

Table 5-1 summarizes the pavement geometry and assigned material input properties. Two different AC thicknesses, 76-mm and 102-mm, were considered. A finite element mesh consisting of 300-second order elements and 981-nodes was used (see Figure 5-5). A uniform pressure of 0.83-MPa was applied over the circular area with a radius of 102-mm. Pavement responses were predicted from the ABAQUS$^{TM}$ and GT-PAVE solutions for the following pavement layer material characterizations with isotropic and linear elastic asphalt concrete material: (1) nonlinear base and linear subgrade, (2) linear base and nonlinear subgrade, and (3) nonlinear base and nonlinear subgrade. In the case of linear analyses, the linear elastic properties given in Table 5-1 were used in the subgrade and base layers. Thin AC surfaced pavements, e.g., 76-mm and 102-mm AC thicknesses were considered here for low volume roads to represent the more drastic influence of nonlinear resilient behavior in the base and subgrade layers.

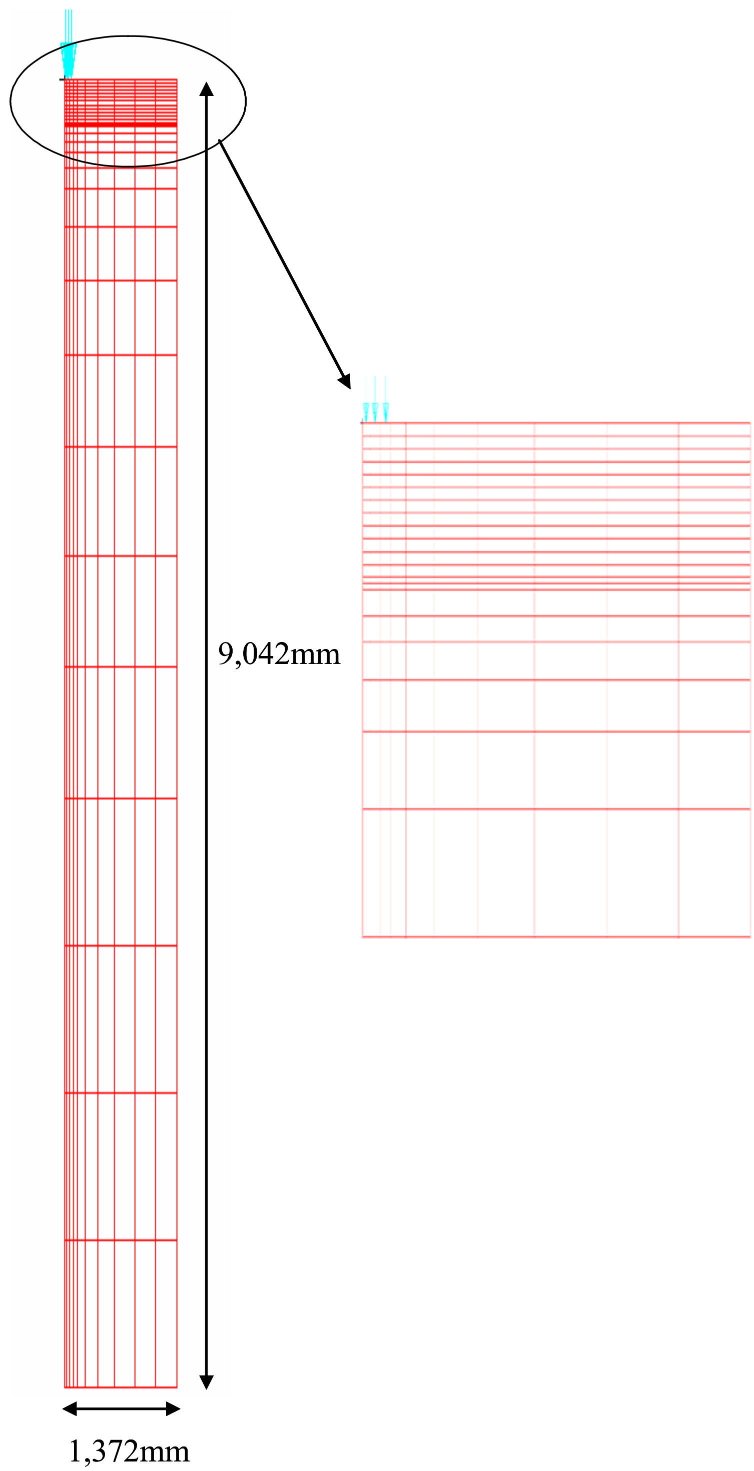


Figure 5-5 Finite Element Mesh used for the Axisymmetric Verification Analysis Case

Table 5-1 Material Properties used in the Nonlinear Finite Element Analysis

<table>
<tr><th>Section</th><th>Element</th><th>Thickness (mm)</th><th>E (MPa)</th><th>$\nu$</th><th colspan="4">Material Properties</th></tr>
<tr><td>AC</td><td>8-noded solid</td><td>76 or 102</td><td>2759</td><td>0.35</td><td colspan="4">Isotropic and Linear Elastic</td></tr>
<tr><td rowspan="3">Base</td><td rowspan="3">8-noded solid</td><td rowspan="3">254</td><td rowspan="3">138 or 207 (initial)</td><td rowspan="3">0.40</td><td colspan="4">Nonlinear: Uzan model (Uzan, 1985)</td></tr>
<tr><td colspan="2">$K_1$ (kPa)</td><td>$K_2$</td><td>$K_3$</td></tr>
<tr><td colspan="2">4,100</td><td>0.64</td><td>0.065</td></tr>
<tr><td rowspan="3">Subgrade</td><td rowspan="3">8-noded solid</td><td rowspan="3">-</td><td rowspan="3">41 (initial)</td><td rowspan="3">0.45</td><td colspan="4">Nonlinear: Bilinear model (Thompson and Robnett, 1979)</td></tr>
<tr><td>$E_{RI}$ (kPa)</td><td>$\sigma_{di}$ (kPa)</td><td>$K_3$ (kPa/kPa)</td><td>$K_4$ (kPa/kPa)</td></tr>
<tr><td>41,400</td><td>41</td><td>1,000</td><td>200</td></tr>
</table>

Table 5-2 and Table 5-3 compare pavement responses predicted by the nonlinear analyses from ABAQUS™ and GT-PAVE programs. Table 5-2 shows the vertical stresses predicted at the centerline of loading and Table 5-3 lists radial stresses at the centerline of loading. As indicated in both tables, two nonlinear finite element analysis programs are in very good agreement producing similar responses. This verified the applicability of the developed ABAQUS™ UMAT subroutine to nonlinear axisymmetric pavement analysis.

Table 5-2 Predicted Vertical Stresses at the Centerline of Loading

| 76-mm AC and 254-mm base section | | | | | | |
|---|---|---|---|---|---|---|
| Pavement Response | Nonlinear base and linear subgrade | | Linear base and nonlinear subgrade | | Nonlinear base and nonlinear subgrade | |
| | ABAQUS | GT-PAVE | ABAQUS | GT-PAVE | ABAQUS | GT-PAVE |
| Top surface (MPa) | -0.771 | -0.759 | -0.767 | -0.767 | -0.770 | -0.760 |
| Bottom of AC (MPa) | -0.394 | -0.342 | -0.390 | -0.390 | -0.389 | -0.350 |
| Top of base (MPa) | -0.245 | -0.231 | -0.279 | -0.279 | -0.256 | -0.237 |
| Bottom of base (MPa) | -0.041 | -0.040 | -0.046 | -0.046 | -0.054 | -0.053 |
| Top of subgrade (MPa) | -0.037 | -0.036 | -0.040 | -0.041 | -0.048 | -0.048 |

| 102-mm AC and 254-mm base section | | | | | | |
|---|---|---|---|---|---|---|
| Pavement Response | Nonlinear base and linear subgrade | | Linear base and nonlinear subgrade | | Nonlinear base and nonlinear subgrade | |
| | ABAQUS | GT-PAVE | ABAQUS | GT-PAVE | ABAQUS | GT-PAVE |
| Top surface (MPa) | -0.785 | -0.782 | -0.787 | -0.787 | -0.782 | -0.781 |
| Bottom of AC (MPa) | -0.300 | -0.282 | -0.327 | -0.327 | -0.269 | -0.275 |
| Top of base (MPa) | -0.138 | -0.143 | -0.189 | -0.189 | -0.129 | -0.137 |
| Bottom of base (MPa) | -0.035 | -0.035 | -0.036 | -0.036 | -0.044 | -0.044 |
| Top of subgrade (MPa) | -0.033 | -0.032 | -0.032 | -0.032 | -0.039 | -0.040 |

Table 5-3 Predicted Radial Stresses at the Centerline of Loading

| 76-mm AC and 254-mm base section | | | | | | |
|---|---|---|---|---|---|---|
| Pavement Response | Nonlinear base and linear subgrade | | Linear base and nonlinear subgrade | | Nonlinear base and nonlinear subgrade | |
| | ABAQUS | GT-PAVE | ABAQUS | GT-PAVE | ABAQUS | GT-PAVE |
| Top surface (MPa) | -1.690 | -1.829 | -1.554 | -1.557 | -1.681 | -1.690 |
| Bottom of AC (MPa) | 1.121 | 1.259 | 0.943 | 0.944 | 1.186 | 1.121 |
| Top of base (MPa) | -0.007 | -0.029 | -0.043 | -0.043 | -0.005 | -0.007 |
| Bottom of base (MPa) | 0.030 | 0.067 | 0.073 | 0.075 | 0.023 | 0.030 |
| Top of subgrade (MPa) | -0.014 | -0.003 | -0.003 | -0.004 | -0.009 | -0.014 |
| 102-mm AC and 254-mm base section | | | | | | |
| Pavement Response | Nonlinear base and linear subgrade | | Linear base and nonlinear subgrade | | Nonlinear base and nonlinear subgrade | |
| | ABAQUS | GT-PAVE | ABAQUS | GT-PAVE | ABAQUS | GT-PAVE |
| Top surface (MPa) | -1.528 | -1.605 | -1.354 | -1.356 | -1.548 | -1.603 |
| Bottom of AC (MPa) | 0.873 | 0.945 | 0.672 | 0.673 | 0.943 | 0.987 |
| Top of base (MPa) | -0.005 | -0.004 | -0.016 | -0.016 | -0.001 | -0.010 |
| Bottom of base (MPa) | 0.020 | 0.030 | 0.056 | 0.057 | 0.003 | 0.007 |
| Top of subgrade (MPa) | -0.009 | -0.004 | -0.003 | -0.003 | -0.006 | -0.007 |

Further, Table 5-4 presents the vertical deflection predictions at the center of loading and Table 5-5 lists the predicted strains. Again, the close matches and good agreements between the ABAQUS$^{TM}$ and GT-PAVE results verify the applicability of the developed ABAQUS$^{TM}$ user defined material model subroutine to nonlinear axisymmetric pavement analysis.

Table 5-4 Predicted Vertical Deflections at the Centerline of Loading

| 76-mm AC and 254-mm base section | | | | | | |
|---|---|---|---|---|---|---|
| Pavement Responses | Nonlinear base and linear subgrade | | Linear base and nonlinear subgrade | | Nonlinear base and nonlinear subgrade | |
| | ABAQUS | GT-PAVE | ABAQUS | GT-PAVE | ABAQUS | GT-PAVE |
| Top surface (mm) | -0.912 | -0.909 | -0.594 | -0.597 | -0.775 | -0.777 |
| Bottom of AC (mm) | -0.902 | -0.899 | -0.584 | -0.587 | -0.762 | -0.767 |
| Top of base (mm) | -0.866 | -0.864 | -0.554 | -0.556 | -0.726 | -0.731 |
| Bottom of base (mm) | -0.655 | -0.655 | -0.401 | -0.404 | -0.505 | -0.503 |
| Top of subgrade (mm) | -0.612 | -0.607 | -0.368 | -0.371 | -0.467 | -0.462 |
| 102-mm AC and 254-mm base section | | | | | | |
| Pavement Responses | Nonlinear base and linear subgrade | | Linear base and nonlinear subgrade | | Nonlinear base and nonlinear subgrade | |
| | ABAQUS | GT-PAVE | ABAQUS | GT-PAVE | ABAQUS | GT-PAVE |
| Top surface (mm) | -0.772 | -0.772 | -0.505 | -0.508 | -0.665 | -0.658 |
| Bottom of AC (mm) | -0.759 | -0.757 | -0.493 | -0.495 | -0.650 | -0.645 |
| Top of base (mm) | -0.732 | -0.732 | -0.470 | -0.472 | -0.622 | -0.615 |
| Bottom of base (mm) | -0.564 | -0.564 | -0.358 | -0.361 | -0.429 | -0.427 |
| Top of subgrade (mm) | -0.531 | -0.526 | -0.333 | -0.335 | -0.404 | -0.396 |

Table 5-5 Predicted Strains at the Centerline of Loading

| 76-mm AC and 254-mm base section | | | | | | |
|---|---|---|---|---|---|---|
| Pavement Responses | Nonlinear base and linear subgrade | | Linear base and nonlinear subgrade | | Nonlinear base and nonlinear subgrade | |
| | ABAQUS | GT-PAVE | ABAQUS | GT-PAVE | ABAQUS | GT-PAVE |
| Bottom of AC (με) | 324 | 339 | 271 | 271 | 328 | 349 |
| Top of subgrade (με) | -962 | -971 | -646 | -658 | -874 | -868 |
| **102-mm AC and 254-mm base section** | | | | | | |
| Pavement Responses | Nonlinear base and linear subgrade | | Linear base and nonlinear subgrade | | Nonlinear base and nonlinear subgrade | |
| | ABAQUS | GT-PAVE | ABAQUS | GT-PAVE | ABAQUS | GT-PAVE |
| Bottom of AC (με) | 243 | 258 | 199 | 199 | 256 | 267 |
| Top of subgrade (με) | -729 | -739 | -503 | -509 | -642 | -625 |

Figure 5-6, Figure 5-7, and Figure 5-8 show predicted vertical stress, radial stress, and vertical deformation distributions at the centerline of loading, respectively. All analyses shown were conducted for the nonlinear base and nonlinear subgrade case. In general, a very good agreement was achieved between ABAQUS™ and GT-PAVE finite element analysis results.

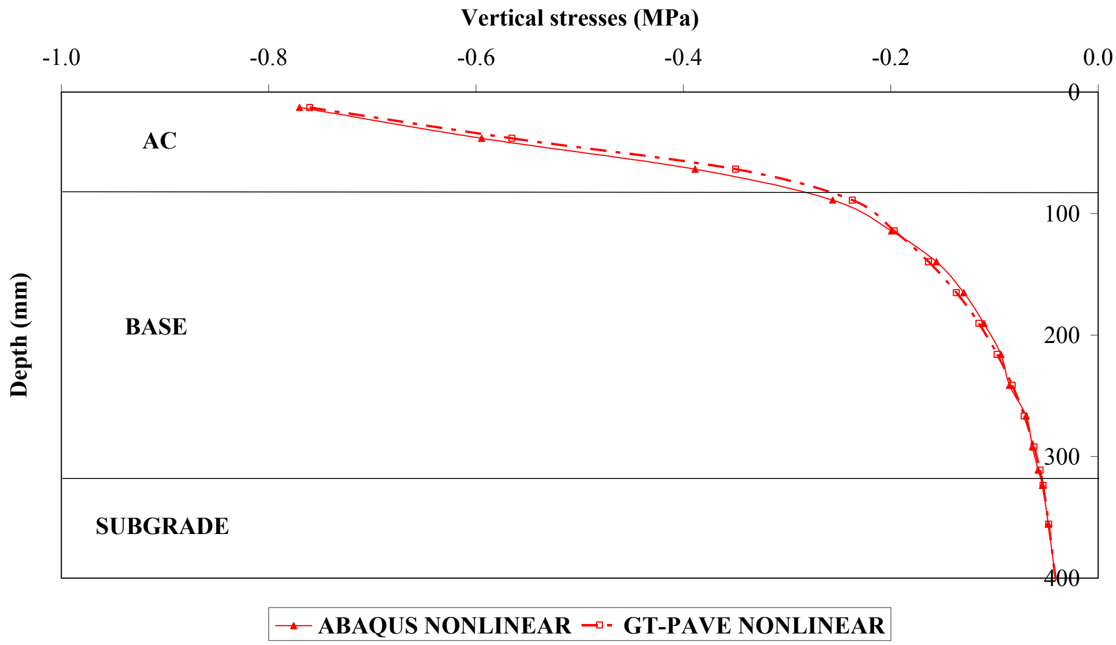


(a) 76-mm AC and 254-mm base section

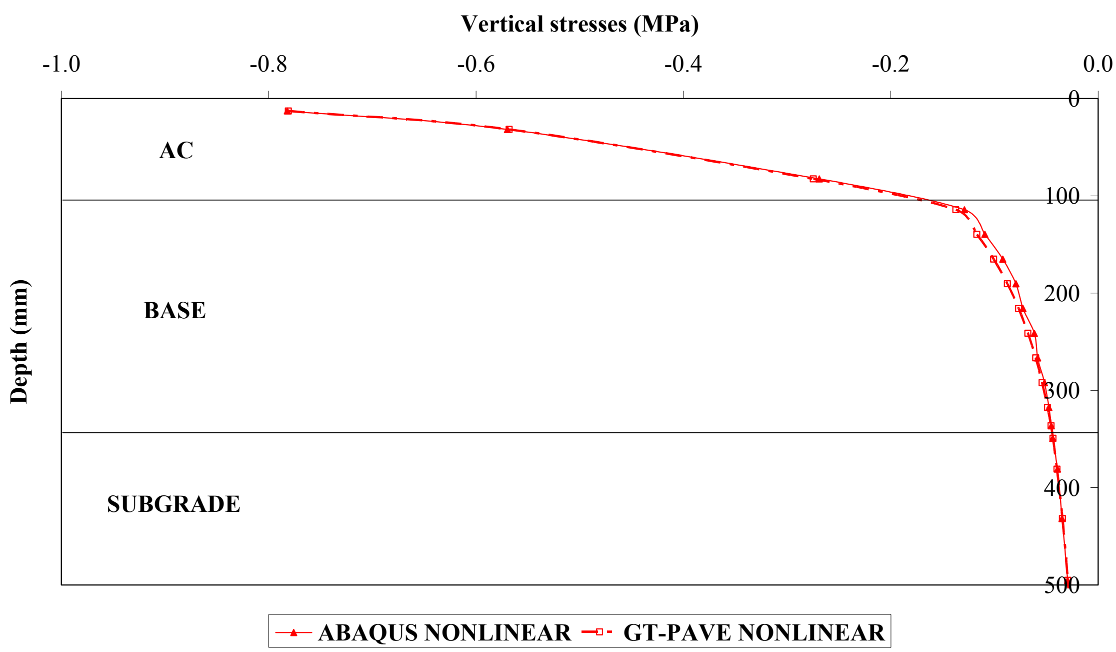


(b) 102-mm AC and 254-mm base section

Figure 5-6 Predicted Vertical Stress Distributions at the Centerline of Loading

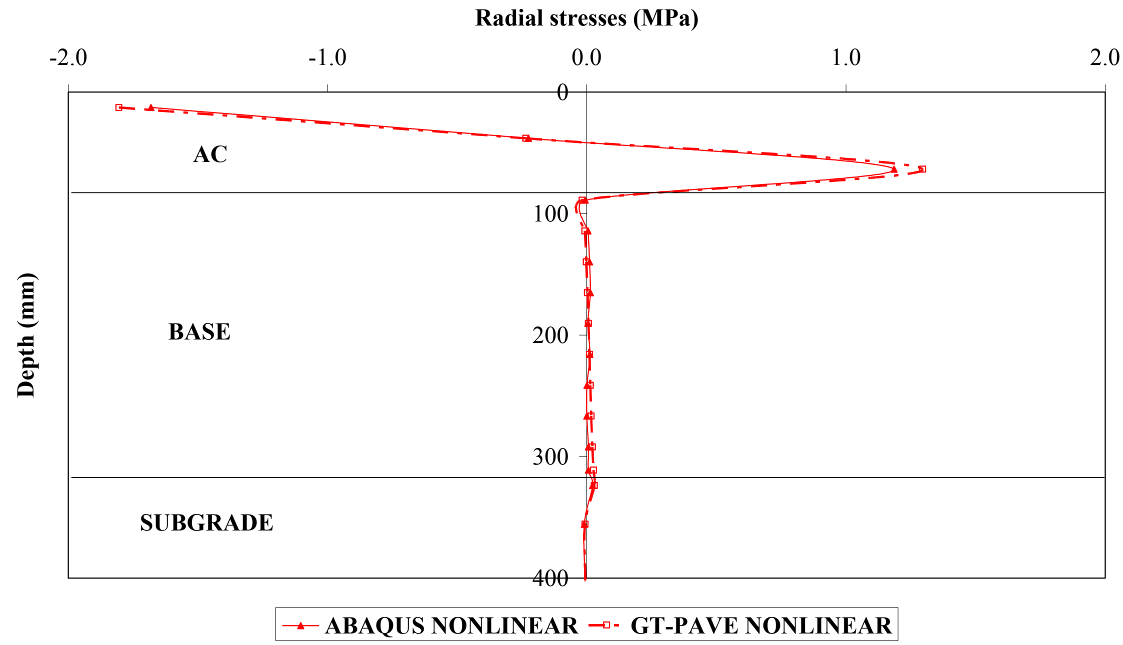


(a) 76-mm AC and 254-mm base section

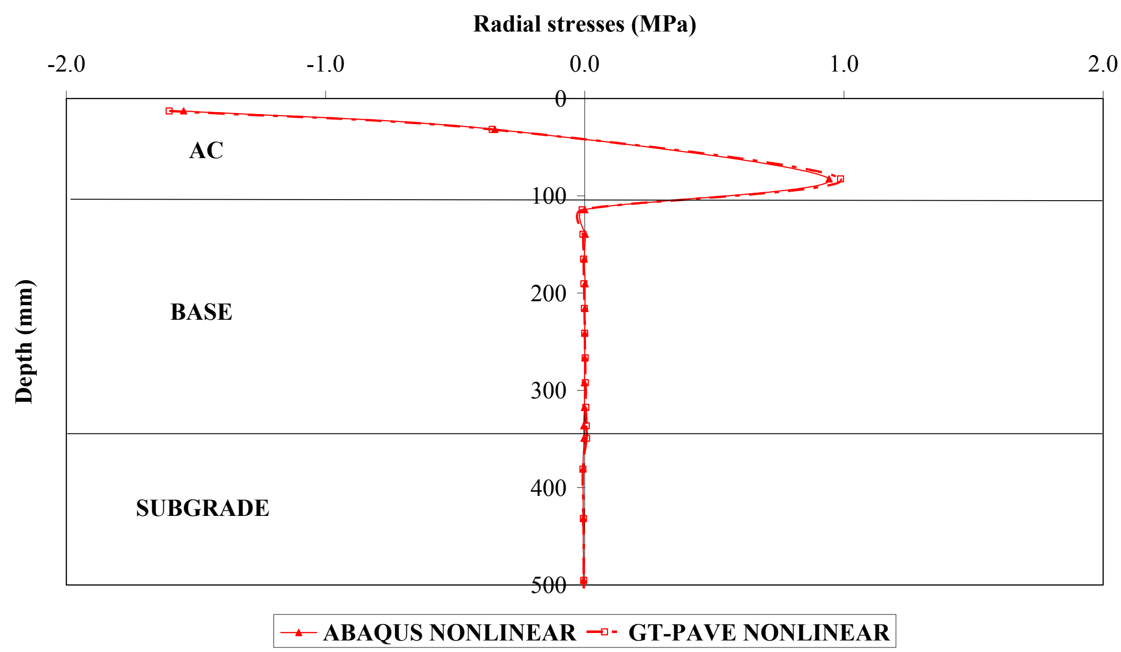


(b) 102-mm AC and 254-mm base section

Figure 5-7 Predicted Radial Stress Distributions at the Centerline of Loading

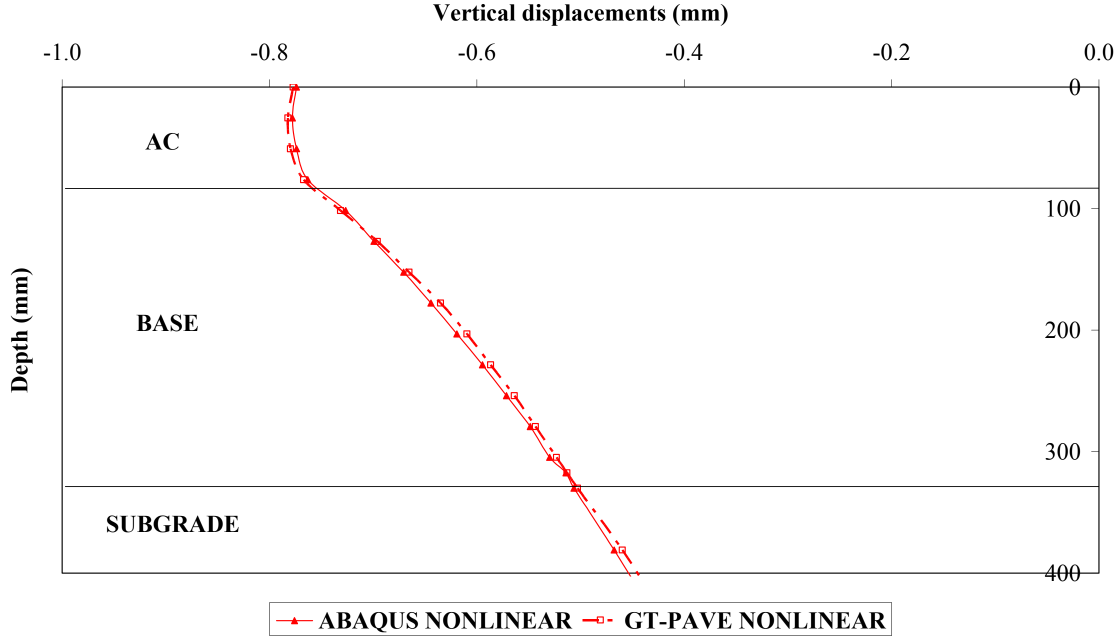


(a) 76-mm AC and 254-mm base section

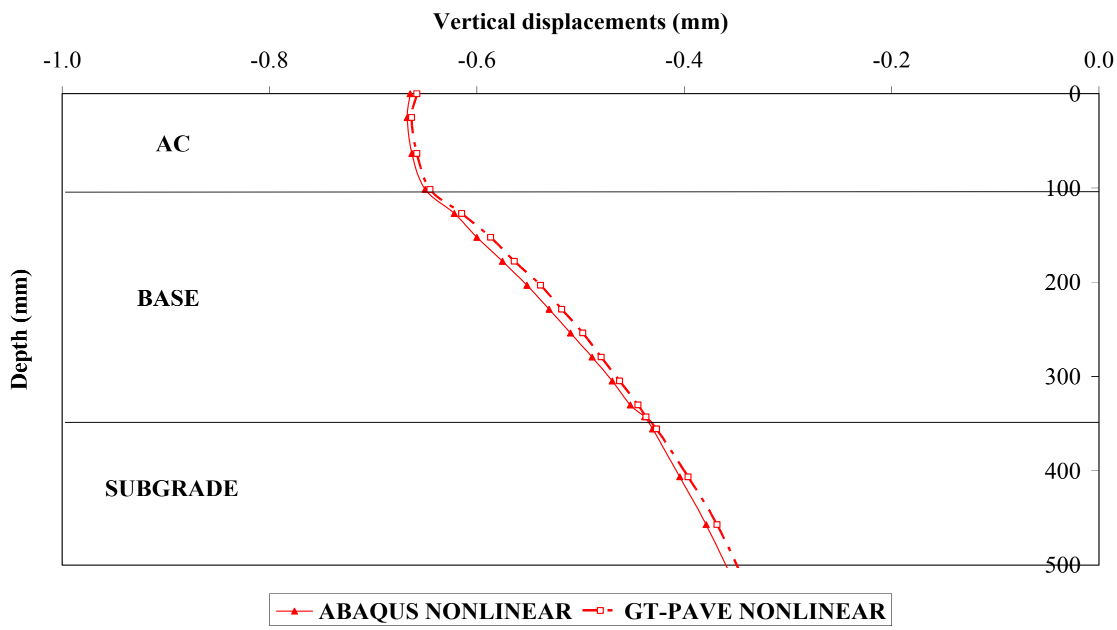


(b) 102-mm AC and 254-mm base section

Figure 5-8 Predicted Vertical Displacement Distributions at the Centerline of Loading

Previous tables and figures present the predicted critical pavement responses at the centerline of loading by the different combinations of ABAQUS$^{TM}$ and GT-PAVE finite element linear and nonlinear analyses. Overall, the two nonlinear finite element analysis programs were in very good agreement producing the same responses for each case, thus verifying the applicability of the developed the ABAQUS$^{TM}$ user defined material model subroutine to nonlinear pavement analysis.

Figure 5-9 shows the modulus distributions of the 76-mm AC and 254-mm base pavement section. The resilient moduli were obtained from the results with both nonlinear base and nonlinear subgrade cases. The two contour plots show very similar modulus distributions throughout the nonlinear base and subgrade layers to further verify and confirm the nonlinear analysis predictions of the developed material user subroutine.

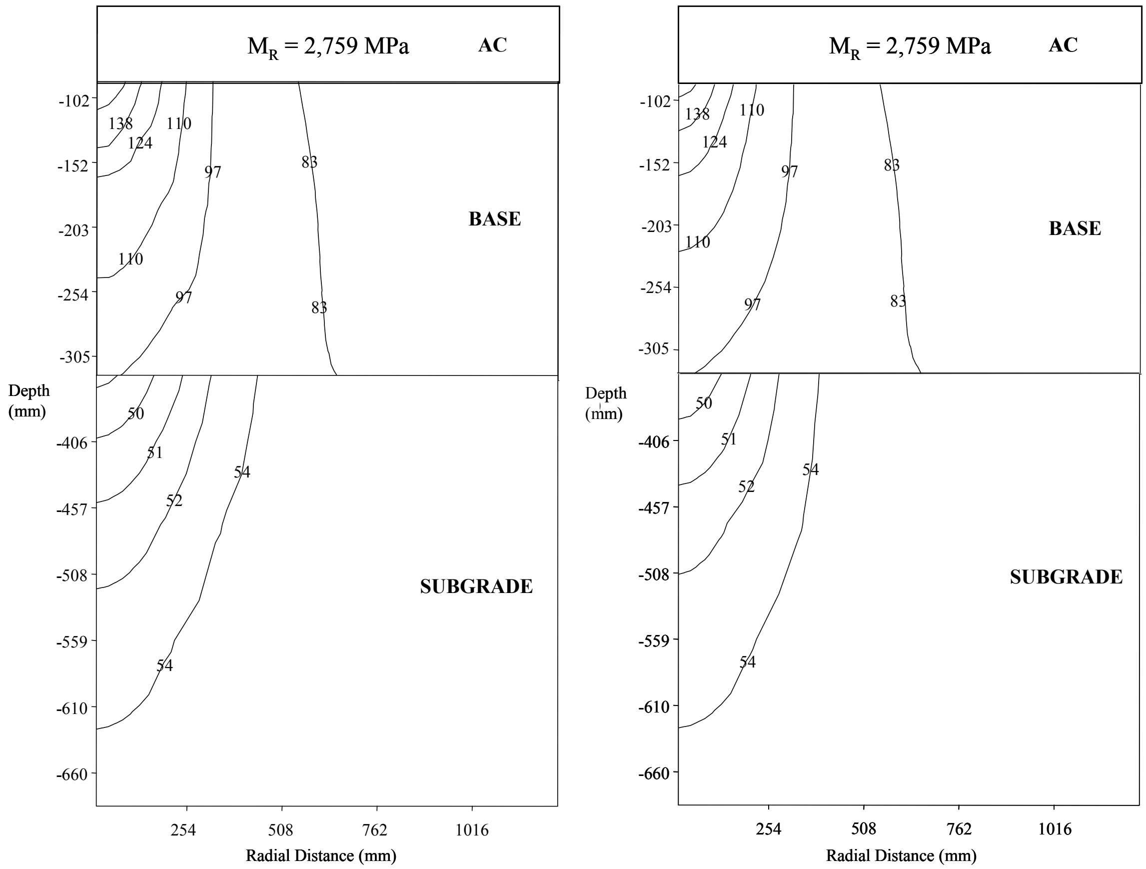


(a) ABAQUS (b) GT-PAVE

Figure 5-9 Predicted Vertical Modulus Distributions in the Base and Subgrade

### 5.2.2 Investigation of Additional Pavement Geometries and Domain Sizes in Axisymmetric Finite Element Analysis

After verifying, the axisymmetric ABAQUS™ analyses with nonlinear pavement foundation geomaterials with the results of the GT-PAVE finite element analyses, another conventional flexible pavement was analyzed as an axisymmetric solid consisting of linear and nonlinear elastic layers in order to employ the nonlinear response models in both the ABAQUS™ and GT-PAVE finite element programs. The investigated finite element models here had a domain size of 20-times the radius of loading area in the horizontal direction and 140-times the radius of loading area in the vertical direction with regular elements shown in Figure 4-6(a). Table 5-6 summarizes the pavement geometry and assigned material input properties. 300-second order elements and 981-nodes were used in the axisymmetric finite element mesh. A uniform pressure of 0.55-MPa was applied over the circular area with a radius of 152-mm Pavement responses were again predicted from the ABAQUS$^{TM}$ and GT-PAVE solutions for the following pavement layer material characterizations with isotropic and linear elastic asphalt concrete material: (1) nonlinear base and linear subgrade, (2) linear base and nonlinear subgrade, and (3) nonlinear base and nonlinear subgrade.

Table 5-6 Material Properties used in the Nonlinear Finite Element Analyses

<table>
<tr><th>Section</th><th>Element</th><th>Thickness (mm)</th><th>E (MPa)</th><th>ν</th><th colspan="4">Material Properties</th></tr>
<tr><td>AC</td><td>8-noded solid</td><td>76 or 102</td><td>2759</td><td>0.35</td><td colspan="4">Isotropic and Linear Elastic</td></tr>
<tr><td rowspan="3">Base</td><td rowspan="3">8-noded solid</td><td rowspan="3">254, 305, or 457</td><td rowspan="3">207 (initial)</td><td rowspan="3">0.40</td><td colspan="4">Nonlinear: Uzan model (Uzan, 1985)</td></tr>
<tr><td colspan="2">$K_1$ (kPa)</td><td>$K_2$</td><td>$K_3$</td></tr>
<tr><td colspan="2">4,100</td><td>0.64</td><td>0.065</td></tr>
<tr><td rowspan="3">Subgrade</td><td rowspan="3">8-noded solid</td><td rowspan="3">20802, 20980, or 20955</td><td rowspan="3">41 (initial)</td><td rowspan="3">0.45</td><td colspan="4">Nonlinear: Bilinear model (Thompson and Robnett, 1979)</td></tr>
<tr><td>$E_{RI}$ (kPa)</td><td>$\sigma_{di}$ (kPa)</td><td>$K_3$ (kPa/kPa)</td><td>$K_4$ (kPa/kPa)</td></tr>
<tr><td>41,400</td><td>41</td><td>1,000</td><td>200</td></tr>
</table>

Table 5-7 through Table 5-9 compare pavement responses predicted by the nonlinear analyses from ABAQUS$^{TM}$ and GT-PAVE programs. Table 5-7 shows predicted pavement responses from the 76-mm AC and 305-mm base section whereas,

Table 5-8 shows predicted pavement responses from the 102-mm AC and 254-mm base section. The computed pavement responses further agreed between the ABAQUS™ and GT-PAVE solutions. Table 5-9 shows the predicted pavement responses from the 76-mm AC and 457-mm base section. Again, the two nonlinear finite element analysis programs are in very good agreement producing the same responses. This also indicates the validation of nonlinear solution approach for the developed UMAT subroutine. Especially, thin AC surfaced pavements for low volume roads were considered to represent the more drastic influence of nonlinear resilient behavior in the base and subgrade layers in all analyses.

Table 5-7 Predicted Pavement Responses of 76-mm AC and 305-mm Base Section

| 76-mm AC and 305-mm base section | | | | | | |
|---|---|---|---|---|---|---|
| Pavement Response | Nonlinear base and linear subgrade | | Linear base and nonlinear subgrade | | Nonlinear base and nonlinear subgrade | |
| | ABAQUS | GT-PAVE | ABAQUS | GT-PAVE | ABAQUS | GT-PAVE |
| $\delta_{\text{surface}}$ (mm) | -1.240 | -1.240 | -0.757 | -0.754 | -0.968 | -0.965 |
| $\delta_{\text{top of subgrade}}$ (mm) | -0.945 | -0.942 | -0.513 | -0.511 | -0.671 | -0.668 |
| $\sigma_{r \text{ bottom of AC}}$ (MPa) | 0.873 | 0.955 | 0.772 | 0.773 | 0.846 | 0.907 |
| $\sigma_{v \text{ top of subgrade}}$ (MPa) | -0.067 | -0.067 | -0.050 | -0.050 | -0.079 | -0.079 |
| $\varepsilon_{r \text{ bottom of AC}}$ ($\mu\varepsilon$) | 267 | 268 | 227 | 227 | 257 | 269 |
| $\varepsilon_{v \text{ top of subgrade}}$ ($\mu\varepsilon$) | -1203 | -1216 | -772 | -778 | -937 | -950 |

Table 5-8 Predicted Pavement Responses of 102-mm AC and 254-mm Base Section

| 102-mm AC and 254-mm base section | | | | | | |
|---|---|---|---|---|---|---|
| Pavement Response | Nonlinear base and linear subgrade | | Linear base and nonlinear subgrade | | Nonlinear base and nonlinear subgrade | |
| | ABAQUS | GT-PAVE | ABAQUS | GT-PAVE | ABAQUS | GT-PAVE |
| $\delta_{\text{surface}}$ (mm) | -1.113 | -1.113 | -0.688 | -0.686 | -0.864 | -0.861 |
| $\delta_{\text{top of subgrade}}$ (mm) | -0.887 | -0.881 | -0.513 | -0.511 | -0.630 | -0.630 |
| $\sigma_{r \text{ bottom of AC}}$ (MPa) | 1.148 | 1.164 | 0.852 | 0.854 | 1.081 | 1.119 |
| $\sigma_{v \text{ top of subgrade}}$ (MPa) | -0.060 | -0.060 | -0.048 | -0.048 | -0.071 | -0.071 |
| $\varepsilon_{r \text{ bottom of AC}}$ ($\mu\varepsilon$) | 310 | 302 | 234 | 234 | 292 | 293 |
| $\varepsilon_{v \text{ top of subgrade}}$ ($\mu\varepsilon$) | -1090 | -1113 | -730 | -738 | -837 | -845 |

Table 5-9 Predicted Pavement Responses of 76-mm AC and 457-mm Base Section

| 76-mm AC and 457-mm base section | | | | | | |
|---|---|---|---|---|---|---|
| Pavement Response | Nonlinear base and linear subgrade | | Linear base and nonlinear subgrade | | Nonlinear base and nonlinear subgrade | |
| | ABAQUS | GT-PAVE | ABAQUS | GT-PAVE | ABAQUS | GT-PAVE |
| $\delta_{\text{surface}}$ (mm) | -1.166 | -1.168 | -0.680 | -0.678 | -0.947 | -0.947 |
| $\delta_{\text{top of subgrade}}$ (mm) | -0.747 | -0.747 | -0.389 | -0.386 | -0.521 | -0.523 |
| $\sigma_{r\text{ bottom of AC}}$ (MPa) | 0.848 | 0.922 | 0.743 | 0.743 | 0.837 | 0.903 |
| $\sigma_{v\text{ top of subgrade}}$ (MPa) | -0.040 | -0.040 | -0.030 | -0.030 | -0.040 | -0.039 |
| $\varepsilon_{r\text{ bottom of AC}}$ ($\mu\varepsilon$) | 247 | 260 | 221 | 221 | 241 | 253 |
| $\varepsilon_{v\text{ top of subgrade}}$ ($\mu\varepsilon$) | -839 | -831 | -470 | -469 | -580 | -572 |

### 5.2.3 Comparisons of Linear and Nonlinear Finite Element Analyses

Nonlinear ABAQUS™ axisymmetric finite element analysis results were next compared to linear elastic analysis solutions to draw conclusions and emphasize the importance of proper nonlinear stress-dependent geomaterial characterizations. A number of findings can be drawn.

The results show that the nonlinear base has a considerable influence on the pavement responses. The case of only nonlinear base material characterization has a remarkable effect on critical pavement responses, especially, tensile strain at the bottom of the AC and vertical strain on the top of subgrade. Nonlinear characterization of the base material caused a maximum increase of 29% in the tensile strain at the bottom of the AC, 49% in the vertical strain on the top of subgrade, and 44% in the surface deflection. The nonlinearity of subgrade also affects the critical pavement responses. The nonlinear subgrade characteristics resulted in 23% decrease in the vertical subgrade strain and 26% decrease in the surface deflection. On the other hand, the nonlinearity of subgrade soils had a little impact on the tensile strain at the bottom of the AC. Since these differences resulted from particular case studies analyzed in this research, these differences can vary on different modeling conditions. Table 5-10 shows the predicted critical pavement responses in each case. For the combined nonlinear base and subgrade characterizations, the most accurate pavement responses, still considerably different from the linear elastic solutions, were predicted especially for the tensile strain at the bottom of asphalt concrete and the vertical strain on the top of subgrade. Note that these differences in pavement responses, in these cases specific to the pavement geometries, layer material properties and the loading condition considered, were contrasted to demonstrate the important effects nonlinear pavement foundation modeling.

Table 5-10 Comparisons of Predicted Critical Pavement Responses

| 76-mm AC and 305-mm base section | | | | |
|---|---|---|---|---|
| Pavement Response | Linear base and linear subgrade | Nonlinear base and linear subgrade | Linear base and nonlinear subgrade | Nonlinear base and nonlinear subgrade |
| $\delta_{\text{surface}}$ (mm) | -0.930 | -1.240 | -0.757 | -0.968 |
| $\varepsilon_{\text{r bottom of AC}}$ ($\mu\varepsilon$) | 227 | 267 | 227 | 257 |
| $\varepsilon_{\text{v top of subgrade}}$ ($\mu\varepsilon$) | -932 | -1203 | -772 | -937 |
| 102-mm AC and 254-mm base section | | | | |
| Pavement Response | Linear base and linear subgrade | Nonlinear base and linear subgrade | Linear base and nonlinear subgrade | Nonlinear base and nonlinear subgrade |
| $\delta_{\text{surface}}$ (mm) | -0.866 | -1.113 | -0.688 | -0.864 |
| $\varepsilon_{\text{r bottom of AC}}$ ($\mu\varepsilon$) | 240 | 310 | 234 | 292 |
| $\varepsilon_{\text{v top of subgrade}}$ ($\mu\varepsilon$) | -896 | -1090 | -730 | -837 |
| 76-mm AC and 457-mm base section | | | | |
| Pavement Response | Linear base and linear subgrade | Nonlinear base and linear subgrade | Linear base and nonlinear subgrade | Nonlinear base and nonlinear subgrade |
| $\delta_{\text{surface}}$ (mm) | -0.968 | -1.166 | -0.680 | -0.947 |
| $\varepsilon_{\text{r bottom of AC}}$ ($\mu\varepsilon$) | 219 | 247 | 221 | 241 |
| $\varepsilon_{\text{v top of subgrade}}$ ($\mu\varepsilon$) | -560 | -839 | -470 | -580 |

## 5.3 Summary

To properly characterize the resilient response of geomaterials, i.e., coarse-grained unbound aggregates and fine-grained subgrade soils, the Uzan model (1985) type aggregate modulus stress dependency and a bilinear variation of subgrade soil modulus with deviator stress (Thompson and Robnett, 1979) were both programmed in a user defined material model subroutine in the general purpose ABAQUS$^{\text{TM}}$ finite element program. The stress- dependent characterizations of the base and subgrade layers were made part of the ABAQUS$^{TM}$ finite element nonlinear solutions for pavement analysis. To converge smoothly in each loading, a direct secant stiffness approach used in nonlinear analysis was found to be the most efficient and suitable to pavement analysis to characterize stress- dependent resilient behavior of geomaterials.

For a conventional flexible pavement analyzed, good agreements were achieved between the predicted pavement responses by the axisymmetric GT-PAVE and ABAQUS$^{TM}$ finite element programs. The pavement displacement and stress distributions predicted from the nonlinear analyses were also very similar and validated the nonlinear solution approach taken in the ABAQUS$^{TM}$ material model subroutine. Compared to the linear elastic solutions, i.e., one modulus assigned to the whole subgrade or base layer obtained from computing the nonlinear analysis, significantly different critical pavement responses, often directly linked to pavement deterioration modes in the context of mechanistic-empirical pavement design, were predicted when nonlinear analyses were performed in the aggregate base and fine-grained subgrade soil layers. Moreover, the analysis results from three pavement geometry case studies also demonstrated a considerable impact of nonlinear geomaterial behavior on the predicted critical pavement responses, i.e., tensile strain at the bottom of AC (asphalt concrete) linked fatigue cracking and vertical strain on the top of subgrade linked to rutting.

# Chapter 6 Three-dimensional Nonlinear Finite Element Analysis of Flexible Pavements

Many existing finite element flexible pavement models have been limited to axisymmetric analysis, although the actual pavement structure exists in full three dimensions. Two-dimensional analysis is often easier to generate meshes and requires less computation time and memory. However, many inherent limitations of two-dimensional analysis reduce the accuracy of the results. Although two-dimensional analyses have been prevalent, there is great demand for a three-dimensional model to solve the nonlinear pavement material problem currently. Moreover, two-dimensional stress analysis is known to be limited in its capacity especially for modeling different geometries, such as for a pavement geosynthetic layer having anisotropic properties on the horizontal plane, and loading conditions, such as multiple wheel loading scenarios, which do not fit with the axial symmetry assumptions.

The three-dimensional finite element method has been increasingly viewed as the best approach to analyze more accurately critical pavement responses by minimizing or eliminating shortcomings/assumptions of two-dimensional analysis. Three-dimensional behavior of structural systems has differences with that of two-dimensional. The analysis in three-dimensional space is more complex than in axisymmetric space because extra coupling can occur in additional direction that is not included in two-dimensional analysis. The three-dimensional structural analysis, however, is more expensive due to the large problem size caused by extra degrees of freedom. Three-dimensional finite element analysis of flexible pavements is currently the state-of-the-art structural analysis approach.

The accuracy of three-dimensional finite element analysis is dependent on the geometric characteristics and mesh refinements which include element aspect ratio and smooth transition of elements. Particularly, the mesh generation of three-dimensional finite element pavement model has some difficulties because the applied wheel load is localized and each layer is relatively thin compared with infinite horizontal and vertical domains. The computational time is also governed by the number of elements used in two and three-dimensional models along each axis, $n^2$ and $n^3$, respectively. Therefore, well constructed meshes are essential for proper three-dimensional pavement analysis. With the advent of the development of finite element techniques and computer capabilities, a well-developed three-dimensional finite element model is capable of analyzing complex engineering problems. In this study, the ABAQUS™ general purpose finite element program has been used to develop a powerful and versatile three-dimensional model for analysis of flexible pavements.

This chapter will discuss the development of proper material characterizations in the three-dimensional finite element analysis and examine effects of geomaterial nonlinearity on pavement response predictions. Various implications of the nonlinear, stress-dependent geomaterial modulus characterizations will be also shown using three-dimensional pavement analysis.

### 6.1 Comparisons of Linear and Nonlinear Finite Element Analyses

The generated three-dimensional finite element mesh, consisting of 15,168 20-noded hexahedron elements and 67,265 nodes, is shown in Figure 4-5. The area subjected to wheel loading had a finer mesh to simulate an almost perfectly circular loading region, which gradually transitioned into to a square mesh construction. The lateral remote boundaries were truncated at a distance of 3,048-mm, 20-times radius of loading (R) away from the center of the loading, and the total depth of the pavement structure was taken as 21,336-mm, 140-times R.

As shown in Chapter 4, to verify the accuracy of the three-dimensional finite element pavement model, the linear elastic solutions were first obtained from both the ABAQUS$^{TM}$ axisymmetric and the three-dimensional finite element analyses. Like in the axisymmetric cases, a uniform pressure of 0.55-MPa was applied in the three-dimensional finite element analyses over the circular area of 152-mm radius. The pavement geometry and the linear elastic layer input properties listed in Table 4-5 were also assigned in this study with the exception of the 20-noded solid elements used in the three-dimensional finite element analysis instead of the 8-noded quadrilateral elements.

The computing time depends on the complexity of nonlinear pavement analysis and the number of nodes and elements used in the finite element mesh. The computing time for axisymmetric analysis using nonlinear base and nonlinear subgrade materials was less than 60 seconds. One three-dimensional nonlinear analysis took approximately 20,000 seconds or 5.6 hours using a 266-Mhz Pentium 4 computer system with a 2-Gbyte RAM.

Results were summarized in Table 4-6 to show the differences in predicted responses between the axisymmetric and three-dimensional analyses for the linear elastic case studied. Overall, the differences in predicted pavement responses are quite small with the largest being for the surface deflection not more than 3%. Some of the critical pavement responses, such as the horizontal tensile stress ($\sigma_h$) at the bottom of AC and vertical strain ($\varepsilon_v$) on the top of subgrade are even less than 1%. These comparisons between the linear axisymmetric and three-dimensional analyses are in general quite acceptable especially when considering all the assumptions made in the axisymmetric finite element formulations and the circular shaped mesh discretization concerns for the wheel loading. Therefore, the developed three-dimensional finite element model was deemed accurate enough to study next the nonlinear pavement foundation modeling concepts in three-dimensional finite element analysis of flexible pavements.

To perform three-dimensional nonlinear finite element analysis, the universal octahedral shear stress model (Witczak and Uzan, 1988) given in Equation 2-18 was used for the unbound aggregate base while the bilinear model (Thompson and Robnett, 1979) was utilized in the fine-grained subgrade as the ABAQUS™ UMAT inputs. The Uzan aggregate base model (Uzan, 1985) was used earlier in all the axisymmetric finite element analyses. However, the universal octahedral shear stress model (Witczak and Uzan, 1988) with the octahedral shear stress ($\tau_{oct}$) term, at this time, had to be utilized in the three-dimensional analyses since the three-dimensional pavement finite element model had the consideration for all three directional components including the intermediate principal stress ($\sigma_2$) now different than the minor principal stress ($\sigma_3$). This difference between the two aggregate base models inherently would be responsible for differences in predicted responses.

The universal octahedral shear stress model is in the same form as originally developed by the Uzan model (Uzan, 1985). This model considers octahedral shear stress ($\tau_{oct}$) to characterize three-dimensional properties instead of deviator stress ($\sigma_d$). To make the model dimensionally consistent, atmospheric pressure was also used in this model. The Uzan model parameters are shown in Table 5-6 and the universal octahedral shear stress model is shown in Table 6-1. The parameters of universal octahedral shear stress model (Witczak and Uzan, 1988) were correlated to the Uzan model (Uzan, 1985) using the same repeated load triaxial test data.

Pavement responses were predicted from the ABAQUS$^{TM}$ for the following pavement layer material characterizations with isotropic and linear elastic AC material: (1) nonlinear base and linear subgrade, (2) linear base and nonlinear subgrade, and (3) nonlinear base and nonlinear subgrade. The same uniform pressure of 0.55-MPa is applied over the circular area with a radius of 152-mm and an investigated three-layered pavement section consists of three-dimensional finite element model with details shown in Table 6-1.

Table 6-1 Pavement Layer Thicknesses and Material Properties used in the Three-dimensional Nonlinear Finite Element Analyses

<table>
<tr><th>Section</th><th>Element</th><th>Thickness (mm)</th><th>E (MPa)</th><th>$\nu$</th><th colspan="4">Material Properties</th></tr>
<tr><td>AC</td><td>20-noded solid</td><td>76 or 102</td><td>2,759</td><td>0.35</td><td colspan="4">Isotropic and Linear Elastic</td></tr>
<tr><td rowspan="3">BASE</td><td rowspan="3">20-noded solid</td><td rowspan="3">254, 305, or 457</td><td rowspan="3">207 (initial)</td><td rowspan="3">0.40</td><td colspan="4">Nonlinear: Universal Model with octahedral shear stress, $\tau_{oct}$ (Witczak and Uzan, 1988)</td></tr>
<tr><td colspan="2">$K_1$</td><td>$K_2$</td><td>$K_3$</td></tr>
<tr><td colspan="2">1,940</td><td>0.64</td><td>0.065</td></tr>
<tr><td rowspan="3">SUBGRADE</td><td rowspan="3">20-noded solid</td><td rowspan="3">20,802, 20,980, or 20,955</td><td rowspan="3">41.4 (initial)</td><td rowspan="3">0.45</td><td colspan="4">Nonlinear: Bilinear model (Thompson and Robnett, 1979)</td></tr>
<tr><td>$E_{RI}$ (kPa)</td><td>$\sigma_{di}$ (kPa)</td><td>$K_3$ (kPa/kPa)</td><td>$K_4$ (kPa/kPa)</td></tr>
<tr><td>41,400</td><td>41</td><td>1,000</td><td>200</td></tr>
</table>

Table 6-2 and Table 6-3 compare pavement responses predicted by the linear and nonlinear analyses from ABAQUS$^{TM}$ three-dimensional modeling. Table 6-2 presents vertical stresses predicted at the center of loading and Table 6-3 lists radial stresses at the center of loading. As indicated in both tables, nonlinear analysis results are considerably different from the linear elastic solutions for the predicted vertical and horizontal stresses.

Table 6-2 Predicted Vertical Stresses at the Center of Loading

| 76-mm AC and 305-mm base section | | | | |
|---|---|---|---|---|
| Pavement Response | Linear base and linear subgrade | Nonlinear base and linear subgrade | Linear base and nonlinear subgrade | Nonlinear base and nonlinear subgrade |
| Top surface (MPa) | -0.524 | -0.550 | -0.525 | -0.549 |
| Bottom of AC (MPa) | -0.355 | -0.515 | -0.357 | -0.499 |
| Top of base (MPa) | -0.296 | -0.468 | -0.300 | -0.462 |
| Bottom of base (MPa) | -0.045 | -0.089 | -0.055 | -0.085 |
| Top of subgrade (MPa) | -0.040 | -0.064 | -0.050 | -0.079 |

Table 6-3 Predicted Horizontal Stresses at the Center of Loading

| 76-mm AC and 305-mm base section | | | | |
|---|---|---|---|---|
| Pavement Response | Linear base and linear subgrade | Nonlinear base and linear subgrade | Linear base and nonlinear subgrade | Nonlinear base and nonlinear subgrade |
| Top surface (MPa) | -1.483 | -1.330 | -1.418 | -1.267 |
| Bottom of AC (MPa) | 0.770 | 0.717 | 0.768 | 0.684 |
| Top of base (MPa) | -0.068 | -0.020 | -0.072 | -0.028 |
| Bottom of base (MPa) | 0.107 | 0.152 | 0.079 | 0.067 |
| Top of subgrade (MPa) | -0.002 | -0.020 | -0.002 | -0.015 |

Table 6-4 and Table 6-5 compare pavement responses predicted by the linear and nonlinear analyses from ABAQUS™ three-dimensional modeling. Table 6-4 presents the vertical deflection predictions at the center of loading and Table 6-5 lists predicted strains. Again, the significantly different results were predicted according to the linear and nonlinear material characterizations.

Table 6-4 Predicted Vertical Deflections at the Center of Loading

| 76-mm AC and 305-mm base section | | | | |
|---|---|---|---|---|
| Pavement Response | Linear base and linear subgrade | Nonlinear base and linear subgrade | Linear base and nonlinear subgrade | Nonlinear base and nonlinear subgrade |
| Top surface (mm) | -0.909 | -1.163 | -0.744 | -0.922 |
| Top of base (mm) | -0.904 | -1.155 | -0.737 | -0.912 |
| Top of subgrade (mm) | -0.660 | -0.907 | -0.500 | -0.665 |

Table 6-5 Predicted Strains at the Center of Loading

| 76-mm AC and 305-mm base section | | | | |
|---|---|---|---|---|
| Pavement Response | Linear base and linear subgrade | Nonlinear base and linear subgrade | Linear base and nonlinear subgrade | Nonlinear base and nonlinear subgrade |
| $\varepsilon_{h\ \mathrm{bottom\ of\ AC}}(\mu\varepsilon)$ | 227 | 235 | 226 | 225 |
| $\varepsilon_{v\ \mathrm{top\ of\ subgrade}}(\mu\varepsilon)$ | -930 | -1126 | -770 | -946 |

As indicated in the Table 6-2 through Table 6-5, nonlinear finite element analyses have different results from those of linear analyses. The largest difference was obtained between the linear and nonlinear base analysis cases. Nonlinear characterization of the base course material causes the maximum increases of 3% in the tensile strain at the bottom of the AC, 21% in the vertical strain on the top of subgrade, and 36% in the surface deflections. The nonlinearity of subgrade also affects the critical pavement responses. The nonlinear subgrade characteristics resulted in 17% decrease in the vertical strain and 18% decrease in the surface deflection. On the other hand, the nonlinearity of subgrade soils had little impact on the tensile strain at the bottom of the AC. Since these differences result from particular case studies with specific pavement layer thicknesses and material properties considered, the differences in predictions were expected to vary considerably for different input properties as well. Figure 6-1 through Figure 6-3 show the pavement responses predicted at the centerline of loading in the AC, base, and subgrade layers as obtained from the three different pavement layer material characterization cases.

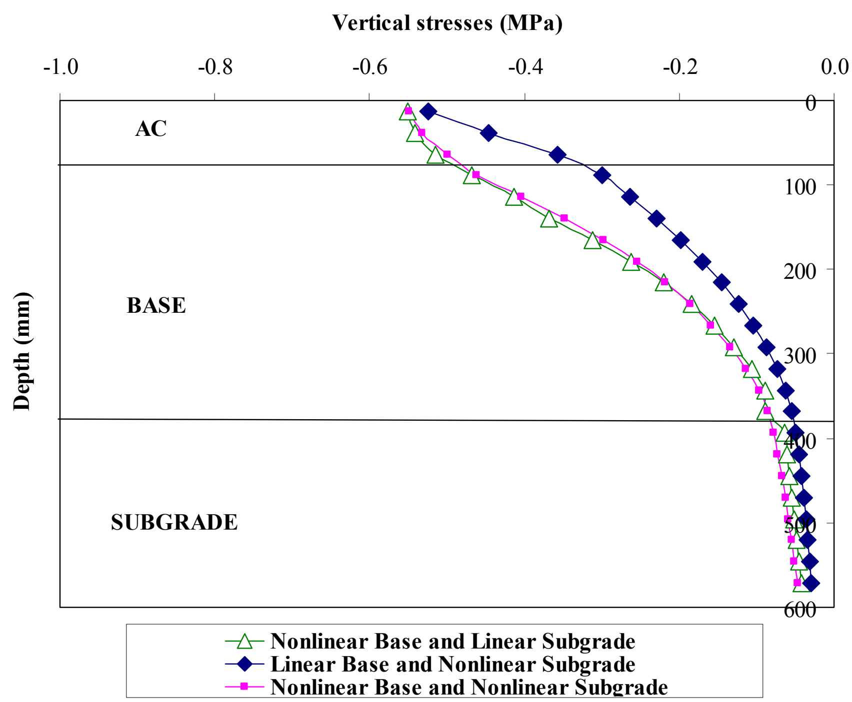


Figure 6-1 Predicted Vertical Stress Distributions at the Centerline of Loading

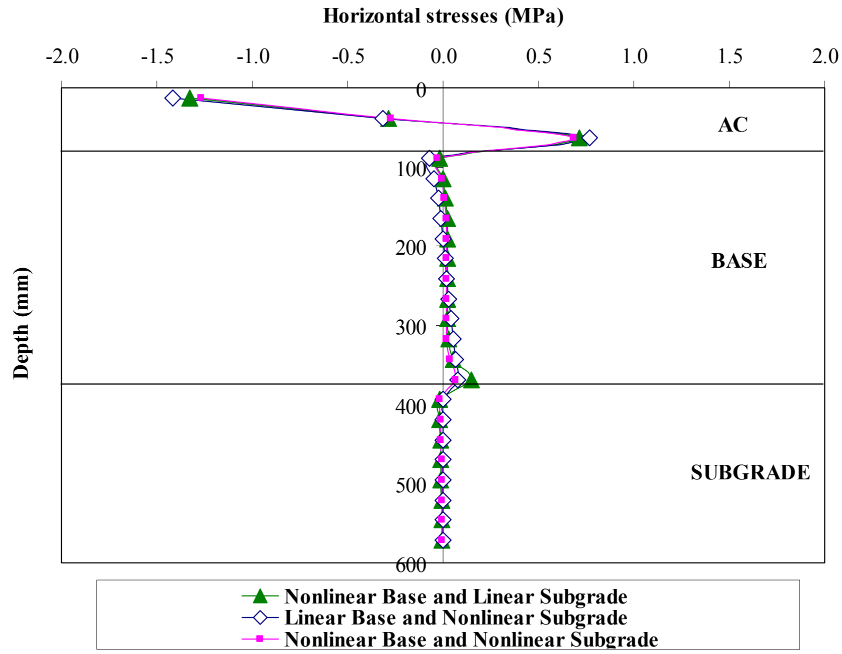


Figure 6-2 Predicted Horizontal Stress Distributions at the Centerline of Loading

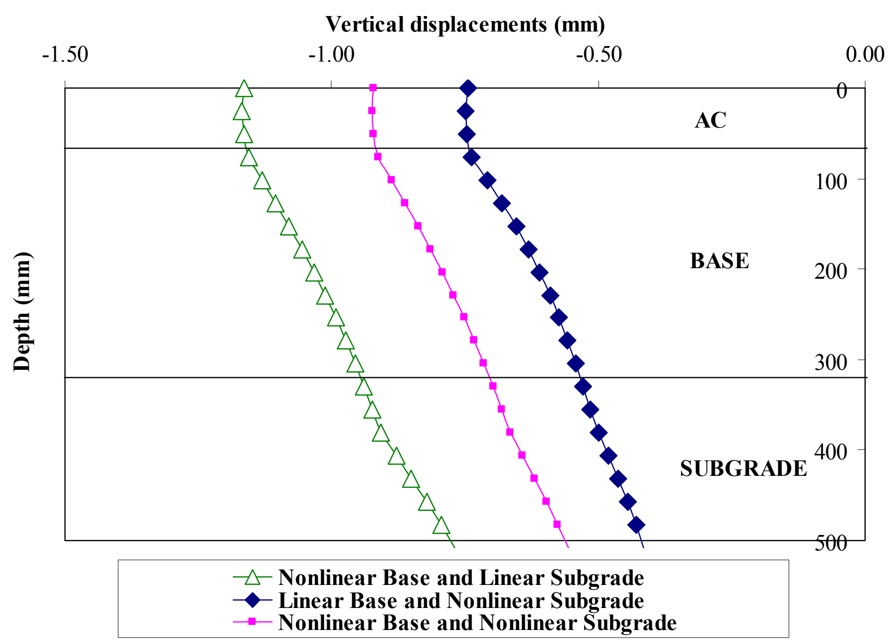


Figure 6-3 Predicted Vertical Displacement Distributions at the Centerline of Loading

Furthermore, Table 6-6 and Table 6-7 list the predicted critical pavement responses for the different analysis cases. The case of 102-mm AC and 254-mm base section is given in Table 6-6 and the case of 76-mm AC and 457-mm base section is presented in Table 6-7.

Table 6-6 Comparisons of Predicted Critical Pavement Responses

| 102-mm AC and 254-mm base section | | | | |
|---|---|---|---|---|
| Pavement Response | Linear base and linear subgrade | Nonlinear base and linear subgrade | Linear base and nonlinear subgrade | Nonlinear base and nonlinear subgrade |
| $\delta_{\text{surface}}$ (mm) | -0.846 | -1.059 | -0.676 | -0.833 |
| $\delta_{\text{top of subgrade}}$ (mm) | -0.665 | -0.861 | -0.500 | -0.630 |
| $\sigma_{\text{h bottom of AC}}$ (MPa) | 0.876 | 1.009 | 0.858 | 0.961 |
| $\varepsilon_{\text{h bottom of AC}}$ ($\mu\varepsilon$) | 239 | 283 | 235 | 270 |
| $\sigma_{\text{v top of subgrade}}$ (MPa) | -0.039 | -0.059 | -0.048 | -0.073 |
| $\varepsilon_{\text{v top of subgrade}}$ ($\mu\varepsilon$) | -895 | -1043 | -737 | -844 |

Table 6-7 Comparisons of Predicted Critical Pavement Responses

| 76-mm AC and 457-mm base section | | | | |
|---|---|---|---|---|
| Pavement Response | Linear base and linear subgrade | Nonlinear base and linear subgrade | Linear base and nonlinear subgrade | Nonlinear base and nonlinear subgrade |
| $\delta_{surface}$ (mm) | -0.787 | -1.118 | -0.668 | -0.922 |
| $\delta_{top\ of\ subgrade}$ (mm) | -0.495 | -0.765 | -0.378 | -0.564 |
| $\sigma_{h\ bottom\ of\ AC}$ (MPa) | 0.731 | 0.644 | 0.747 | 0.646 |
| $\varepsilon_{h\ bottom\ of\ AC}$ ($\mu\varepsilon$) | 218 | 219 | 221 | 216 |
| $\sigma_{v\ top\ of\ subgrade}$ (MPa) | -0.024 | -0.047 | -0.029 | -0.056 |
| $\varepsilon_{v\ top\ of\ subgrade}$ ($\mu\varepsilon$) | -559 | -876 | -467 | -685 |

From the results of 102-mm AC and 254-mm base section analysis, nonlinear characterization of the base layer material caused a maximum increase of 18% in the tensile strain at the bottom of the AC, 17% in the vertical strain on the top of subgrade, and 25% in the surface deflection. The nonlinearity of subgrade also affects the critical pavement responses. The nonlinear subgrade characteristics resulted in 18% decrease in the vertical strain and 20% decrease in the surface deflection. The nonlinearity of subgrade soils had little impact on the tensile strain at the bottom of the AC. Moreover, from the results of 76-mm AC and 457-mm base section analysis, nonlinear characterization of the base material caused the maximum increases of only 1% in the tensile strain at the bottom of the AC, 57% in the vertical strain on top of the subgrade, and 42% in the surface deflection. The nonlinear subgrade characteristics resulted in 17% decrease in the vertical strain and 15% decrease in the surface deflection. For the combined nonlinear base and subgrade characterizations, one can clearly see the differences from the linear elastic solutions. Note that these differences in pavement responses, in these specific cases of pavement geometries and layer material properties, were computed from particular case studies. Nonlinear finite element analyses should result in more accurate critical pavement responses and these analyses are essential to realistic pavement responses.

## 6.2 Comparisons of Axisymmetric and Three-dimensional Finite Element Analyses

Comparisons were made between axisymmetric and three-dimensional analysis results emphasizing the importance of nonlinear geomaterial characterizations on the predicted critical pavement responses in contrast to linear elastic results. Table 6-8 lists the layer thicknesses and material properties including the nonlinear model parameters assigned to comparison study of axisymmetric and three-dimensional analyses of three pavement geometry cases. The finite element models for this study are shown in Figure 4-6.

Table 6-8 Pavement Layer Thicknesses and Material Properties used in the Comparison Study of Nonlinear Finite Element Analyses

<table>
<tr><th>Section</th><th>Element</th><th>Thickness (mm)</th><th>$\nu$</th><th colspan="4">Material Properties</th></tr>
<tr><td>AC</td><td>8-noded solid, 20-noded solid</td><td>76 or 102</td><td>0.35</td><td colspan="4">Isotropic and Linear Elastic<br>(E = 2,759-MPa)</td></tr>
<tr><td rowspan="6">BASE</td><td rowspan="6">8-noded solid, 20-noded solid</td><td rowspan="6">254, 305, or 457</td><td rowspan="6">0.40</td><td colspan="4">Nonlinear (Axisymmetric)<br>: Uzan model (Uzan, 1985)</td></tr>
<tr><td colspan="2">$K_1$ (kPa)</td><td>$K_2$ (kPa)</td><td>$K_3$ (kPa)</td></tr>
<tr><td colspan="2">4,100</td><td>0.64</td><td>0.065</td></tr>
<tr><td colspan="4">Nonlinear (Three-dimensional) : Universal Model with octahedral shear stress, $\tau_{oct}$ (Witczak and Uzan, 1988)</td></tr>
<tr><td colspan="2">$K_1$</td><td>$K_2$</td><td>$K_3$</td></tr>
<tr><td colspan="2">1,940</td><td>0.64</td><td>0.065</td></tr>
<tr><td rowspan="3">SUBGRADE</td><td rowspan="3">8-noded solid, 20-noded solid</td><td rowspan="3">20,802, 20,980, or 20,955</td><td rowspan="3">0.45</td><td colspan="4">Nonlinear: Bilinear model<br>(Thompson and Robnett, 1979)</td></tr>
<tr><td>$E_{RI}$ (kPa)</td><td>$\sigma_{di}$ (kPa)</td><td>$K_3$ (kPa/kPa)</td><td>$K_4$ (kPa/kPa)</td></tr>
<tr><td>41,400</td><td>41</td><td>1,000</td><td>200</td></tr>
</table>

Pavement responses were predicted from the ABAQUS three-dimensional analyses with the linear elastic AC layer and for the following pavement geomaterial layer characterizations: (i) nonlinear base and linear subgrade and (ii) nonlinear base and nonlinear subgrade. Table 6-9 gives detailed comparisons of the predicted critical pavement responses for all the three pavement geometry cases studied between the three-dimensional finite element analysis results and the axisymmetric finite element analysis results. From the comparisons of base characterized nonlinear only, surface deflections were somewhat different by up to 6%, tensile strains at the bottom of AC up to 12%, vertical deviator stresses on the top subgrade up to 18%, and vertical strains on the top of subgrade by up to 6%. However, each response variable did not consistently increase or decrease between the two analyses. For the combined nonlinear base and subgrade results, the predicted responses from the axisymmetric and the three-dimensional finite element analyses show 5% difference of surface deflection, 12% difference of tensile strains at the bottom of AC, and 18% difference of vertical strains on the top of subgrade.

Table 6-9 Predicted Critical Pavement Responses between Three-dimensional and Axisymmetric Nonlinear Finite Element Analyses

| Case (1): 76 mm AC and 305 mm base | | | | |
|---|---|---|---|---|
| Pavement Response | Nonlinear base and linear subgrade | | Nonlinear base and nonlinear subgrade | |
| | Axisymmetric | Three-dimensional | Axisymmetric | Three-dimensional |
| $\delta_{\text{surface}}$ (mm) | -1.240 | -1.163 (-6%)* | -0.968 | -0.922 (-5%) |
| $\varepsilon_{\text{h bottom of AC}}$ ($\mu\varepsilon$) | 267 | 235 (-12%) | 257 | 225 (-12%) |
| $\sigma_{\text{v top of subgrade}}$ (MPa) | -0.067 | -0.064 (-4%) | -0.080 | -0.079 (-1%) |
| $\varepsilon_{\text{v top of subgrade}}$ ($\mu\varepsilon$) | -1,203 | -1,126 (-6%) | -937 | -946 (+1%) |
| **Case (2): 102 mm AC and 254 mm base** | | | | |
| Pavement Response | Nonlinear base and linear subgrade | | Nonlinear base and nonlinear subgrade | |
| | Axisymmetric | Three-dimensional | Axisymmetric | Three-dimensional |
| $\delta_{\text{surface}}$ (mm) | -1.113 | -1.059 (-5%) | -0.864 | -0.833 (-4%) |
| $\varepsilon_{\text{h bottom of AC}}$ ($\mu\varepsilon$) | 310 | 283 (-9%) | 292 | 270 (-8%) |
| $\sigma_{\text{v top of subgrade}}$ (MPa) | -0.060 | -0.059 (-2%) | -0.071 | -0.073 (+3%) |
| $\varepsilon_{\text{v top of subgrade}}$ ($\mu\varepsilon$) | -1,090 | 1,043 (-4%) | -837 | -844 (+1%) |
| **Case (3): 76 mm AC and 457 mm base** | | | | |
| Pavement Response | Nonlinear base and linear subgrade | | Nonlinear base and nonlinear subgrade | |
| | Axisymmetric | Three-dimensional | Axisymmetric | Three-dimensional |
| $\delta_{\text{surface}}$ (mm) | -1.166 | -1.118 (-4%) | -0.947 | -0.922 (-3%) |
| $\varepsilon_{\text{h bottom of AC}}$ ($\mu\varepsilon$) | 247 | 219 (-11%) | 241 | 216 (-10%) |
| $\sigma_{\text{v top of subgrade}}$ (MPa) | -0.040 | -0.047 (+18%) | -0.055 | -0.056 (+2%) |
| $\varepsilon_{\text{v top of subgrade}}$ ($\mu\varepsilon$) | -839 | -876 (+4%) | -580 | -685 (+18%) |

*: Change from axisymmetric result, %

Three-dimensional nonlinear finite element analysis of flexible pavements is currently the state-of-the-art structural analysis approach, and the three-dimensional analysis results for the three pavement geometry cases studied here do not differ significantly from the results of the axisymmetric analyses. This is in a way good news indicating that axisymmetric analysis with nonlinear geomaterial layer characterizations can still be used confidently for predicting reasonably accurate responses. However, before one can confidently make that statement, further work in this area should closely investigate whether the use of a nonlinear resilient model developed from true triaxial tests that can fully apply and simulate the three-dimensional stress states in material modeling would bring out any discrepancies in results from the three-dimensional analyses of flexible pavements.

## 6.3 True Triaxial Tests on Unbound Granular Materials

This section describes a pavement finite element analysis focusing on incorporating proper characterizations of the granular materials using true triaxial test data, not a standard type test. The intermediate principal stresses ($\sigma_2$) are also taken into account in the modulus model development. In the axisymmetric finite element analyses, the Uzan model is used since the Uzan model assumes the intermediate principal stress ($\sigma_2$) to be the same with the minor principal stress ($\sigma_3$). The universal model, on the other hand, can take into account separately the major ($\sigma_1$), intermediate ($\sigma_2$), and the minor principal stresses ($\sigma_3$) in both axisymmetric and three-dimensional finite element resilient response analyses for base layers. To properly account for the three-dimensional stress states in modeling, true triaxial test data are therefore utilized in this study to include realistic three-dimensional stress components applied on cubical aggregate specimens. Comparisons are made between axisymmetric and three-dimensional finite element analysis results emphasizing the effects of different nonlinear geomaterial model characterizations on the predicted critical pavement responses.

In the previous section, a three-dimensional pavement modeling effort with the consideration of the nonlinear pavement foundation geomaterial behavior did not show significant differences in pavement response predictions as obtained from the axisymmetric and three-dimensional analyses, although three-dimensional nonlinear finite element analysis of flexible pavements is currently the state-of-the-art structural analysis approach. This was partly due to the fact that the stress-dependent aggregate characterization model used in the nonlinear analyses was developed from the commonly used repeated load triaxial tests without any consideration for an applied intermediate principal stress ($\sigma_2$) and therefore was primarily applicable to the axisymmetric stress analysis.

A true triaxial apparatus allows three independently controlled normal stresses to be applied the faces of a cubical sample. Such a device can evaluate the influence of the intermediate principal stress ($\sigma_2$) on the strength and deformation characteristics of geomaterials. The main feature of this device is that the principal directions of stresses and strains correspond to the sides of a cubical sample. This assumption is true only if the sample is orthotropic along the axes. In this case, the feasible stress and strain paths consist of every path in the principal stress and strain space, respectively. Nevertheless, the true triaxial apparatus represents a limited advancement in rotating the principal axes over the conventional triaxial test.

The limitation of a repeated load triaxial test, especially its inability to simulate arbitrary applied stresses in three orthogonal directions, necessitates the use of a true triaxial device. Rowshanzamir (1995) used the true triaxial testing machine for determining the resilient properties of a base course granular material, well-graded crushed basalt, in the laboratory. To conduct each test in this experimental study, the requirements of Australian Standards (1977) were used in sample preparation. A fixed corner compaction mold was used as the test chamber. To stabilize the loading platens and reduce the effects of the residual stresses due to the sample preparation, the preconditioning stage including an initial range of stress states was applied. In the experimental study, after initial conditioning, the sample was subjected to the following stress states:

i) stress combination No 1.: $\sigma_1$ = 550-kPa, $\sigma_2$ = 350-kPa, and $\sigma_3$ = 350-kPa for 200 repetitions;

ii) a series of different stress states including 27 combinations of $\sigma_1$, $\sigma_2$, and $\sigma_3$ each applied for 200 repetitions.

The original laboratory data by Rowshanzamir (1995) were used in this study to develop nonlinear stress-dependent models of the Uzan and the universal forms. Table 6-10 gives the resilient model parameters and regression results obtained using the true triaxial test data. The axisymmetric universal model was obtained by assuming $\sigma_2=\sigma_3$ in triaxial conditions.

Table 6-10 Aggregate Nonlinear Model Parameters determined from Rowshanzamir (1995) Test Data

| Model Parameters | | | | |
|---|---|---|---|---|
| Model Type | $K_1$ | $K_2$ | $K_3$ | $R^{2*}$ |
| Uzan Model (axisymmetric) | 3,502 (kPa) | 0.635 | 0.010 | 0.79 |
| Universal Model (axisymmetric) | 1,360 | 0.635 | 0.010 | 0.79 |
| Universal Model (three-dimensional) | 417 | 1.071 | -0.107 | 0.98 |

*: $R^2$ is the regression correlation coefficient.

### 6.3.1 Comparisons of Nonlinear Pavement Responses using Different Material Characterizations

The nonlinear resilient modulus models introduced earlier were next incorporated into the finite element analyses to represent the most realistic stress-dependent pavement geomaterial behavior. Important design parameters such as the horizontal strain ($\varepsilon_h$) at the bottom of AC and the vertical strain ($\varepsilon_v$) on the top of subgrade were obtained to compare the predictions of several case studies.

The three-dimensional finite element mesh and the axisymmetric finite element mesh given in Figure 4-6 were utilized. The universal model (Witczak and Uzan, 1988) in three-dimensional analysis was used and the Uzan model (Uzan, 1985) in axisymmetric analysis was employed for the base layer. The bilinear model (Thompson and Robnett, 1979) for subgrade was also employed with the assumption of linear elastic

AC layer behavior. Table 6-11 lists the pavement geometry and the assigned input properties including nonlinear model parameters in the three-dimensional finite element analyses. A uniform pressure of 0.55-MPa was applied over a circular area of 152-mm radius.

Table 6-11 Pavement Geometry and Material Properties Assigned according to Rowshanzamir (1995) Data in the Three-dimensional Nonlinear Finite Element Analyses

<table>
<tr><th>Section</th><th>Element</th><th>Thickness (mm)</th><th>E (MPa)</th><th>ν</th><th colspan="4">Material Properties</th></tr>
<tr><td>AC</td><td>20-noded solid</td><td>76 or 102</td><td>2,759</td><td>0.35</td><td colspan="4">Isotropic and Linear Elastic</td></tr>
<tr><td rowspan="9">BASE</td><td rowspan="9">20-noded solid</td><td rowspan="9">254 or 305</td><td rowspan="9">207 (initial)</td><td rowspan="9">0.40</td><td colspan="4">Nonlinear: Uzan model (Uzan, 1985)</td></tr>
<tr><td colspan="2">$K_1$ (kPa)</td><td>$K_2$</td><td>$K_3$</td></tr>
<tr><td colspan="2">3,502</td><td>0.635</td><td>0.010</td></tr>
<tr><td colspan="4">Nonlinear: Universal Model* (Witczak and Uzan, 1988)</td></tr>
<tr><td colspan="2">$K_1$</td><td>$K_2$</td><td>$K_3$</td></tr>
<tr><td colspan="2">1,360</td><td>0.635</td><td>0.010</td></tr>
<tr><td colspan="4">Nonlinear: Universal Model** (Witczak and Uzan, 1988)</td></tr>
<tr><td colspan="2">$K_1$</td><td>$K_2$</td><td>$K_3$</td></tr>
<tr><td colspan="2">417</td><td>1.071</td><td>-0.107</td></tr>
<tr><td rowspan="3">SUBGRADE</td><td rowspan="3">20-noded solid</td><td rowspan="3">20,955 or 20,980</td><td rowspan="3">41.4 (initial)</td><td rowspan="3">0.45</td><td colspan="4">Nonlinear: Bilinear Model (Thompson and Robnett, 1979)</td></tr>
<tr><td>$E_{RI}$ (kPa)</td><td>$\sigma_{di}$ (kPa)</td><td>$K_3$ (kPa/kPa)</td><td>$K_4$ (kPa/kPa)</td></tr>
<tr><td>41,400</td><td>41</td><td>1,000</td><td>200</td></tr>
</table>

*: The resilient model considered triaxial conditions ($\sigma_2 = \sigma_3$).

**: The resilient model considered all three stress components.

Four different modeling cases using different base course characterizations were selected for finite element analyses:

**Case (1)** – Axisymmetric finite element analysis using the Uzan model;

**Case (2)** – Axisymmetric finite element analysis using the universal model with triaxial $\sigma_2=\sigma_3$ assumption;

**Case (3)** – Three-dimensional finite element analysis using the universal model with triaxial $\sigma_2=\sigma_3$ assumption;

**Case (4)** – Three-dimensional finite element analysis using the universal model with all three stress components and $\tau_{oct}$.

Since the stress-dependent resilient modulus ($M_R$) models developed using the true triaxial test data were used in the base layer, various comparisons showing the effects of advanced testing and characterization on pavement response predictions could be made successfully. Table 6-12 through Table 6-14 give detailed comparisons of the predicted critical pavement responses in two different pavement geometries. In all the nonlinear analyses, the bilinear $M_R$ model (Thompson and Robnett, 1979) was used in the subgrade layers. The predicted pavement responses were investigated in relation to different combinations of linear and nonlinear analyses in the base and subgrade: (i) nonlinear base and linear subgrade and (ii) nonlinear base and nonlinear subgrade.

By comparing responses predicted between cases (2) and (3), mesh and geometry related differences between axisymmetric and three-dimensional finite element analyses could be realistically investigated. The effects of intermediate principal stress ($\sigma_2$) on nonlinear behavior could be studied by comparing results from cases (3) and (4). And finally, by comparing axisymmetric and three-dimensional analyses between cases (2) and (4) the limitations and applicability of triaxial testing and characterization could be investigated in three-dimensional analyses.

Table 6-12 Predicted Pavement Responses from Cases (2) and (3)

| Pavement response | Nonlinear base and linear subgrade | | Nonlinear base and nonlinear subgrade | |
|---|---|---|---|---|
| | Axisymmetric (case 2) | Three-dimensional (case 3) | Axisymmetric (case 2) | Three-dimensional (case 3) |
| 76mm AC and 305mm base section | | | | |
| $\delta_{surface}$ (mm) | -1.102 | -1.059 (-4) * | -0.859 | -0.840 (-2) |
| $\sigma_{h\ bottom\ of\ AC}$ (MPa) | 0.531 | 0.563 (+6) | 0.517 | 0.547 (+6) |
| $\varepsilon_{h\ bottom\ of\ AC}$ ($\mu\varepsilon$) | 192 | 196 (+2) | 188 | 191 (+2) |
| $\sigma_{v\ top\ of\ subgrade}$ (MPa) | -0.059 | -0.057 (-5) | -0.073 | -0.070 (-4) |
| $\varepsilon_{v\ top\ of\ subgrade}$ ($\mu\varepsilon$) | -1042 | -974 (-7) | -818 | -793 (-3) |
| 102mm AC and 254mm base section | | | | |
| $\delta_{surface}$ (mm) | -1.019 | -0.978 (-4) | -0.787 | -0.775 (-2) |
| $\sigma_{h\ bottom\ of\ AC}$ (MPa) | 0.828 | 0.823 (-1) | 0.789 | 0.819 (+4) |
| $\varepsilon_{h\ bottom\ of\ AC}$ ($\mu\varepsilon$) | 245 | 240 (-2) | 235 | 238 (+1) |
| $\sigma_{v\ top\ of\ subgrade}$ (MPa) | -0.055 | -0.053 (-4) | -0.068 | -0.067 (-2) |
| $\varepsilon_{v\ top\ of\ subgrade}$ ($\mu\varepsilon$) | -979 | -922 (-6) | -769 | -759 (-1) |

*: The values in parentheses indicate percentage change from case (2) to case (3) results.

In Table 6-12, axisymmetric and three-dimensional finite element analysis results are compared for the same modulus models obtained from triaxial testing. From both linear and nonlinear analyses considered in the subgrade with nonlinear aggregate base, the three-dimensional analysis results were not much different from those of the axisymmetric analyses. This indicated no major mesh or geometry related differences were found between axisymmetric and three-dimensional analyses of the single wheel loading approximation.

Table 6-13 Predicted Pavement Responses from Cases (3) and (4)

| Pavement response | Nonlinear base and linear subgrade | | Nonlinear base and nonlinear subgrade | |
|---|---|---|---|---|
| | Three-dimensional (case 3) | Three-dimensional (case 4) | Three-dimensional (case 3) | Three-dimensional (case 4) |
| 76mm AC and 305mm Base Section | | | | |
| $\delta_{\text{surface}}$ (mm) | -1.059 | -1.061 (0)* | -0.840 | -0.839 (0) |
| $\sigma_{\text{h bottom of AC}}$ (MPa) | 0.563 | 0.464 (-18) | 0.547 | 0.447 (-18) |
| $\varepsilon_{\text{h bottom of AC}}$ ($\mu\varepsilon$) | 196 | 179 (-8) | 191 | 175 (-9) |
| $\sigma_{\text{v top of subgrade}}$ (MPa) | -0.057 | -0.058 (+3) | -0.070 | -0.073 (+4) |
| $\varepsilon_{\text{v top of subgrade}}$ ($\mu\varepsilon$) | -974 | -958 (-2) | -793 | -789 (-1) |
| 102mm AC and 254mm Base Section | | | | |
| $\delta_{\text{surface}}$ (mm) | -0.978 | -0.983 (+1) | -0.775 | -0.782 (+1) |
| $\sigma_{\text{h bottom of AC}}$ (MPa) | 0.823 | 0.727 (-12) | 0.819 | 0.744 (-9) |
| $\varepsilon_{\text{h bottom of AC}}$ ($\mu\varepsilon$) | 240 | 223 (-7) | 238 | 227 (-5) |
| $\sigma_{\text{v top of subgrade}}$ (MPa) | -0.053 | -0.054 (+3) | -0.067 | -0.070 (+5) |
| $\varepsilon_{\text{v top of subgrade}}$ ($\mu\varepsilon$) | -922 | -904 (-2) | -759 | -765 (+1) |

*: The values in parentheses indicate percentage change from case (3) to case (4) results.

The effects of intermediate principal stress ($\sigma_2$) are indicated in Table 6-13. The two finite element models had the exact same three-dimensional finite element meshes and nonlinear material models with the only difference being the intermediate principal stress, which was replaced with the minor principal stress ($\sigma_3$) in finding granular material model parameters of case (3). The use of the true triaxial test data by Rowshanzamir (1995) made this comparison possible. The use of intermediate principal stress ($\sigma_2$) had the most impact on the horizontal strain and stress predictions at the bottom of AC as they showed the largest percent differences, e.g., up to 18% differences in radial stresses at the bottom of AC layer, between case (3) and case (4) results.

Table 6-14 Predicted Pavement Responses from Cases (2) and (4)

| Pavement response | Nonlinear base and linear subgrade | | Nonlinear base and nonlinear subgrade | |
|---|---|---|---|---|
| | Axisymmetric (case 2) | Three-dimensional (case 4) | Axisymmetric (case 2) | Three-dimensional (case 4) |
| 76mm AC and 305mm Base Section | | | | |
| $\delta_{surface}$ (mm) | -1.102 | -1.061 (-4) * | -0.859 | -0.839 (-2) |
| $\sigma_{h\ bottom\ of\ AC}$ (MPa) | 0.531 | 0.464 (-13) | 0.517 | 0.447 (-14) |
| $\varepsilon_{h\ bottom\ of\ AC}$ ($\mu\varepsilon$) | 192 | 179 (-7) | 188 | 175 (-7) |
| $\sigma_{v\ top\ of\ subgrade}$ (MPa) | -0.059 | -0.058 (-2) | -0.073 | -0.073 (0) |
| $\varepsilon_{v\ top\ of\ subgrade}$ ($\mu\varepsilon$) | -1042 | -958 (-8) | -818 | -789 (-4) |
| 102mm AC and 254mm Base Section | | | | |
| $\delta_{surface}$ (mm) | -1.019 | -0.983 (-4) | -0.787 | -0.782 (-1) |
| $\sigma_{h\ bottom\ of\ AC}$ (MPa) | 0.828 | 0.727 (-12) | 0.789 | 0.744 (-6) |
| $\varepsilon_{h\ bottom\ of\ AC}$ ($\mu\varepsilon$) | 245 | 223 (-9) | 235 | 227 (-3) |
| $\sigma_{v\ top\ of\ subgrade}$ (MPa) | -0.055 | -0.054 (-1) | -0.068 | -0.070 (+3) |
| $\varepsilon_{v\ top\ of\ subgrade}$ ($\mu\varepsilon$) | -979 | -904 (-8) | -769 | -765 (-1) |

*: The values in parentheses indicate percentage change from case (2) to case (4) results.

Table 6-14 summarize the results of the combined effects of the applicability of both triaxial testing and characterization and also adequately take into account the intermediate principal stress ($\sigma_2$) in three-dimensional analyses. The horizontal strain and stress predictions at the bottom of AC indicated the largest percent differences between case (2) and case (4) results. In addition, with the linear subgrade, vertical subgrade strains also indicated a difference of up to 8%. Interestingly, considering all the results presented in Table 6-12 to Table 6-14, one can realize that different cases and analyses studied had compensating effects, positive and negative percent differences, on the computed critical pavement responses.

Table 6-15 Predicted Pavement Responses from Cases (1) and (4)

| Pavement response | Nonlinear base and linear subgrade | | Nonlinear base and nonlinear subgrade | |
|---|---|---|---|---|
| | Axisymmetric (case 1) | Three-dimensional (case 4) | Axisymmetric (case 1) | Three-dimensional (case 4) |
| 76mm AC and 305mm Base Section | | | | |
| $\delta_{surface}$ (mm) | -1.130 | -1.061 (-6) * | -0.886 | -0.839 (-5) |
| $\sigma_{h\ bottom\ of\ AC}$ (MPa) | 0.665 | 0.464 (-30) | 0.654 | 0.447 (-32) |
| $\varepsilon_{h\ bottom\ of\ AC}$ ($\mu\varepsilon$) | 219 | 179 (-18) | 215 | 175 (-19) |
| $\sigma_{v\ top\ of\ subgrade}$ (MPa) | -0.060 | -0.058 (-2) | -0.073 | -0.073 (0) |
| $\varepsilon_{v\ top\ of\ subgrade}$ ($\mu\varepsilon$) | -1047 | -958 (-9) | -840 | -789 (-6) |
| 102mm AC and 254mm Base Section | | | | |
| $\delta_{surface}$ (mm) | -1.039 | -0.983 (-5) | -0.805 | -0.782 (-3) |
| $\sigma_{h\ bottom\ of\ AC}$ (MPa) | 0.952 | 0.727 (-24) | 0.908 | 0.744 (-18) |
| $\varepsilon_{h\ bottom\ of\ AC}$ ($\mu\varepsilon$) | 268 | 223 (-17) | 257 | 227 (-12) |
| $\sigma_{v\ top\ of\ subgrade}$ (MPa) | -0.055 | -0.054 (-1) | -0.067 | -0.070 (+5) |
| $\varepsilon_{v\ top\ of\ subgrade}$ ($\mu\varepsilon$) | -988 | -904 (-9) | -784 | -765 (-2) |

*: The values in parentheses indicate percentage change from case (1) to case (4) results.

Finally, Table 6-15 presents the most drastic results, i.e., highest percent differences, in the computed responses when predicted responses are compared between cases (1) and (4). Note that this is often what most researchers studied and compared in the past such as Schwartz (2002). These results indeed agree well with the differences between the axisymmetric Uzan model and three-dimensional universal model finite element analysis results seen in cases (1) and (4). Since different models were used in the base layer with different axisymmetric and three-dimensional stress components, the largest differences, up to 32% change in radial stresses at the bottom of AC layer and 9% change in vertical strain on the top of subgrade, occurred as shown in Table 6-15. Also, the results obtained from different cases and analyses studied again had compensating effects, positive and negative percent differences, on the computed critical pavement responses.

## 6.4 Summary

This chapter focused on an investigation of appropriate stress-dependent resilient modulus characterization models considered in the unbound aggregate base and fine-grained subgrade layers for the nonlinear analyses of three-dimensional finite element analyses.

The developed three-dimensional finite element model was verified for accuracy based on good agreements in the linear elastic solutions with the axisymmetic finite element analyses. Comparisons between the results of axisymmetric and three-dimensional ABAQUS$^{TM}$ analyses using the developed UMAT subroutine for nonlinear solutions did not indicate major differences in the predicted pavement responses. This could be due to the fact that the stress-dependent aggregate characterization model used in the nonlinear analyses was developed from typical repeated load triaxial tests with the axisymmetric stress analysis conditions. Therefore, to properly account for the impacts of triaxial and true triaxial testing options in the laboratory on the stress-dependent modulus model characterizations, the most realistic true triaxial test data for unbound aggregate base materials were utilized as obtained from a previous study.

Several comparative analyses were undertaken to study the effects of axisymmetric and three-dimensional finite element analyses for a single wheel loading approximation and the consideration of the intermediate principal stress ($\sigma_2$). In the comparison of axisymmetric and three-dimensional finite element results, both linear and nonlinear analyses did not indicate major differences only when the exact same modulus characterization models defined from axisymmetric stress conditions were used in both analyses. Next, including the intermediate principal stress ($\sigma_2$) in the aggregate base modulus characterization model was found to be important in three-dimensional analyses especially when somewhat different AC horizontal strain and stress responses were predicted. This means that neglecting intermediate principal stresses as we always do in the axisymmetric solution may cause computing different pavement responses than found in the field. The largest and the most drastic differences, up to 30% change in radial stresses at the bottom of AC layer and 9% change in vertical strain on the top of subgrade, were obtained when comparing responses predicted from the axisymmetric and three-dimensional nonlinear finite element analyses using just the Uzan model developed from triaxial test data with the triaxial assumption of equal minor and intermediate stresses ($\sigma_2$=$\sigma_3$) and the universal model for three-dimensional analysis employing additional intermediate stress ($\sigma_2$) and the octahedral shear stress ($\tau_{oct}$) instead of the deviator stress ($\sigma_d$) for shear stress effects. In conclusion, the investigations proved that the use of true triaxial test data in the laboratory and appropriate three-dimensional modulus model characterizations would result in more accurate pavement response predictions in three-dimensional nonlinear finite element analyses of conventional flexible pavements with unbound aggregate bases.

# Chapter 7 Field Validation of Nonlinear Finite Element Analysis

In a mechanistic-empirical flexible pavement analysis and design procedure, pavement structural responses have to be determined accurately from mechanistic structural models. Accordingly, the developed nonlinear geomaterial models employed in the ABAQUS$^{TM}$ finite element program need to be validated for accurately predicting pavement responses. Since three-dimensional ABAQUS$^{TM}$ finite element program is capable of considering multiple wheel loads and wheel load interaction effects, proper nonlinear pavement foundation models have to be used to predict responses of field pavement sections. For this purpose, the field measured responses of the National Airport Pavement Test Facility (NAPTF) flexible pavement test sections were utilized.

## 7.1 National Airport Pavement Test Facility

The National Airport Pavement Test Facility (NAPTF) at the Federal Aviation Administration (FAA) was constructed to test full-scale instrumented pavement sections to investigate pavement performance subjected to complex gear loading of next generation aircraft. The NAPTF pavement test strip was 274.3-m long and 18.3-m wide. The first built group of test sections, named as Construction Cycle 1 (CC1) included nine test pavements composed of six flexible and three rigid pavements. These were built on three different subgrade materials, i.e., low, medium, and high strength and two base sections, i.e., conventional and stabilized bases. The structural thickness requirements of CC1 cross sections are shown in Figure 7-1.

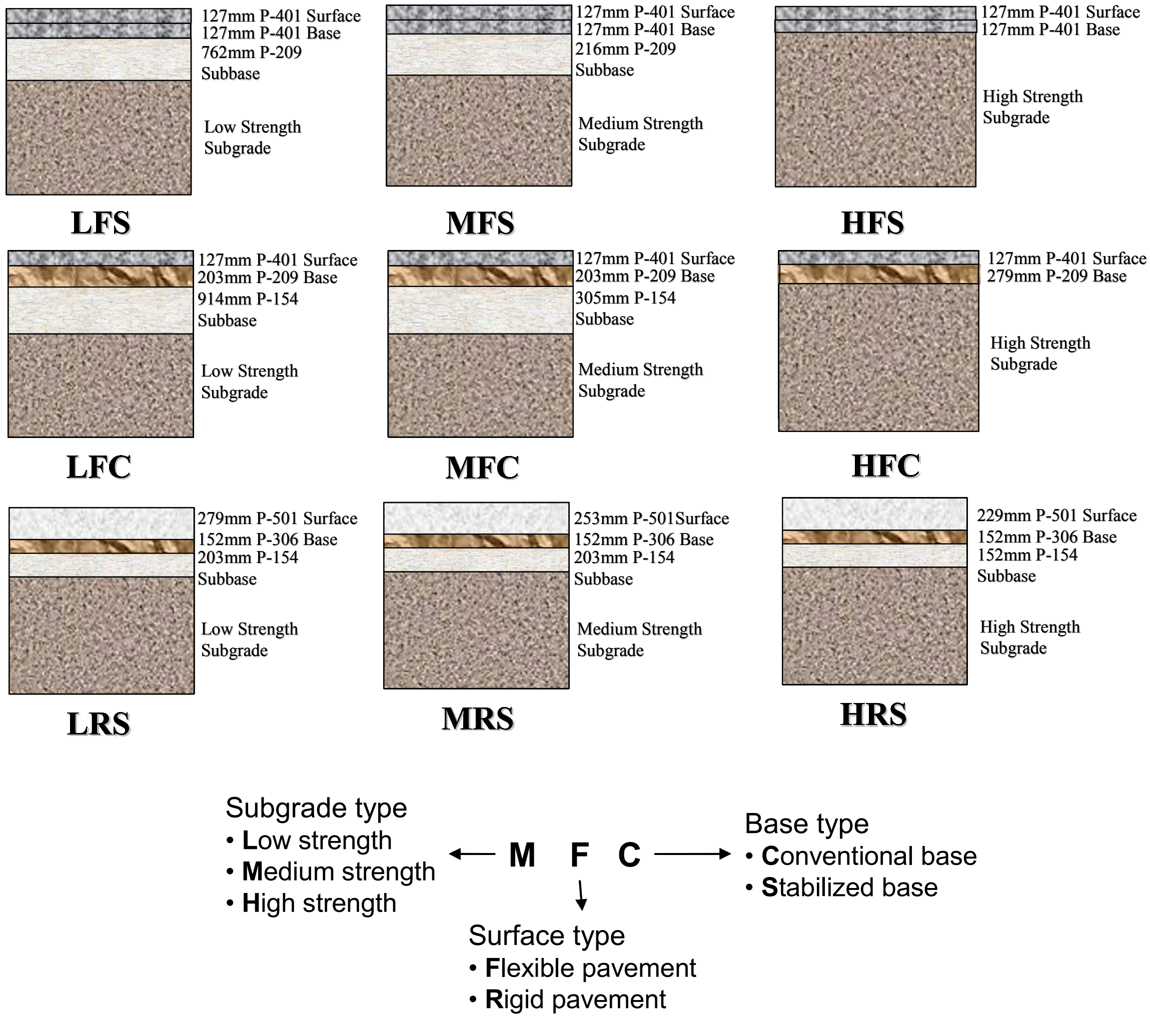


Figure 7-1 Cross Sections of NAPTF Pavement Test Sections (Garg, 2003)

The National Airport Pavement Test Machine (NAPTM) was used to load the NAPTF test sections. The NAPTM can carry up to 34-ton per wheel on two loading gears with 6-wheel per gear. Typical aircraft gear configurations, i.e., single, dual single, dual tandem, dual tridem, can be accommodated with the capability to change wheel load, wheel spacing, and wheel speed. This NAPTF pavement testing was conducted within two phases: response testing and trafficking testing. The response testing was performed to determine the effects of static, monotonic and slow rolling gear configuration (0.55

km/hour). The trafficking tests were conducted at 8 km/hour to investigate gear configuration and wander effects by monitoring pavement responses and performances as a function of number of load repetitions.

To measure the structural responses in the CC1 test sections, several sensors were installed within the pavement sections. The NAPTF structural response instrumentations were Multi-Depth Deflectometers (MDD), Pressure Cells (PC), and Asphalt Strain Gauges (ASG). MDDs were installed to record the load-induced displacement at multi-depths within the pavement sections. Each MDD consisted of seven displacement tranducers at the position to capture multiple wheel load interaction effects. These measured displacements at different depths, i.e., surface displacement, top and bottom of base layer, bottom of subbase layer, top of subgrade, in the subgrade. Five sets of MDDs were placed in each test pavement; one in the centerline of the test pavement and two in each traffic path. In the placement of pressure cells, 152-mm pressure cells were used to measure stresses in the unbound aggregates in the base layers and 51-mm pressure cells measured stresses in the subgrade layers. H-bar type strain gages were installed at the bottom of the asphalt concrete layer in both the longitudinal and transverse directions. Figure 7-2 and Figure 7-3 show the cross sections used for the CC1 sections of NAPTF along with the locations of the sensors such as MDDs and pressure cells.

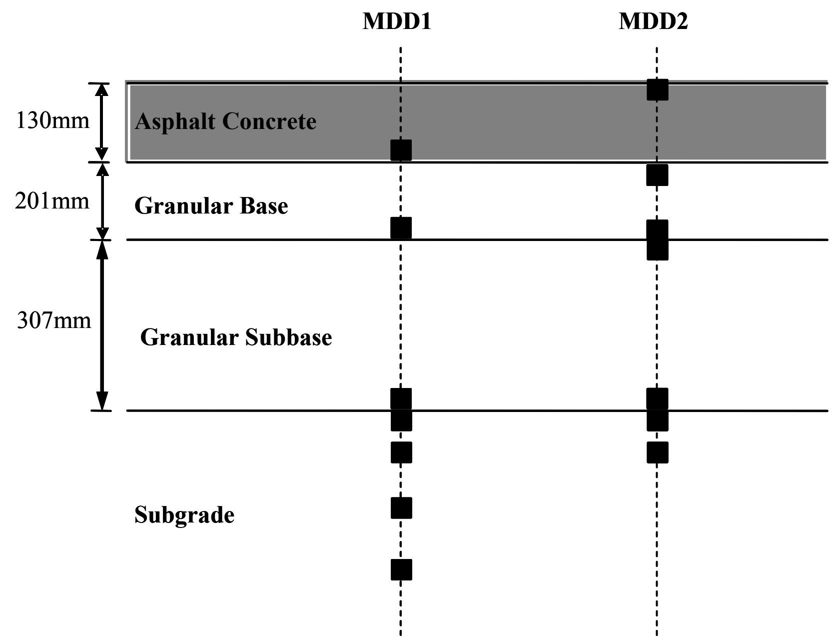


(a) MDD gages in MFC

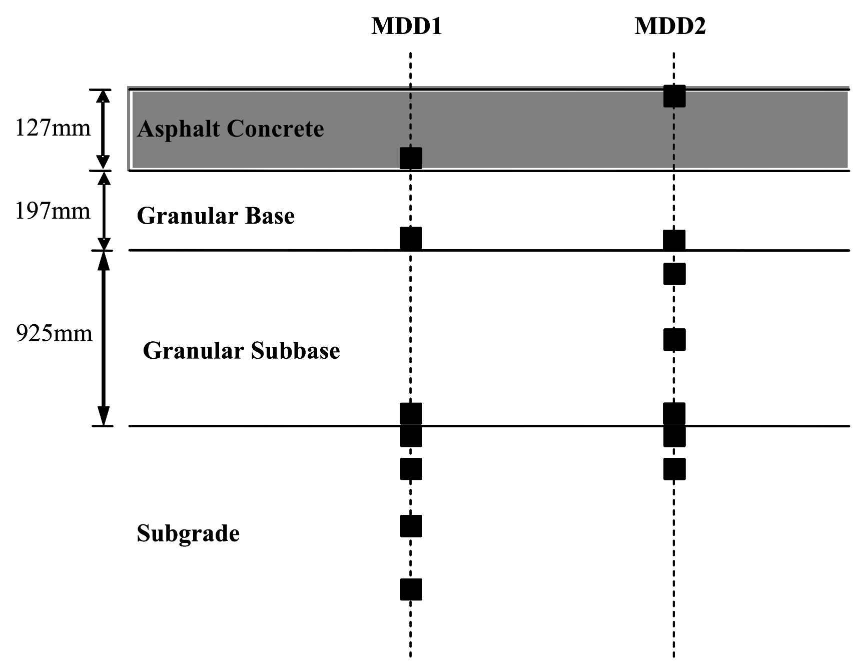


(b) MDD gages in LFC

Figure 7-2 Vertical Locations of MDD sensors in CC1 of NAPTF Test Sections (CTL, 1998)

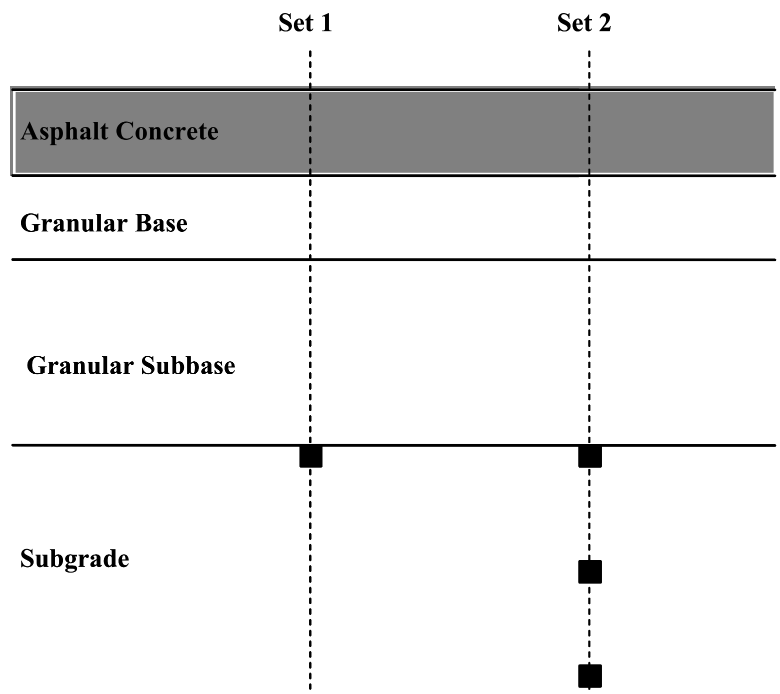


Figure 7-3 Vertical Locations of Subgrade Pressure Cells in CC1 of NAPTF Test Sections (CTL, 1998)

### 7.1.1 Comparisons between Measured Subgrade Stresses and Predicted Stresses

Three-dimensional ABAQUS™ finite element analyses were performed to compute the pavement responses under aircraft gear loadings and to compare them with the measured CC1 section responses of NAPTF. The conventional section, herein MFC and LFC, were chosen for validation in order to obtain the distinct effect of nonlinear stress-dependent materials. The P-401 AC surface, P-209 granular base and P-154 granular subbase layers were used in both sections. Laboratory modulus characterization tests for both unbound aggregates and subgrade soils were performed to determine stress dependencies and develop resilient modulus models as given in Table 7-1. Table 7-1 also lists the different backcalculated modulus properties and model parameters obtained from previous studies referred to here as backcalculation 1 and 2 by Gopalakrishnan (2004) and Gomez-Ramirez (2002), respectively. The reasons why different model parameters were reported is due to the various environmental effects and applied loading in the slow rolling gear response test at the initial loading stage. These results were used in this study as inputs for MDD based deflection and PC based stress prediction using three-dimensional finite element analyses. Model parameters $K_i$ are given for the Uzan model (1985) used in the granular base (see Equations 2-13) and for the bilinear approximation used in the subgrade (see Equations 2-28). Since the K-θ model was used for laboratory tests, the Uzan model assigned was assumed to drop $K_3$ term ($K_3$=0), in the base and subbase layers. Note that the study results by Gopalakrishnan (2004) are indicated by backcalculation 1 and the study results by Gomez-Ramirez (2002) are indicated by backcalculation 2 for the data provided in Table 7-1.

Table 7-1 Pavement Geometries and Material Properties used in the Three-dimensional Finite Element Analyses of NAPTF Pavement Sections

| Materials | Section | Thickness (mm) | ν | Modulus Properties | | | |
|---|---|---|---|---|---|---|---|
| AC | | | | Isotropic and linear behavior (kPa) | | | |
| | Backcalculation 1 - MFC | 130 | 0.35 | 8,268,000 | | | |
| | Backcalculation 1 - LFC | 127 | 0.35 | 7,579,000 | | | |
| | Backcalculation 2 – MFC | 130 | 0.35 | 1,036,000 | | | |
| | Backcalculation 2 - LFC | 127 | 0.35 | 861,000 | | | |
| Base | | | | Nonlinear: Uzan model | | | |
| | | | | $K_1$ (kPa) | $K_2$ | $K_3$ | |
| | Backcalculation 1 - MFC | 201 | 0.38 | 10,300 | 0.40 | 0 | |
| | Backcalculation 1 - LFC | 197 | 0.38 | 8,300 | 0.60 | 0 | |
| | Backcalculation 2 – MFC | 201 | 0.38 | 10,300 | 0.00 | 0 | |
| | Backcalculation 2 - LFC | 197 | 0.38 | 31,000 | 0.40 | 0 | |
| Subbase | | | | Nonlinear: Uzan model | | | |
| | | | | $K_1$ (kPa) | $K_2$ | $K_3$ | |
| | Backcalculation 1 - MFC | 307 | 0.38 | 6,900 | 0.64 | 0 | |
| | Backcalculation 1 - LFC | 925 | 0.38 | 6,900 | 0.64 | 0 | |
| | Backcalculation 2 – MFC | 307 | 0.38 | 6,900 | 0.64 | 0 | |
| | Backcalculation 2 - LFC | 925 | 0.38 | 15,800 | 0.64 | 0 | |
| Subgrade | | | | Nonlinear: Bilinear model | | | |
| | | | | $E_{RI}$ (kPa) | $\sigma_{di}$ (kPa) | $K_3$ | $K_4$ |
| | Backcalculation 1 - MFC | 2,408 | 0.40 | 62,800 | 42 | 420 | 570 |
| | Backcalculation 1 - LFC | 2,408 | 0.40 | 13,800 | 41 | 872 | 155 |
| | Backcalculation 2 – MFC | 2,408 | 0.40 | 89,600 | 41 | 470 | 570 |
| | Backcalculation 2 - LFC | 2,408 | 0.40 | 24,100 | 40 | 872 | 152 |

The finite element mesh and modeled pavement geometry are shown in Figure 7-4. The three-dimensional finite element mesh was used to analyze both the MFC and LFC sections as nonlinear elastic layered systems. All elements used were parabolic 20-noded hexahedron solid elements. The subgrade and the unbound aggregate base layers were treated as nonlinear elastic materials while the AC surface layer was modeled as linear elastic.

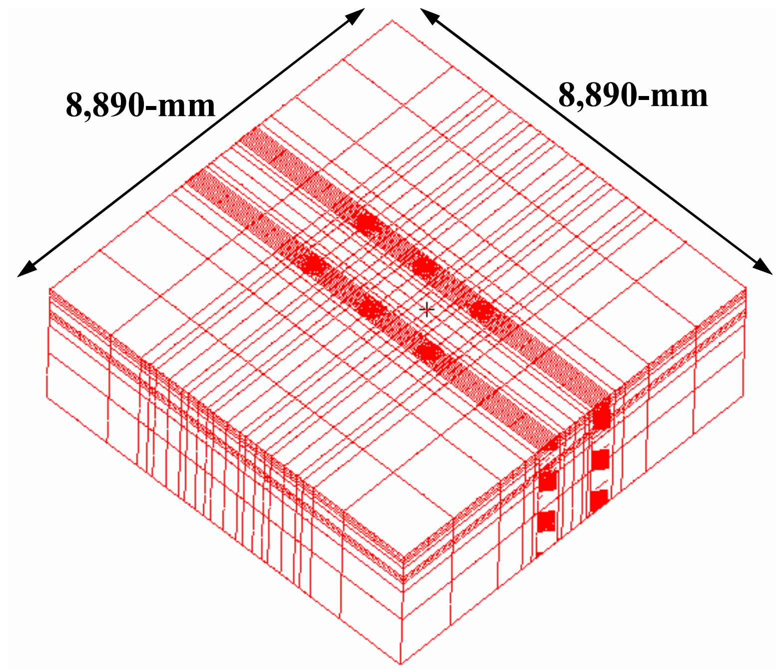


Figure 7-4 Three-dimensional Finite Element Mesh for CC1 NAPTF Test Sections

To model the test sections, the wheel loads were approximated as a uniform pressure over a circular area as shown in Figure 7-5. A six-wheel dual tridem aircraft gear configuration similar to that of Boeing 777 aircraft with 1372-mm wheel spacing and 1448-mm axle spacing was applied. The tire pressure was 1.3-MPa for backcalculation 1.

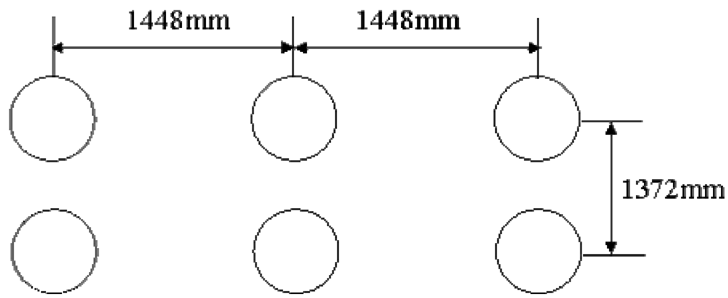


Figure 7-5 Six-wheel Gear Configuration Applied on NAPTF Pavement Test Sections

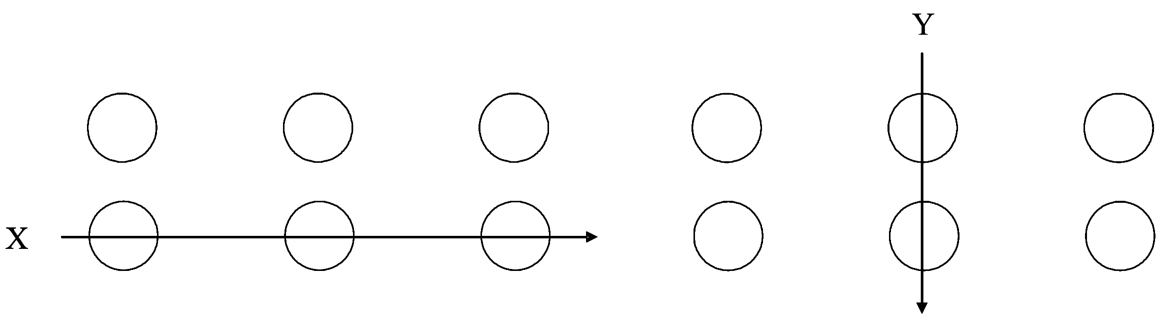


(a) Longitudinal direction (b) Transverse direction

Figure 7-6 Profile Locations of Pavement Responses Associated with 6-wheel Gear Configuration

Figure 7-6 shows the profile locations of predicted pavement responses. Figure 7-7 and Figure 7-8 compare the measured response variables with the finite element mechanistic model predictions for sections MFC and LFC using material properties obtained from backcalculation 1 study in Table 7-1. Subgrade stresses computed in the longitudinal direction (see Figure 7-6) from finite element analyses were compared with the measured pressure cell subgrade stresses. In each test section, the pressure cells were installed on the top of subgrade to measure the vertical stresses. There were two to three different pressure cells on top of the subgrade and the measured pressure cell results showed large variability. A possible reason for such variability would be the actual installation depth of each pressure cell. Gomez-Ramirez and Thompson (2002) reported that only 25.4-mm difference in the pressure cell placement resulted in 34 to 48 kPa differences in measured subgrade vertical stresses. Also, the MDD displacement predictions were made in the transverse direction profile shown in Figure 7-6 to compare with the measured ones and these validate three-dimensional finite element analysis results.

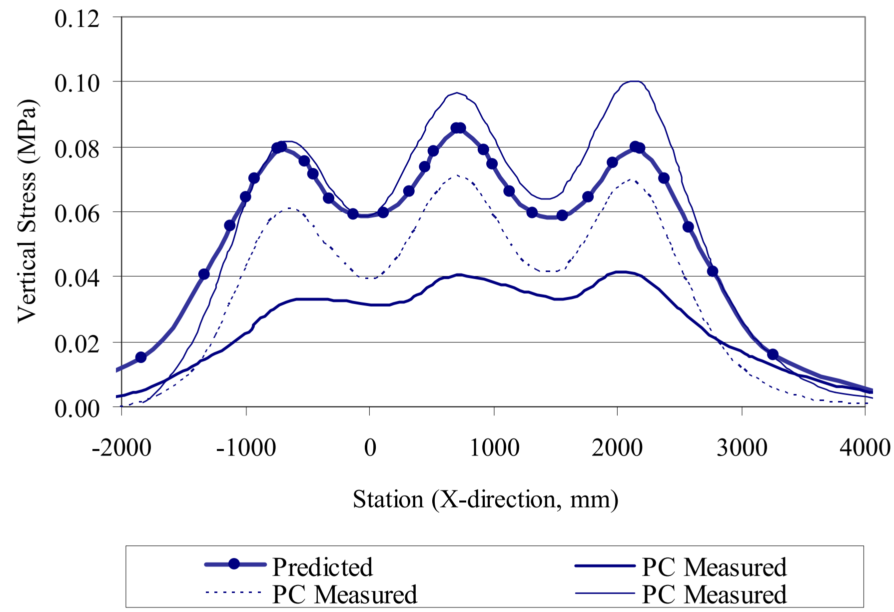


(a) Vertical subgrade stresses

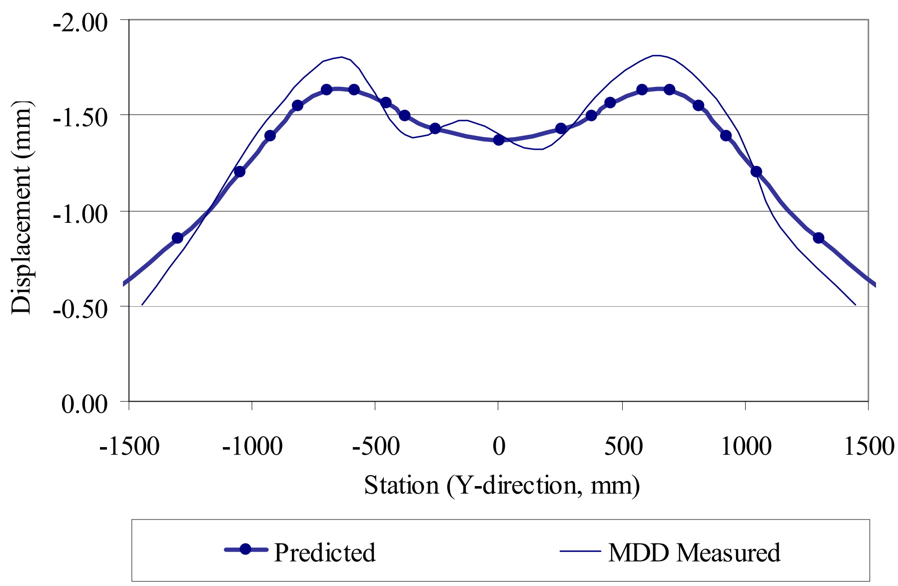


(b) Vertical surface displacements

Figure 7-7, cont. on next page

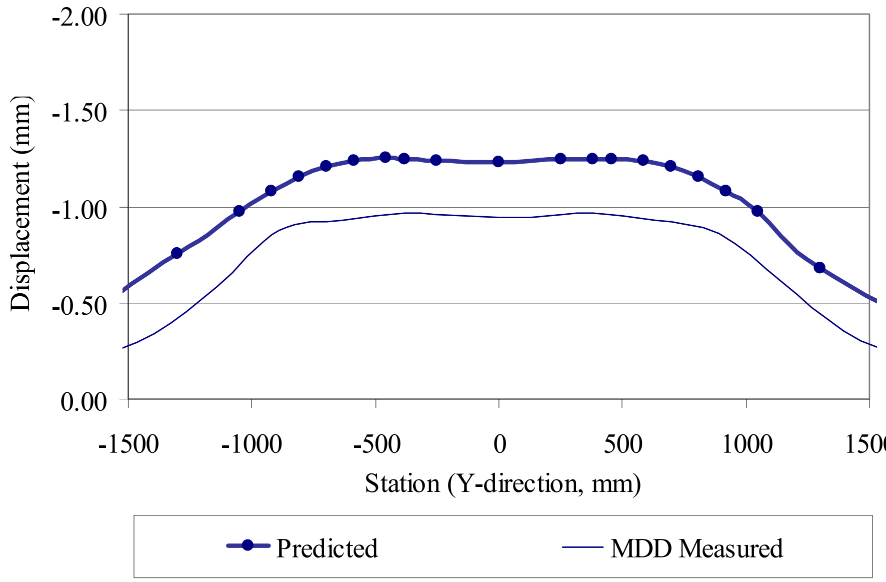


(c) Vertical subgrade displacements

Figure 7-7 Comparisons between Measured and Finite Element Predictions for MFC Test Section

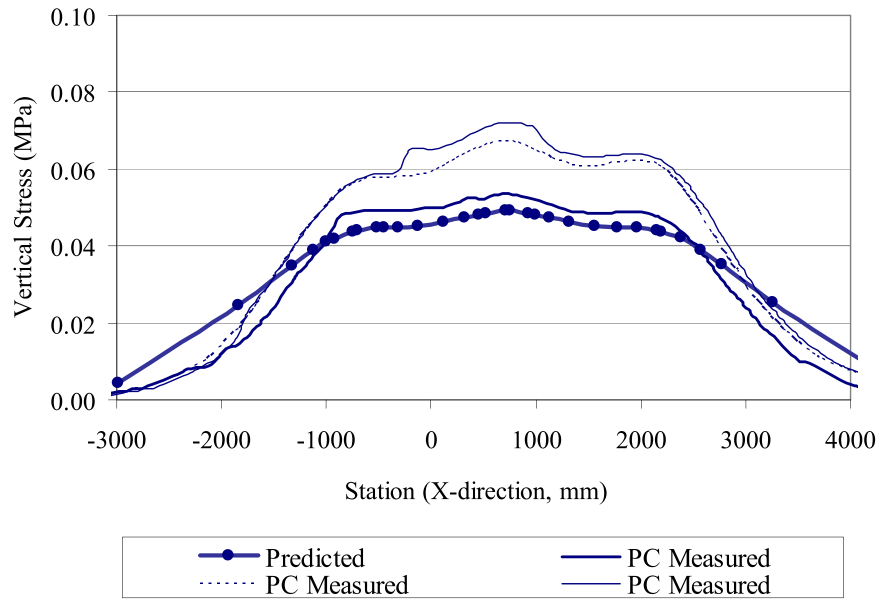


(a) Vertical subgrade stresses

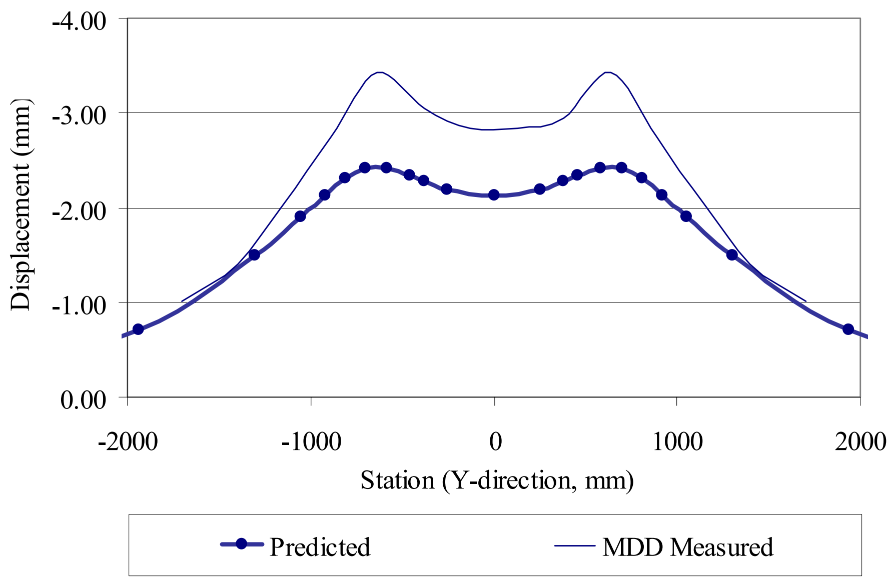


(b) Vertical surface displacements

Figure 7-8, cont. on next page

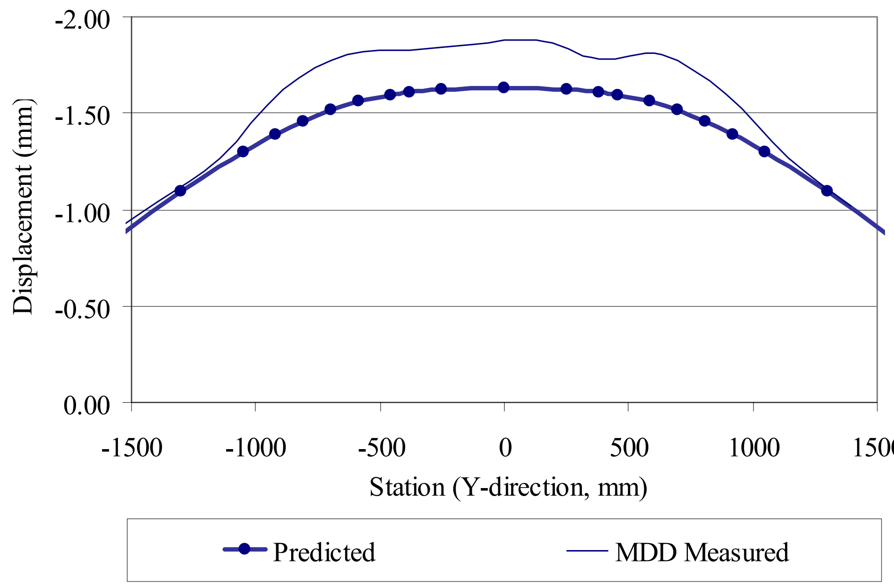


(c) Vertical subgrade displacements

Figure 7-8 Comparisons between Measured and Finite Element Predictions for LFC Test Section

In general, the nonlinear finite element model predictions were in reasonably good agreement with the measured responses of the test sections and the predictions from nonlinear analyses. The predicted values of subgrade vertical stress, subgrade displacement, and surface deflection compared reasonably well with the order of magnitudes of the measured responses in both sections, except the predicted surface deflection at LFC section. Especially, good agreements were found between measured and predicted values of subgrade vertical stress and surface deflection on MFC section. The better agreement was found for the MFC sections than for the LFC section.

From the comparisons, the differences found can be attributed to the dynamic nature of moving wheel loads. The developed mechanistic model performed a static analysis to approximate the wheel load as applied uniform circular pressure. Accordingly, important effects of the moving loads, i.e., tire configuration, speed, interaction of tire and pavement, and non-uniform tire contact pressures on pavement distress were ignored. Even low strength subgrade material can be more subjective by localized effects due to moving wheel loads.

Figure 7-9 shows the profile locations of predicted pavement responses shown in Figure 7-10 and Figure 7-11. Using the material properties from backcalculation 2 case given in Table 7-1, another validation study was conducted for subgrade responses. Figure 7-10 and Figure 7-11 show the measured vertical stresses on the top of subgrade layer, from three different pressure cells, for the MFC and LFC section. To model the test sections, the wheel load was applied as a uniform pressure over a circular area as shown in Figure 7-5. Compared to the validation study using backcalculation 1 data, both six-wheel dual tridem and four-wheel dual tandem aircraft gear configurations were used. The wheel and axle spacings were the same as in Figure 7-5, but the tire pressure was 1.02-MPa.

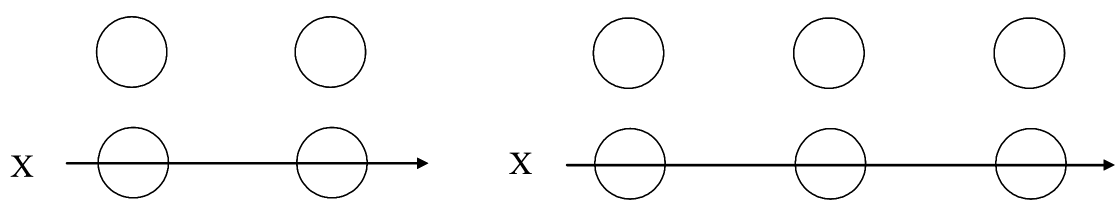


(a) Four-wheel dual tandem (b) Six-wheel dual tridem

Figure 7-9 Profile Locations of Pavement Response Predictions Associated with Two Gear Configurations

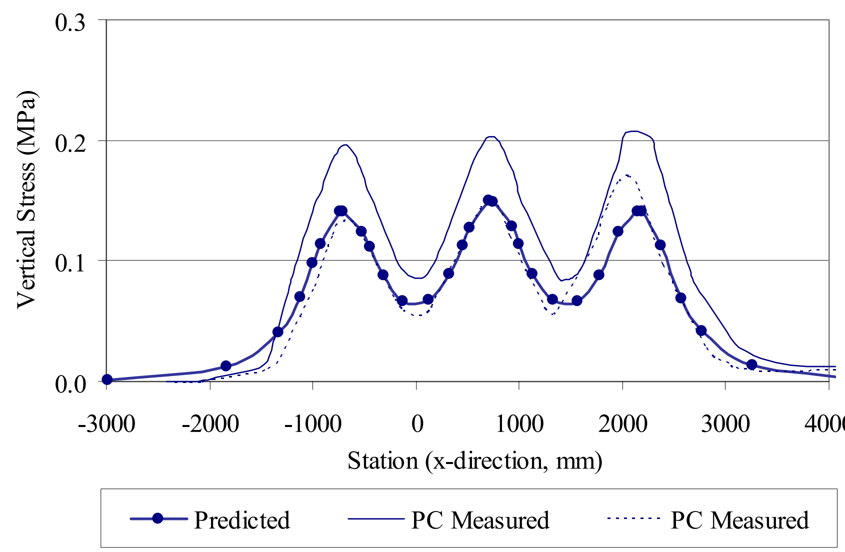


(a) Vertical subgrade stresses for tridem gear

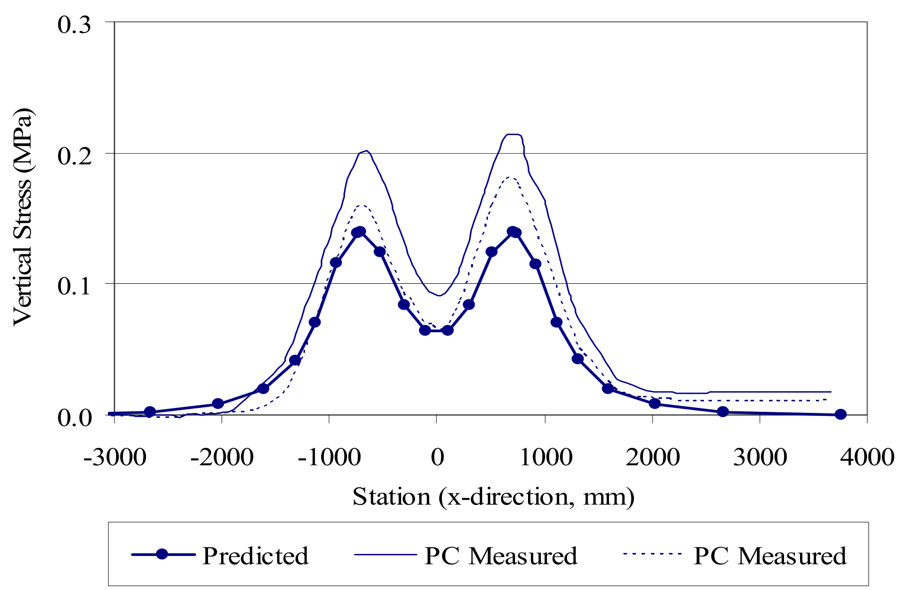


(b) Vertical subgrade stresses for tandem gear

Figure 7-10 Comparisons between Measured and Predicted Responses for the MFC Test Section

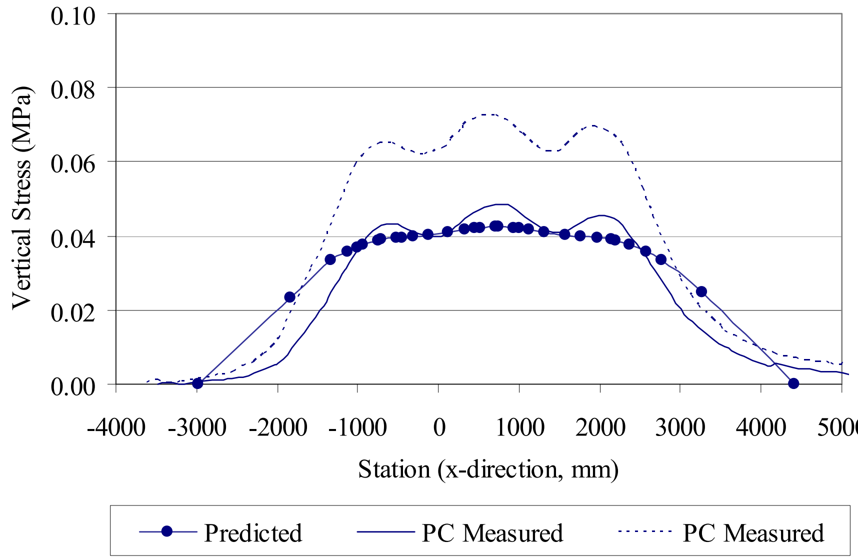


(a) Vertical subgrade stresses for tridem gear

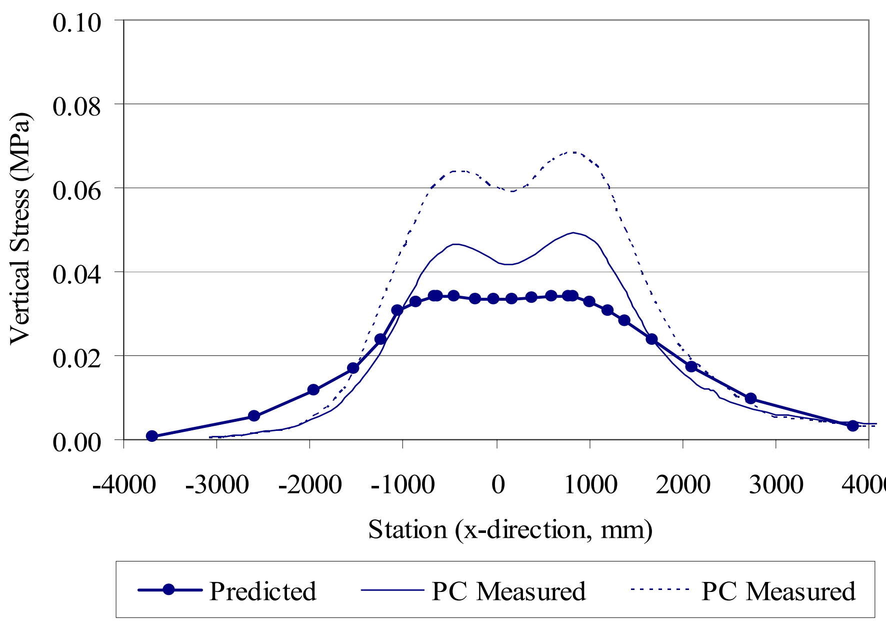


(b) Vertical subgrade stresses for tandem gear

Figure 7-11 Comparisons between Measured and Predicted Responses for the MFC Test Section

Considering the variability of the pressure cell measurements, predicted ABAQUS™ nonlinear finite element results showed good agreement with measured values. The measured responses had a tendency of exhibiting higher responses than predicted ones. This was possibly due to localized effects of wheel loads in the actual tests. The predicted responses, due to the symmetry of wheel loading, indicated first and last peak values to be the same which was in contrast to measured responses.

## 7.2 Effect of Pavement Layer Thickness on Subgrade Responses

Rutting is a major distress in flexible pavements and three-dimensional finite element response analysis results are integrally linked to establishing rutting distress models for mechanistic-empirical pavement design procedures. Ruts appear as longitudinal depressions in the wheel paths and are often related to subgrade critical responses. Depending on the magnitude of the wheel loads and the relative strength of the pavement layers, a significant portion of the total rutting can occur in the pavement foundation due to weak subgrade or the use of a low quality aggregate layer. Such significant rutting can often be the main cause of pavement structural failures.

A major factor contributing to subgrade rutting is the subgrade vertical stress/strain level, which is governed by the pavement thickness and the magnitude of the wheel loads. The layer thickness of base/subbase has the main purpose of distributing wheel loads to allow only limited stress levels over weak subgrade soils. Especially, airport pavements are designed with substantially thicker granular base/subbase layers to resist heavy aircraft wheel/gear loadings and to protect the weakest subgrade layer. For example, estimating the needed base/subbase thickness to protect the subgrade and at the same time minimize rutting in granular base/subbase layers has been a key consideration in the FAA's NAPTF Construction Cycle 3 (CC3) full-scale pavement tests. The CC3 tests included four different subbase thicknesses to evaluate pavement rutting performances under the application of 4- and 6-wheel gear load configurations (Hayhoe, 2004). According to the FAA, the research objective of first trafficking test of NAPTF (CC1) was to determine the number of load applications to cause the shear failure in the subgrade. The HFC and HFS sections out of CC1 test items, were hard to fail in contrast to other test sections due to high strength subgrade. This brought to more investigations of low strength subgrade sections and reconstructed all pavement subgrade layers to low strength subgrade materials. These reconstructed test sections were referred as Construction Cycle 3 (CC3) and are shown in Figure 7-12. In this section, the response data from the CC3 tests are analyzed and then the influence of subbase thickness on the pavement responses is studied.

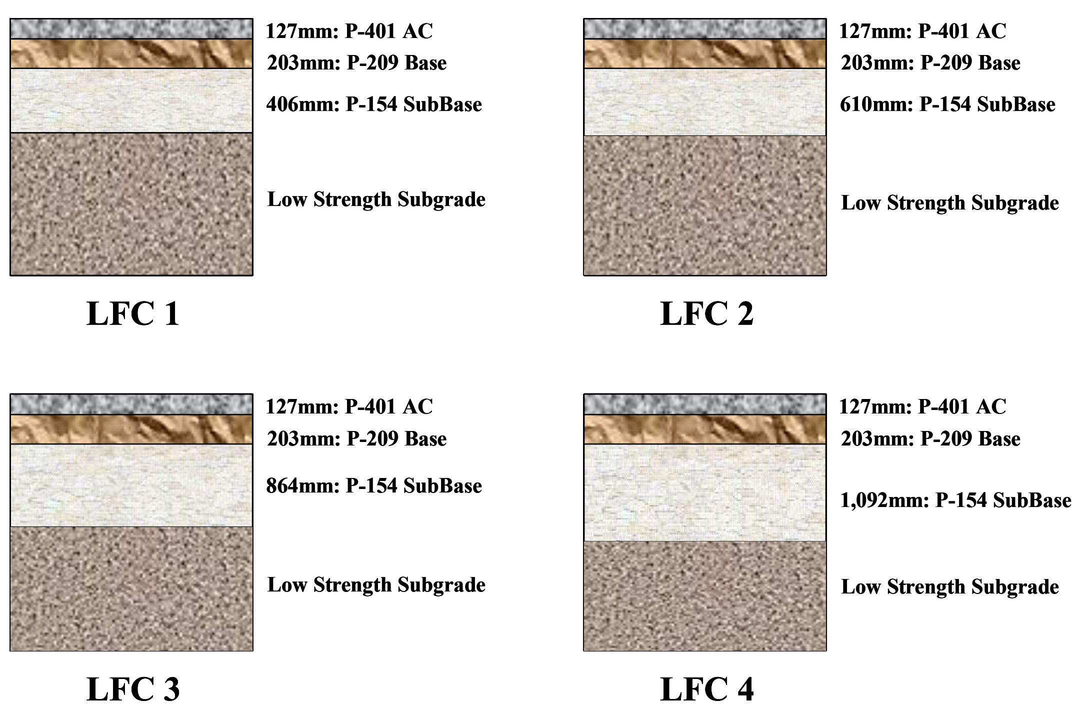


Figure 7-12 Cross Sections of NAPTF CC3 Pavement Test Sections (Garg, 2003)

The NAPTF flexible pavement test sections were analyzed as three-dimensional solids consisting of linear and nonlinear elastic layers in order to employ the nonlinear response models in the ABAQUS™ finite element programs. To employ the nonlinear resilient material models in the finite element solutions, the universal model for base and subbase layers and the bilinear subgrade model were selected. Table 7-2 summarizes the pavement geometry and assigned material input properties. The applied wheel pressure was set to 1.69-MPa and the same loading configuration was used in Figure 7-5.

Table 7-2 Material Properties used in the Nonlinear Finite Element Analysis of NAPTF CC3 Pavement Test Sections

<table>
<tr><th>Section</th><th>Element</th><th>Thickness (mm)</th><th>E (MPa)</th><th>ν</th><th colspan="4">Material Properties</th></tr>
<tr><td>AC</td><td>8-noded solid</td><td>127</td><td>3,445</td><td>0.35</td><td colspan="4">Isotropic and Linear Elastic</td></tr>
<tr><td rowspan="3">Base</td><td rowspan="3">8-noded solid</td><td rowspan="3">203</td><td rowspan="3">159 (initial)</td><td rowspan="3">0.38</td><td colspan="4">Nonlinear: Uzan model (Uzan, 1985)</td></tr>
<tr><td colspan="2">$K_1$ (MPa)</td><td>$K_2$</td><td>$K_3$</td></tr>
<tr><td colspan="2">79</td><td>0.33</td><td>0.01</td></tr>
<tr><td rowspan="3">Subbase</td><td rowspan="3">8-noded solid</td><td rowspan="3">Various</td><td rowspan="3">124 (initial)</td><td rowspan="3">0.38</td><td colspan="4">Nonlinear: Uzan model (Uzan, 1985)</td></tr>
<tr><td colspan="2">$K_1$ (MPa)</td><td>$K_2$</td><td>$K_3$</td></tr>
<tr><td colspan="2">37.1</td><td>0.49</td><td>-0.08</td></tr>
<tr><td rowspan="3">Subgrade</td><td rowspan="3">8-noded solid</td><td rowspan="3">Various</td><td rowspan="3">20.7 (initial)</td><td rowspan="3">0.40</td><td colspan="4">Nonlinear: Bilinear model (Thompson and Robnett, 1979)</td></tr>
<tr><td>$E_{Ri}$ (MPa)</td><td>$\sigma_{di}$ (MPa )</td><td>$K_3$</td><td>$K_4$</td></tr>
<tr><td>19.3</td><td>0.04</td><td>872</td><td>155</td></tr>
</table>

The pavement geometries, loading conditions, tire pressure, load radius, and layer material properties listed in Table 7-2 were assigned in the three-dimensional finite element analyses of these conventional flexible pavements having different subbase layer thicknesses. Figure 7-13 shows the three-dimensional mesh and the pavement model analyzed.

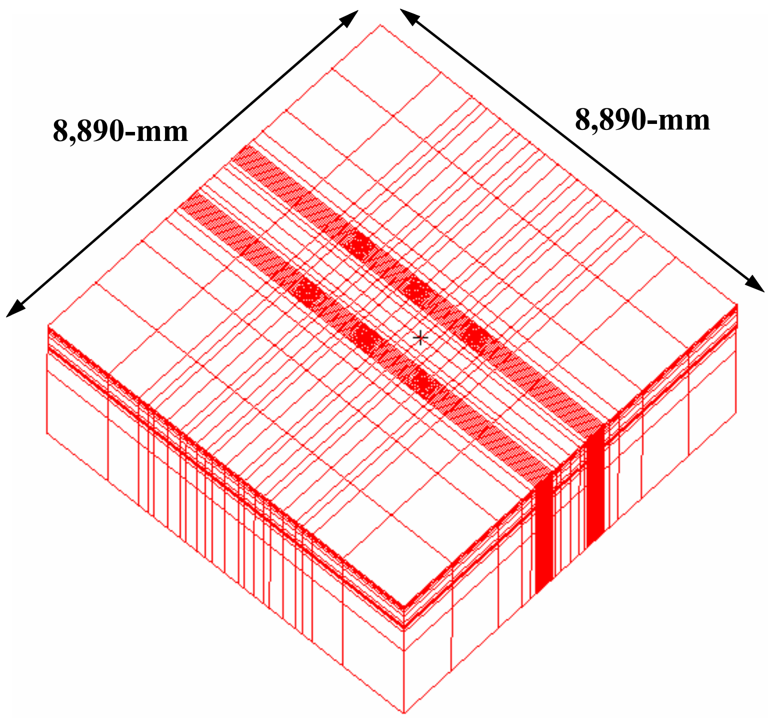


Figure 7-13 Three-dimensional Finite Element Mesh for CC3 NAPTF Test Sections

Figure 7-14 and Figure 7-15 indicate that somewhat thinner sections still yield two peaks directly under the wheels for the highest subgrade vertical deflections and stresses computed. As the granular subbase gets substantially thicker, the one peak response is finally encountered in the middle of the two wheels along that same wheel path. These results are in line with the FAA's NAPTF instrumented pavement test section

MDD results with one exception that often the first axle/wheel passing over the MDD was found to record higher deflection values when compared to the second and third axles due to the dynamic or moving nature of the wheel loading (Donovan and Tutumluer, 2007). Nevertheless, such a methodology utilizing three-dimensional finite element analyses of flexible pavements with nonlinear base/subbase and subgrade, as demonstrated herein, can be used to analyze multiple wheel loads and compute critical subgrade stress/strain profiles in order to adequately consider multiple wheel load interaction and its effects on mechanistic based pavement design.

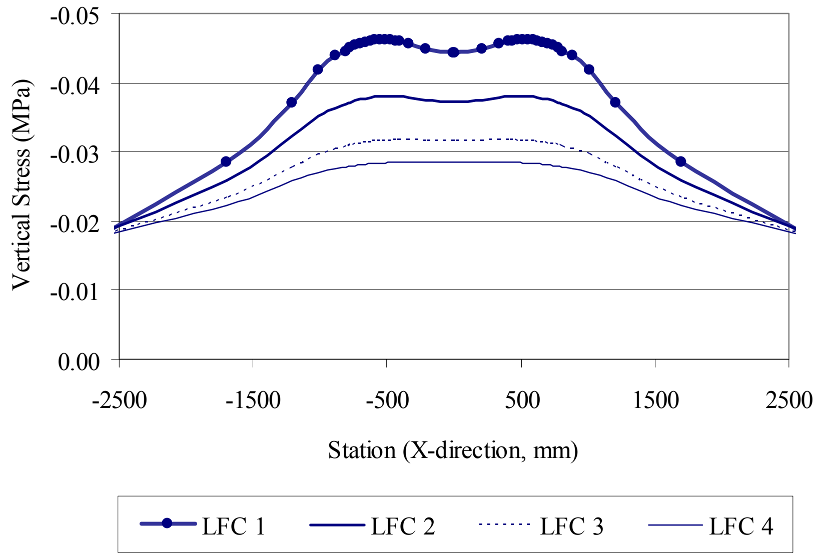


(a) Subgrade vertical stresses

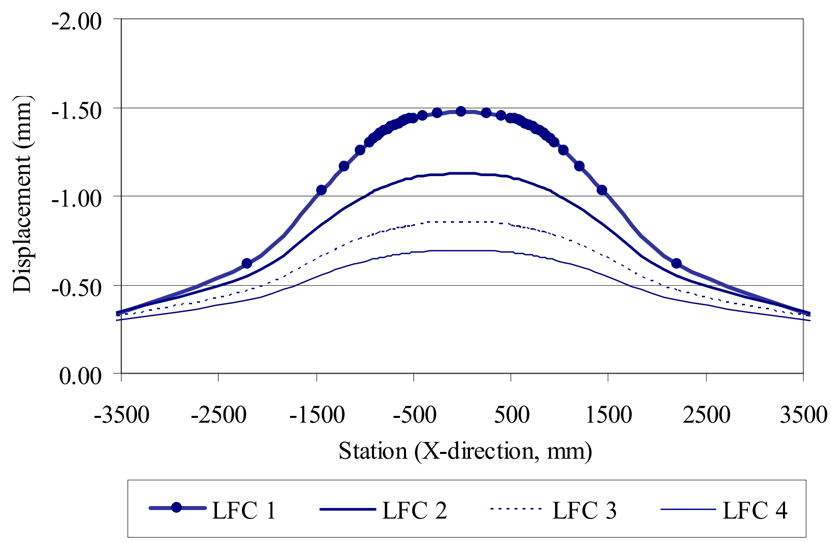


(b) Subgrade vertical displacements

Figure 7-14 Predicted Subgrade Responses in the Direction of Wheel Path subjected to Tandem Axle in CC3 NAPTF Pavement Test Sections

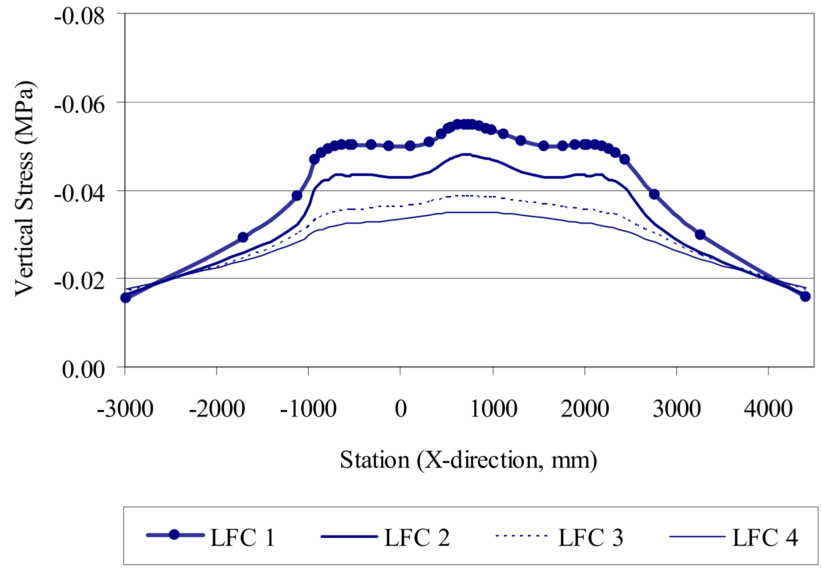


(a) Subgrade vertical stresses

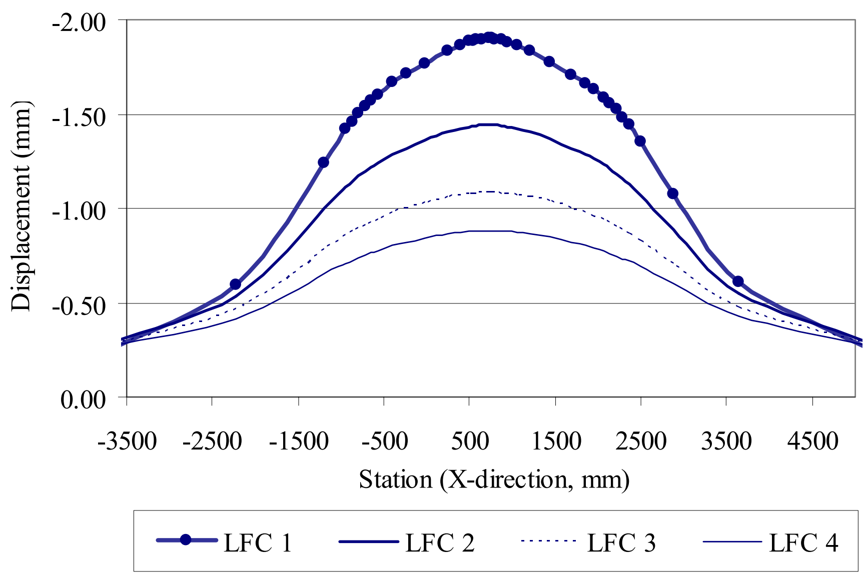


(b) Subgrade vertical displacements

Figure 7-15 Predicted Subgrade Responses in the Direction of Wheel Path subjected to Tridem Axle in CC3 NAPTF Pavement Test Sections

## 7.3 Summary

The objective of this chapter was to conduct three-dimensional finite element analyses using the general purpose ABAQUS$^{TM}$ finite element program by adequately accounting for the nonlinear resilient behavior of geomaterials using the developed UMAT subroutine and validating the prediction ability of accurate pavement responses when compared to field measured pavement responses of the National Airport Pavement Test Facility (NAPTF) traffic testing. Multi-Depth Deflectometers (MDDs) and Pressure Cells (PCs) in the first built group of test sections, named as Construction Cycle 1 (CC1), were installed in the test sections to measure the NAPTF pavement structural responses. The investigation with the developed UMAT subroutine proved that three-dimensional nonlinear flexible pavement analyses could be accurately performed in the case of multiple wheel/gear loading applied on a flexible airport pavement test sections. The predicted pavement responses matched closely with the displacements and stresses measured in the field and the finite element analyses could be reasonably applied to the design of airfield pavements serving multiple wheel gear loads when the nonlinear pavement geomaterials were considered. Especially, good agreements were found between measured and predicted values of subgrade vertical stress and surface deflection in the MFC section.

From the study of pavement layer thickness requirements using CC3 NAPTF pavement sections, the subgrade vertical stresses and deflections were considerably influenced by both loading and the layer thicknesses. In the study of effect of pavement layer thickness on subgrade responses, the thicker base/subbase layer had one peak response on subgrade in the middle of the wheels regardless of wheel configuration. A key consideration was to properly estimate the needed base/subbase thickness to protect the subgrade and at the same time minimize rutting in granular base/subbase layers.

# Chapter 8 Analyzing Multiple Wheel Load Interaction in Flexible Pavements

Flexible pavements are commonly used for low to high volume highway pavements subjected to different truck axle/wheel arrangements and for runways, taxiways, and aprons of major hub airfields subjected to heavy aircraft gear/wheel loads. As the demand for heavier wheel loads and number of load applications continually increases, these multiple wheel loading conditions and their damage potentials in the field should be realistically taken into account in pavement structural analysis. However, computing accurate pavement responses, i.e., stress, strain, deflection, under multiple loads is complex although currently a necessity for mechanistic-empirical pavement design and it requires the consideration of multiple wheel load interaction effects due to adjacent wheel locations.

To study loading effects of multiple wheels, the principle of superposition has been regarded as an essential approach, often using single wheel responses from axisymmetric analysis, when these solutions to flexible pavement problems incorporated isotropic, homogeneous, and linear elastic layers. However, it was recognized that pavement foundation geomaterials, e.g., fine-grained subgrade soils and unbound aggregates used in untreated base/subbase layers, exhibit nonlinear behavior which nullifies the single wheel pavement response superposition principle, which is theoretically valid for linear elastic systems. That leaves three-dimensional nonlinear finite element solutions as the viable means to compute accurate pavement responses at critical locations under multiple wheel loading scenarios, study the extent of error made by using the superposition principle in nonlinear pavement systems, and determine how feasible it is to assume superposition in routine pavement analysis by engineers and practitioners.

This chapter describes the pavement modeling research effort focused on computing more accurate finite element analysis results of pavement structures subjected to different multiple wheel loading scenarios and investigating the adequacy of the superposition principle. The objective is to show that three-dimensional nonlinear finite element analysis of the full multiple wheel loading is capable of accounting for the effects of different axle/wheel and gear configurations. For this purpose, both linear elastic and nonlinear, stress-dependent pavement geomaterial modulus models are employed in the analyses. Comparisons are made between the single wheel superposition and full three-dimensional loading results to emphasize the importance of nonlinear material characterizations on predicting more accurately critical pavement responses and the effects of multiple wheel load interactions.

## 8.1 Previous Studies on Multiple Wheel Load Interaction

Pavements are complex layered systems involving the interaction of different variables, i.e., applied wheel loads, environmental factors, etc. One way of evaluating the effects of wheel load interaction is to conduct full-scale tests on instrumented pavement sections. In-situ instrumentation of pavement structures is a valid approach used to monitor the responses of pavements when subjected to various combinations of axle/wheel types. Another way is to conduct numerical modeling analyses to determine pavement responses and evaluate the interaction effects. These two methods have been mainly used in the analyses of pavements subjected to multiple wheel loads.

Chou and Ledbetter (1973) calculated the final pavement responses, such as stress, strain, deflection, equivalent to the summation of the results from each single wheel load case in a Corps of Engineers (COE) study performed in Stockton Airfield as well as the multiple wheel heavy gear load tests conducted at the Waterways Experiment Station (WES). The main objective of their study was to investigate the validity of the principle of superposition for airfield flexible pavement analysis. Several loading cases were considered for static and dynamic wheel loads. For the superposition of various single wheel load levels, higher measured deflections were reported when compared to the superposed values, and the superposed stress values tended to be lower than the actual measured stresses for a stress-softening clayey silt section. Yet, the opposite was observed for the stress-hardening sand section. In the end, however, they concluded that when single wheel responses were correctly measured and each wheel had the same load, the superposition for multiple wheel loads was a reasonably valid approach.

Federal Aviation Administration (FAA) constructed National Airport Pavement Test Facility (NAPTF) where the primary objective was to develop new airport pavement design procedures for the next generation aircraft configured with complex and large loading gears (Thompson and Garg 1999, Hayhoe and Garg 2002, Gomez-Ramirez 2002). To quantify load induced responses from aircraft multiple wheel gears, six flexible pavement sections were constructed for the first cycle of testing over low, medium, and high strength subgrades at the NAPTF (Hayhoe and Garg, 2002). The pavement sections were loaded by typical aircraft gear configurations, i.e., dual single, dual tandem, dual tridem. Vertical subgrade deformations/strains measured from Multi-Depth Deflectometers (MDDs) in the NAPTF first cycle tests showed that accurately predicting pavement responses was extremely difficult. The elastic pavement layer behavior did not well represent significant strain differences between the first and the last peaks of wheel passages. After terminating trafficking on the first cycle tests, the next set of flexible pavements with variable subbase thicknesses were also built over the low strength subgrade to determine the adequacy of subbase thickness designs needed to protect the weak subgrade.

Thompson and Garg (1999) introduced an "Engineering Approach" to determine critical pavement responses under typical multiple wheel aircraft gear loadings and evaluate wheel load interaction effects on the flexible pavement responses. The "Engineering Approach" used average layer modulus values computed from nonlinear axisymmetric ILLI-PAVE finite element analysis and these values established the inputs for elastic layered analyses to solve for multiple wheel loading scenarios. The actual modulus distributions were, however, different from the single modulus assignment into the entire horizontal pavement layer. Based on the findings of the FAA's NAPTF full scale pavement tests, Gomez-Ramirez (2002) also proposed that the principle of superposition could be applied to the design and analysis of airport pavements subjected to aircraft gear loads, if single wheel nonlinear responses were accurately determined. From the reviews of previous studies, the more accurate way to consider three-dimensional stress-dependent modulus distributions under individual wheel loads would be through performing a full three-dimensional structural analysis for pavements subjected to multiple wheel loads.

## 8.2 Finite Element Analyses of Multiple Wheel Loads

### 8.2.1 Pavement Modeling Considerations

The finite element domain size study in Chapter 4 proved that the domain size of 140-times the radius of circular loading (R) in the vertical direction and 20-times R in the horizontal direction consistently gave accurate and repeatable results for the case of equivalent single wheel loading. Therefore, the same domain size was used in this study.

Using the developed ABAQUS$^{TM}$ UMAT subroutine, conventional flexible pavements analyzed consisted of a linear elastic asphalt concrete (AC) layer underlain by nonlinear elastic unbound base and subgrade layers. A uniform pressure of 0.55-MPa was applied over a circular area of 107-mm radius. As shown in Figure 8-1, the finite element structural analyses were then conducted using the first order 8-noded isoparametric linear hexahedron elements in a square prism three-dimensional mesh having sizes of 21,336-mm in the vertical direction and 6,096-mm in the horizontal direction. All vertical boundary nodes had roller supports with fixed horizontal boundary nodes used at the bottom.

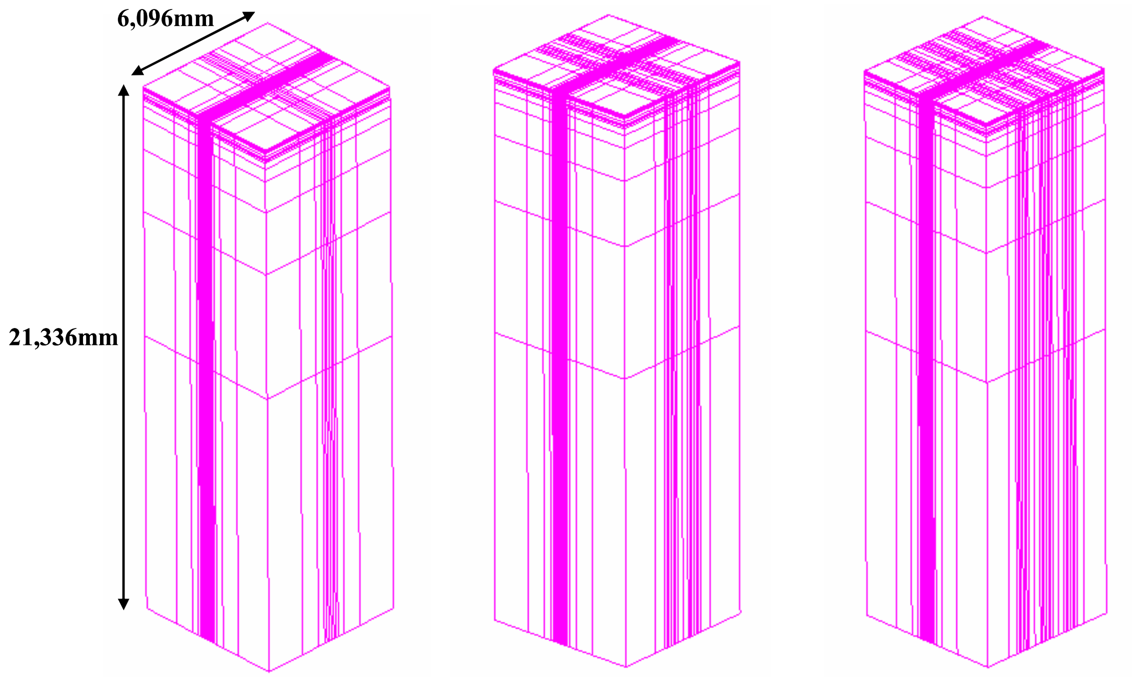


(a) Single axle (b) Tandem axle (c) Tridem axle

Figure 8-1 Three-dimensional Finite Element Meshes used in Various Multiple Wheel Loading Cases

To investigate wheel load interaction, three sets of axle configuration, i.e., single, tandem, and tridem, were investigated. As shown in Figure 8-2, the stress distributions caused by the adjacent load in a tandem configuration are superimposed yielding a different stress distribution caused by adjacent wheel. Due to the close spacing between axles/wheels, the critical pavement responses under multiple loads are different from those under a single load. Even if the passage of each set of multiple loads is assumed to be one repetition, the damage caused by single axle would not be the same as that caused by tandem or tridem axle. The analyses indicated that the primary response parameters of pavement caused by different load configurations were substantially different from each other.

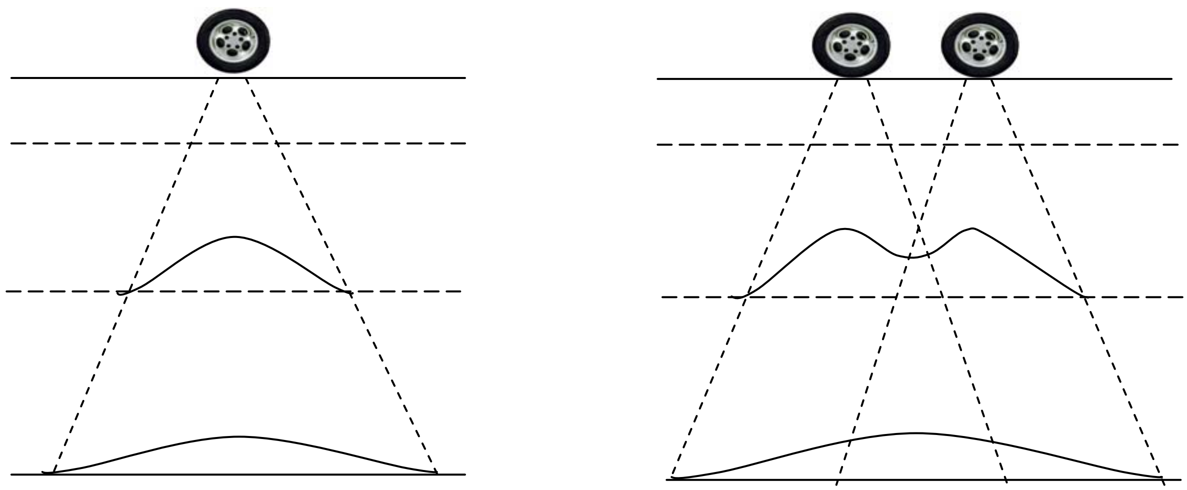

(a) Single axle (b) Tandem axle

Figure 8-2 Vertical Stress Distributions under Single and Tandem Axle Loads

### 8.2.2 Finite Element Analyses of Multiple Wheel Loads

The capabilities of three-dimensional finite element solutions for flexible pavement structural analysis have already been discussed in Chapter 2. However, the computational intensiveness of a three-dimensional finite element analysis still makes it impractical for routine pavement design usage. To overcome this difficulty, axisymmetric finite element analyses with single wheels were used to approximate multiple wheel effects via superposition (Thompson and Garg 1999, Gomez-Ramirez 2002). Such axisymmetric nonlinear finite element solutions for circular wheel loading conducted through the Strategic Highway Research Program (SHRP) by Lytton et al. (1993), however, indicated up to 20% differences in the computed stresses and displacements from nonlinear superposition.

To study wheel load interaction through three-dimensional finite element analyses, Figure 8-3 shows the typical truck axle arrangements consisting of single axle with dual tires, tandem axle with dual tires, and tridem axle with dual tires (Huang, 1993). The spacing of 343-mm was considered for each wheel and 1,219-mm for each axle in this study. Figure 8-3(d) shows the plan view of the generated finite element mesh for the tridem axle arrangement and the middle dual wheel detail.

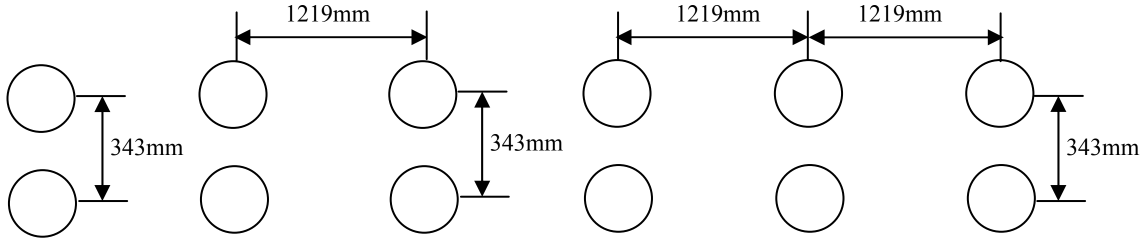


(a) Dual single (b) Dual tandem (c) Dual tridem

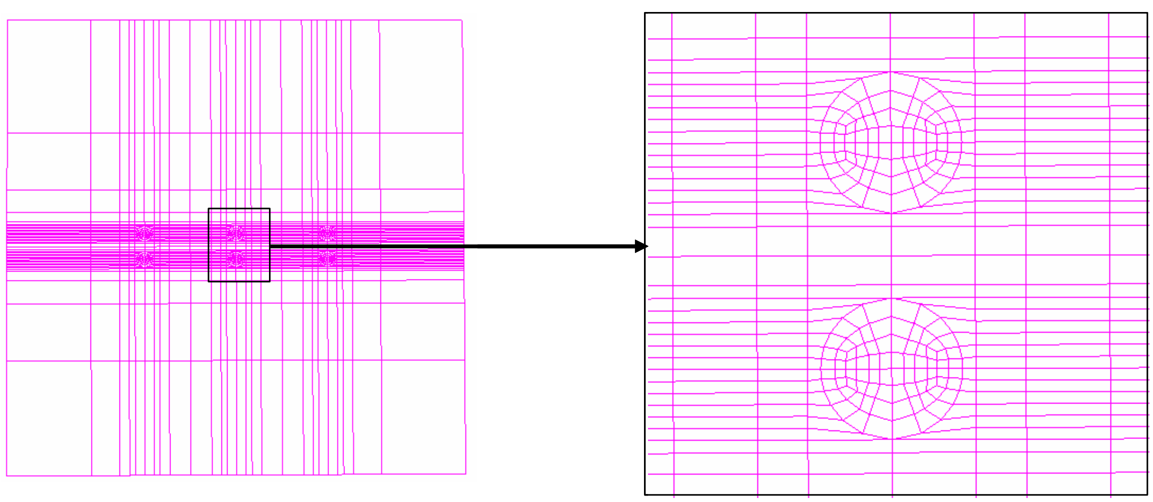

(d) Finite element mesh plan view for the tridem axle showing the dual wheel detail

Figure 8-3 Different Circular Contact Areas Associated with Various Axle Arrangements and the Finite Element Mesh for the Tridem Axle

The three-dimensional finite element analyses for multiple wheel loadings were performed next for single, tandem, and tridem axle arrangements now considering two pavement geometry cases as follows:

Pavement (1): 102-mm of AC and 254-mm of aggregate base;

Pavement (2): 76-mm of AC and 305-mm of aggregate base.

Pavement responses were predicted from three-dimensional ABAQUS™ finite element analyses; all using the linear elastic AC material properties and the following pavement layer characterizations: (i) linear elastic, (ii) nonlinear base and linear subgrade, (iii) nonlinear base and nonlinear subgrade. The layer material properties listed in Table 8-1 were assigned in all the pavement sections analyzed.

Table 8-1 Pavement Geometries and Material Properties used in the Three-dimensional Finite Element Analyses for Studying Multiple Wheel Load Interaction

<table>
<tr><th>Section</th><th>Element</th><th>E (MPa)</th><th>$\nu$</th><th colspan="4">Material Properties</th></tr>
<tr><td>AC</td><td>8-noded solid</td><td>2,759</td><td>0.35</td><td colspan="4">Isotropic and Linear Elastic</td></tr>
<tr><td rowspan="3">BASE</td><td rowspan="3">8-noded solid</td><td rowspan="3">138 (initial)</td><td rowspan="3">0.40</td><td colspan="4">Nonlinear: Universal Model with octahedral shear stress, $\tau_{oct}$ (Witczak and Uzan, 1988)</td></tr>
<tr><td colspan="2">$K_1$</td><td>$K_2$</td><td>$K_3$</td></tr>
<tr><td colspan="2">1,098</td><td>0.64</td><td>0.065</td></tr>
<tr><td rowspan="3">SUBGRADE</td><td rowspan="3">8-noded solid</td><td rowspan="3">41 (initial)</td><td rowspan="3">0.45</td><td colspan="4">Nonlinear: Bilinear model (Thompson and Robnett, 1979)</td></tr>
<tr><td>$E_{RI}$ (kPa)</td><td>$\sigma_{di}$ (kPa)</td><td>$K_3$ (kPa/kPa)</td><td>$K_4$ (kPa/kPa)</td></tr>
<tr><td>41,400</td><td>41</td><td>1,000</td><td>200</td></tr>
</table>

To identify critical pavement response locations under the various axle load arrangements for the full three-dimensional finite element analyses, two different conventional flexible pavement geometries, pavements (1) and (2), were mainly selected to represent typical low volume roads. Figure 8-4 shows possible locations investigated for computing pavement responses in an effort to determine the locations of maximum critical pavement responses, i.e., surface deflection ($\delta_{surface}$), horizontal stress and strain at the bottom of AC ($\sigma_h$ and $\varepsilon_h$), vertical stress and strain on the top of subgrade ($\sigma_v$ and $\varepsilon_v$).

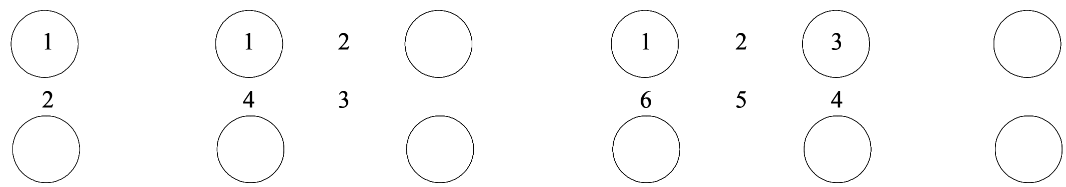


(a) Dual single (b) Dual tandem (c) Dual tridem

Figure 8-4 Locations of Pavement Responses Associated with Various Axle Arrangements

Table 8-2 gives the detailed comparisons of the predicted critical pavement responses for single axle dual wheel loads. While for $\varepsilon_h$ at the bottom of AC the critical pavement response location is directly under the wheel (location 1), for $\delta_{surface}$ and $\varepsilon_v$ on the top of subgrade, the critical pavement response occurs in between the wheels (location 2). The nonlinear base characterizations using the universal model (Witczak and Uzan, 1988) had a considerable effect on the predicted critical responses. For the combined nonlinear base and nonlinear subgrade analyses, percent differences from the linear elastic case are still seen although the discrepancy diminishes especially in surface deflection.

Table 8-2 Comparisons of Predicted Single Axle Pavement Responses from Three-dimensional Linear and Nonlinear Finite Element Analyses

| Pavement (1): 102-mm of AC and 254-mm of aggregate base | | | | |
|---|---|---|---|---|
| Pavement response** / location*** | | Linear base and linear subgrade | Nonlinear base and linear subgrade | Nonlinear base and nonlinear subgrade |
| $\delta_{surface}$ (mm) | 1 | -6.74X10$^{-01}$ | -7.73X10$^{-01}$ (14.8)* | -6.46X10$^{-01}$ (-4.1) |
| | ***2*** | ***-6.84X10$^{-01}$*** | ***-7.89X10$^{-01}$ (15.3)*** | ***-6.73X10$^{-01}$ (-3.6)*** |
| $\varepsilon_{h\ bottom\ of\ AC}$ ($\mu\varepsilon$) | ***1*** | ***188*** | ***214 (13.6)*** | ***204 (8.4)*** |
| | 2 | -21 | 2 (-92.1) | -5 (-78.0) |
| $\varepsilon_{v\ top\ of\ subgrade}$ ($\mu\varepsilon$) | 1 | -616 | -661 (7.3) | -617 (0.2) |
| | ***2*** | ***-680*** | ***-716 (5.3)*** | ***-671 (-1.3)*** |
| Pavement (2): 76-mm of AC and 305-mm of aggregate base | | | | |
| Pavement response** / location*** | | Linear base and linear subgrade | Nonlinear base and linear subgrade | Nonlinear base and nonlinear subgrade |
| $\delta_{surface}$ (mm) | 1 | -7.47X10$^{-01}$ | -8.76X10$^{-01}$ (17.3)* | -7.37X10$^{-01}$ (-1.4) |
| | ***2*** | ***-7.44X10$^{-01}$*** | ***-8.77X10$^{-01}$ (17.9)*** | ***-7.36X10$^{-01}$ (-1.1)*** |
| $\varepsilon_{h\ bottom\ of\ AC}$ ($\mu\varepsilon$) | ***1*** | ***194*** | ***236 (22.0)*** | ***230 (18.7)*** |
| | 2 | -65 | -96 (46.7) | -99 (52.2) |
| $\varepsilon_{v\ top\ of\ subgrade}$ ($\mu\varepsilon$) | 1 | -664 | -743 (12.0) | -710 (6.9) |
| | ***2*** | ***-703*** | ***-797 (13.4)*** | ***-762 (8.5)*** |

* The percentage value in the parenthesis indicates change from the linear elastic result.
** Critical pavement responses are given in bold and italic.
*** 1 and 2 indicate the locations under the wheel and between the wheels shown in Figure 8-2, respectively.

Table 8-3 lists the predicted pavement responses for tandem axle loads according to different material characterizations. While for $\varepsilon_h$ at the bottom of AC the critical pavement response location is again under the wheel (location 1), for $\delta_{surface}$ and $\varepsilon_v$ on the top of subgrade, the critical pavement response again occurs in between the wheels (location 4). In contrast to the results of single axle dual wheel analyses, the differences in the case of nonlinear base and subgrade analyses show large percentages. The multiple axle/wheel loading is likely to produce different nonlinear modulus and stress distributions when compared to single wheel loading and the adjacent wheel loads appreciably affect pavement responses.

Table 8-3 Comparisons of Predicted Tandem Axle Pavement Responses from Three-dimensional Linear and Nonlinear Finite Element Analyses

| Pavement (1): 102-mm of AC and 254-mm of aggregate base | | | | |
|---|---|---|---|---|
| Pavement response** / location*** | | Linear base and linear subgrade | Nonlinear base and linear subgrade | Nonlinear base and nonlinear subgrade |
| $\delta_{surface}$ (mm) | 1 | $-8.48X10^{-01}$ | $-9.36X10^{-01}$ (10.4)* | $-7.63X10^{-01}$ (-10.0) |
| | 2 | $-6.85X10^{-01}$ | $-7.44X10^{-01}$ (8.5) | $-5.63X10^{-01}$ (-17.8) |
| | 3 | $-7.05X10^{-01}$ | $-7.68X10^{-01}$ (9.0) | $-5.84X10^{-01}$ (-17.2) |
| | ***4*** | ***$-8.59X10^{-01}$*** | ***$-9.52X10^{-01}$ (10.8)*** | ***$-7.77X10^{-01}$ (-9.5)*** |
| $\varepsilon_{h\ bottom\ of\ AC}$ ($\mu\varepsilon$) | ***1*** | ***191*** | ***218 (13.9)*** | ***207 (8.3)*** |
| | 2 | 47 | 69 (46.8) | 60 (27.2) |
| | 3 | 55 | 79 (44.9) | 70 (28.5) |
| | 4 | -17 | 7 (-57.3) | 0 (-98.0) |
| $\varepsilon_{v\ top\ of\ subgrade}$ ($\mu\varepsilon$) | 1 | -586 | -623 (6.4) | -581 (-0.7) |
| | 2 | -200 | -190 (-5.3) | -131 (-34.4) |
| | 3 | -224 | -217 (-3.4) | -154 (-31.2) |
| | ***4*** | ***-654*** | ***-683 (4.5)*** | ***-639 (-2.3)*** |
| Pavement (2): 76-mm of AC and 305-mm of aggregate base | | | | |
| Pavement response** / location*** | | Linear base and linear subgrade | Nonlinear base and linear subgrade | Nonlinear base and nonlinear subgrade |
| $\delta_{surface}$ (mm) | 1 | $-9.22X10^{-01}$ | $-10.3X10^{-01}$ (12.2) | $-8.43X10^{-01}$ (-8.6) |
| | 2 | $-6.85X10^{-01}$ | $-7.55X10^{-01}$ (10.3) | $-5.59X10^{-01}$ (-18.4) |
| | 3 | $-7.04X10^{-01}$ | $-7.81X10^{-01}$ (10.9) | $-5.80X10^{-01}$ (-17.6) |
| | ***4*** | ***$-9.21X10^{-01}$*** | ***$-10.4X10^{-01}$ (12.8)*** | ***$-8.44X10^{-01}$ (-8.4)*** |
| $\varepsilon_{h\ bottom\ of\ AC}$ ($\mu\varepsilon$) | ***1*** | ***192*** | ***237 (23.6)*** | ***230 (19.8)*** |
| | 2 | 16 | 68 (323.3) | 61 (274.1) |
| | 3 | 17 | 66 (287.2) | 60 (251.1) |
| | 4 | -52 | -91 (74.2) | -97 (85.7) |
| $\varepsilon_{v\ top\ of\ subgrade}$ ($\mu\varepsilon$) | 1 | -640 | -710 (10.8) | -667 (4.1) |
| | 2 | -248 | -167 (-32.7) | -101 (-59.2) |
| | 3 | -275 | -202 (-26.8) | -122 (-55.5) |
| | ***4*** | ***-688*** | ***-758 (10.3)*** | ***-723 (5.2)*** |

* The percentage value in the parenthesis indicates change from the linear elastic result.
** Critical pavement responses are given in bold and italic.
*** 1 and 4 indicate the locations under the wheel and between the wheels shown in Figure 8-2, respectively.

Table 8-4 lists the predicted pavement responses for the tridem axle loads according to the different material characterizations. While for $\varepsilon_h$ at the bottom of AC the critical pavement response location is under the wheel at location 3, for $\delta_{surface}$ and $\varepsilon_v$ on the top of subgrade, the critical pavement response occurs in between the wheels at location 4 (see Figure 8-4). The wheel/axle load interaction this time is a significant factor affecting pavement responses. Especially, surface displacements are more influenced than others in the nonlinear analyses.

Table 8-4 Comparisons of Predicted Tridem Axle Pavement Responses from Three-dimensional Linear and Nonlinear Finite Element Analyses

| Pavement response** / location*** | | Linear base and linear subgrade | Nonlinear base and linear subgrade | Nonlinear base and nonlinear subgrade |
|---|---|---|---|---|
| Pavement (1): 102-mm of AC and 254-mm of aggregate base | | | | |
| $\delta_{surface}$ (mm) | 1 | -9.67X10$^{-01}$ | -10.5X10$^{-01}$ (9.0)* | -8.35X10$^{-01}$ (-13.6) |
| | 2 | -8.35X10$^{-01}$ | -8.89X10$^{-01}$ (6.5) | -6.54X10$^{-01}$ (-21.7) |
| | 3 | -10.8X10$^{-01}$ | -11.5X10$^{-01}$ (7.3) | -9.08X10$^{-01}$ (-15.6) |
| | ***4*** | ***-10.9X10$^{-01}$*** | ***-11.7X10$^{-01}$ (7.6)*** | ***-9.23X10$^{-01}$ (-15.3)*** |
| | 5 | -8.56X10$^{-01}$ | -9.15X10$^{-01}$ (6.9) | -6.76X10$^{-01}$ (-21.1) |
| | 6 | -9.79X10$^{-01}$ | -10.7X10$^{-01}$ (9.4) | -8.49X10$^{-01}$ (-13.3) |
| $\varepsilon_{h\ bottom\ of\ AC}$ ($\mu\varepsilon$) | 1 | 193 | 220 (14.0) | 207 (7.3) |
| | 2 | 49 | 36 (-26.3) | 30 (-38.7) |
| | ***3*** | ***199*** | ***223 (12.4)*** | ***211 (6.3)*** |
| | 4 | -9 | 14 (-56.6) | 5 (-41.8) |
| | 5 | 57 | 81 (43.1) | 71 (25.0) |
| | 6 | -15 | 9 (-37.1) | 1 (-94.6) |
| $\varepsilon_{v\ top\ of\ subgrade}$ ($\mu\varepsilon$) | 1 | -583 | -623 (6.8) | -583 (0.1) |
| | 2 | -196 | -184 (5.7) | -122 (37.7) |
| | 3 | -609 | -639 (4.9) | -590 (-3.2) |
| | ***4*** | ***-678*** | ***-701 (3.4)*** | ***-648 (-4.4)*** |
| | 5 | -220 | -210 (-4.3) | -144 (-34.4) |
| | 6 | -652 | -684 (4.9) | -638 (-2.2) |
| Pavement (2): 76-mm of AC and 305-mm of aggregate base | | | | |
| Pavement response** / location*** | | Linear base and linear subgrade | Nonlinear base and linear subgrade | Nonlinear base and nonlinear subgrade |
| $\delta_{surface}$ (mm) | 1 | -10.4X10$^{-01}$ | -11.5X10$^{-01}$ (10.8) | -9.21X10$^{-01}$ (-11.5) |
| | 2 | -8.33X10$^{-01}$ | -8.98X10$^{-01}$ (7.9) | -6.54X10$^{-01}$ (-21.5) |
| | 3 | -11.5X10$^{-01}$ | -12.5X10$^{-01}$ (8.7) | -9.87X10$^{-01}$ (-13.8) |
| | ***4*** | ***-11.5X10$^{-01}$*** | ***-12.5X10$^{-01}$ (8.7)*** | ***-9.89X10$^{-01}$ (-13.9)*** |
| | 5 | -8.53X10$^{-01}$ | -9.25X10$^{-01}$ (8.4) | -6.76X10$^{-01}$ (-20.7) |
| | 6 | -10.4X10$^{-00}$ | -11.6X10$^{-01}$ (11.2) | -9.22X10$^{-01}$ (-11.4) |
| $\varepsilon_{h\ bottom\ of\ AC}$ ($\mu\varepsilon$) | 1 | 192 | 241 (25.6) | 230 (20.0) |
| | 2 | 16 | 16 (-1.4) | 13 (-19.3) |
| | ***3*** | ***192*** | ***242 (25.9)*** | ***231 (20.2)*** |
| | 4 | -52 | -92 (77.2) | -94 (81.1) |
| | 5 | 17 | 60 (263.2) | 53 (222.2) |
| | 6 | -52 | -93 (78.2) | -96 (83.3) |
| $\varepsilon_{v\ top\ of\ subgrade}$ ($\mu\varepsilon$) | 1 | -638 | -707 (10.9) | -668 (4.7) |
| | 2 | -242 | -161 (-33.4) | -96 (-60.4) |
| | 3 | -660 | -713 (8.0) | -665 (0.9) |
| | ***4*** | ***-703*** | ***-766 (8.9)*** | ***-725 (3.2)*** |
| | 5 | -269 | -188 (-30.1) | -116 (-57.0) |
| | 6 | -685 | -762 (11.2) | -726 (6.0) |

* The percentage value in the parenthesis indicates change from the linear elastic result.
** Critical pavement responses are given in bold and italic.
*** 3 and 4 indicate the locations under the wheel and between the wheels shown in Figure 8-2, respectively.

### 8.2.3 Response Profiles due to Multiple Wheel Loads

The aforementioned study provides very good evidence to assure the need of three-dimensional finite element study for typical multiple axle/wheel load configurations. So, it is feasible to consider that all possible layouts of flexible pavements, typical layer arrangements and material types should provide useful pavement responses. The focus of this study is to predict pavement profile responses induced by multiple wheel loads. Showing the pavement response profiles along the pavement cross-section can easily show the effect of multiple wheel loads according to pavement material characterizations.

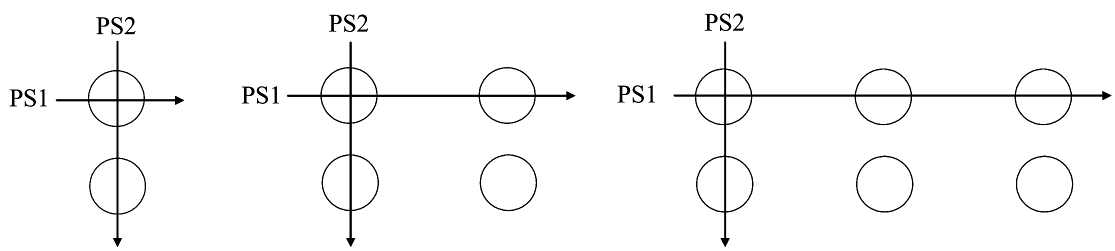


(a) Single axle (b) Tandem axle (c) Tridem axle

Figure 8-5 Profile Locations of Pavement Response Associated with Various Axle Configurations

Figure 8-6 gives detailed comparisons of the pavement responses along wheel load direction, profile section 1 (PS1), according to axle/wheel configurations in Figure 8-5. The axle/wheel configurations are the same as given in Figure 8-3 and the applied load conditions are also the same as in the previous analysis. In all nonlinear analyses, stress-dependent base and subgrade models were used. For surface deflections, the largest peak points are shown in the tridem configuration due to interaction effects and the point under the middle wheel gives a larger deflection than others. The single axle responses of surface deflection are indicated as the minimum deflections. In these figures, the load spreading ability was observed, and the vertical surface deflection basin showed more differences in magnitudes than in the case of vertical subgrade stresses.

Surface vertical displacements

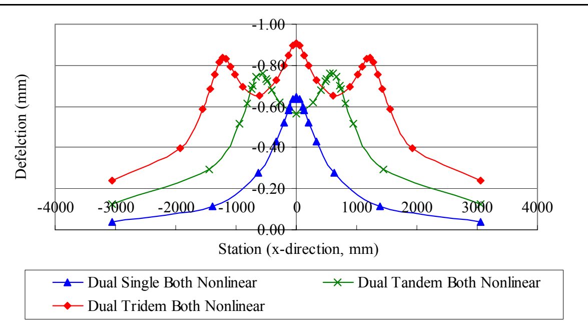


102-mm of AC and 254-mm of aggregate base

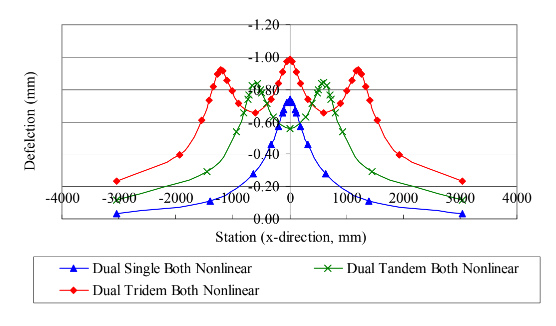


76-mm of AC and 305-mm of aggregate base

Subgrade vertical stresses

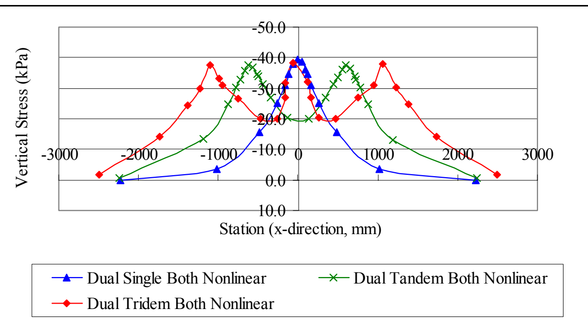


102-mm of AC and 254-mm of aggregate base

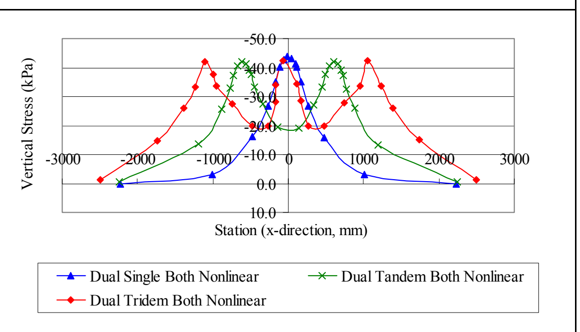


76-mm of AC and 305-mm of aggregate base

Figure 8-6 PS1 Response Profiles of Both Nonlinear Analyses associated with Various Axle Configurations

The response predicted for profiles transverse to loading direction, profile section 2 (PS2), are shown in Figure 8-7. Due to the very close distances between two wheels, the pavement responses are shown with one peak instead of two peaks. As the same trends of PS1, tridem axle has the largest pavement responses, especially for the surface deflections.

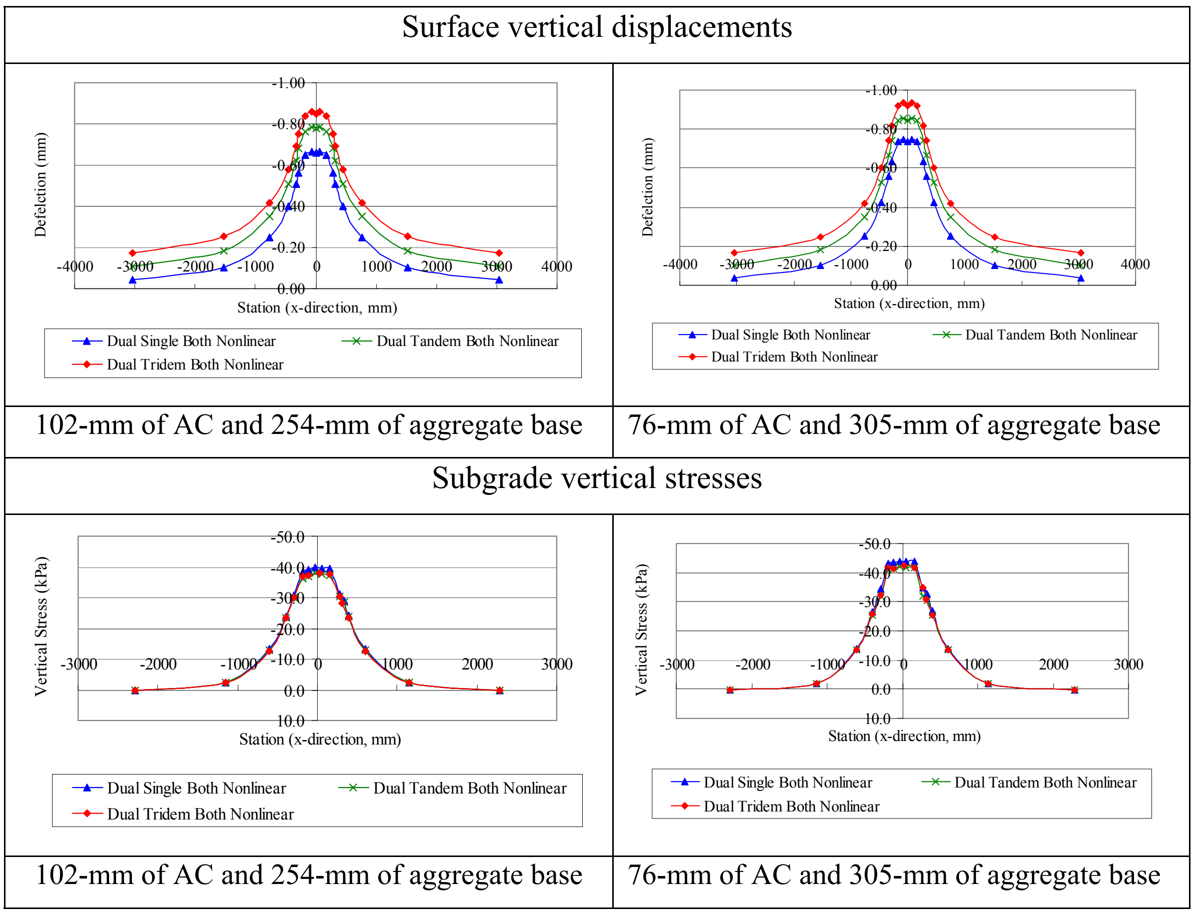


Figure 8-7 PS2 Response Profiles of Both Nonlinear Analyses associated with Various Axle Configurations

### 8.2.4 Differences between Three-dimensional and Superposed Analyses

A large number of three-dimensional finite element analyses were performed to quantify the differences resulting from the single wheel superposition. The goal was to compare between full three-dimensional finite element and the superposition analysis results for several different conventional flexible pavement geometries. In the superposition analysis, single wheel responses were added according to the following procedure exemplified for the maximum horizontal stress at the bottom of AC layer below wheel 1 of the dual tridem axle (see Figure 8-8):

$$\sigma_{multi-1} = \sigma_1 + \sigma_2 + \sigma_3 + \sigma_4 + \sigma_5 + \sigma_6 \qquad (8\text{-}1)$$

where $\sigma_{multi\text{-}1}$ : horizontal stress below wheel 1 due to the dual tridem axle;

$\sigma_1$ : horizontal stress below wheel 1 due to a single wheel at location 1;

$\sigma_2$ : horizontal stress below wheel 1 due to a single wheel at location 2;

$\sigma_3$ : horizontal stress below wheel 1 due to a single wheel at location 3;

$\sigma_4$ : horizontal stress below wheel 1 due to a single wheel at location 4;

$\sigma_5$ : horizontal stress below wheel 1 due to a single wheel at location 5;

$\sigma_6$ : horizontal stress below wheel 1 due to a single wheel at location 6.

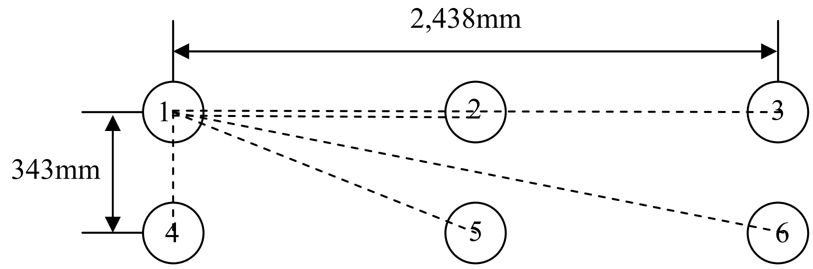


Figure 8-8 Superposition of Single Wheel Responses below Wheel 1

The same procedure was used to evaluate pavement responses at other locations subjected to multiple wheel loads. To evaluate the applicability of superposition, both linear and nonlinear pavement analyses were performed with the nonlinear solutions considering the stress dependencies of the base and subgrade materials. The conventional flexible pavement geometries analyzed included only thin AC layers of 76 and 102-mm with five different base course thicknesses ranging from relatively thin to substantially thick granular layers listed as follows:

Case (1): 102-mm of AC and 152-mm of aggregate base;

Case (2): 102-mm of AC and 254-mm of aggregate base;

Case (3): 76-mm of AC and 305-mm of aggregate base;

Case (4): 76-mm of AC and 457-mm of aggregate base;

Case (5): 76-mm of AC and 914-mm of aggregate base.

Pavement responses were predicted from three-dimensional ABAQUS™ finite element analyses; all using the linear elastic AC material properties and the following pavement layer characterizations: (i) linear elastic, (ii) nonlinear base and linear subgrade, (iii) nonlinear base and nonlinear subgrade. The same layer material properties listed in Table 8-1 were assigned in all the pavement sections analyzed. To start with, the universal model (Witczak and Uzan, 1988) was used in the base and the bilinear model (Thompson and Robnett, 1979) was utilized in the subgrade with the model parameters given in Table 8-1 and obtained from repeated load triaxial tests. The linear elastic solution then used the average modulus values from the modulus distributions of nonlinear analysis obtained at the center of wheel loading, similar to the "Engineering Approach" introduced by Thompson and Garg (1999). The differences in critical pavement responses between full three-dimensional and superposition analyses were computed using the following,

$$Difference\,(\%) = \frac{3D\ Multiple\ Wheel\ Response - Superposed\ Response}{3D\ Multiple\ Wheel\ Response} \times 100 \qquad (8\text{-}2)$$

In the case of linear elastic base and subgrade, the results from full three-dimensional and superposition analyses did not show any differences as expected. However, when nonlinear pavement geomaterial models were considered, the pavement responses from full three-dimensional loading and superposition from single wheel showed differences. Table 8-5 gives detailed comparisons of the predicted critical pavement responses for the selected pavement case studies. These three-dimensional finite element analyses were performed for single, tandem, and tridem axle loadings for two assigned pavement geometry cases, (2) and (3). In each case, the same finite element mesh, boundary conditions, material properties, and tire pressure were used for all analyses. The only different parameter was the axle/wheel configurations, i.e., single, tandem, and tridem.

Table 8-5 summarizes the differences between the full three-dimensional analysis results and the single wheel responses from superposition. For linear elastic analyses, the results from two analyses do not show any differences as expected. However, when nonlinear pavement geomaterial models were considered, the pavement responses from full three-dimensional loading and superposition from single wheel showed differences. In these comparisons, the nonlinear characterizations of the base layer caused a maximum 7.4% difference for the horizontal strain, 10.0% for the vertical strain, and 8.4% for the surface deflection. Since the superposed results from base nonlinearity are higher, the differences show a negative fashion in most comparisons and superposed results can bring conservative pavement responses. For the combined nonlinear base and subgrade characterizations, the most accurate pavement responses are still considerably different between two analyses. These relative differences in pavement responses are calculated from specific pavement geometries, material properties in layers, and loading conditions.

Table 8-5 Differences of Pavement Responses from Single Wheel Superposition

| Pavement Response (%) | Case (2): 102-mm of AC and 254-mm of aggregate base | | | | | | | | |
|---|---|---|---|---|---|---|---|---|---|
| | Linear base and linear subgrade | | | Nonlinear base and linear subgrade | | | Nonlinear base and nonlinear subgrade | | |
| | Single | Tandem | Tridem | Single | Tandem | Tridem | Single | Tandem | Tridem |
| $\delta_{v\_surface}$ | 0.0 | 0.0 | 0.0 | -8.4 | -4.8 | -3.5 | -7.0 | -2.5 | -2.1 |
| $\varepsilon_{h\_AC}$ | 0.0 | 0.0 | 0.0 | -6.0 | -6.3 | -4.6 | -4.7 | -4.0 | -4.6 |
| $\sigma_{h\_AC}$ | 0.0 | 0.0 | 0.0 | -9.4 | -6.7 | -4.5 | -7.7 | -4.4 | -4.9 |
| $\varepsilon_{v\_Subgrade}$ | 0.0 | 0.0 | 0.0 | -5.5 | -7.8 | -10.0 | 1.4 | -1.8 | -3.4 |
| $\sigma_{v\_subgrade}$ | 0.0 | 0.0 | 0.0 | -7.7 | -10.2 | -11.4 | -11.5 | -16.1 | -17.1 |
| Pavement Response (%) | Case (3): 76-mm of AC and 305-mm of aggregate base | | | | | | | | |
| | Linear base and linear subgrade | | | Nonlinear base and linear subgrade | | | Nonlinear base and nonlinear subgrade | | |
| | Single | Tandem | Tridem | Single | Tandem | Tridem | Single | Tandem | Tridem |
| $\delta_{v\_surface}$ | 0.0 | 0.0 | 0.0 | -6.4 | -4.2 | -2.8 | -6.5 | -2.0 | -1.1 |
| $\varepsilon_{h\_AC}$ | 0.0 | 0.0 | 0.0 | -7.4 | -7.3 | -7.2 | -6.4 | -5.7 | -6.0 |
| $\sigma_{h\_AC}$ | 0.0 | 0.0 | 0.0 | -9.9 | -7.4 | -6.1 | -8.5 | -5.5 | -6.3 |
| $\varepsilon_{v\_Subgrade}$ | 0.0 | 0.0 | 0.0 | 1.0 | -3.2 | -5.1 | 5.4 | 2.3 | 2.6 |
| $\sigma_{v\_subgrade}$ | 0.0 | 0.0 | 0.0 | -0.2 | -4.9 | -6.6 | -5.3 | -11.1 | -6.5 |

Figure 8-9 presents the response differences obtained from the analyses using linear elastic AC, nonlinear base, and linear subgrade pavement material characterizations shown in Table 8-1. The analysis results indicate that the superposition from single wheel would not utilize the pavement structural analyses subjected to multiple axles/wheels, since there are significant differences between the two analyses. Since all pavement responses from single wheel superposition are predicted larger in magnitude, the differences show the negative sign making superposition a conservative estimate.

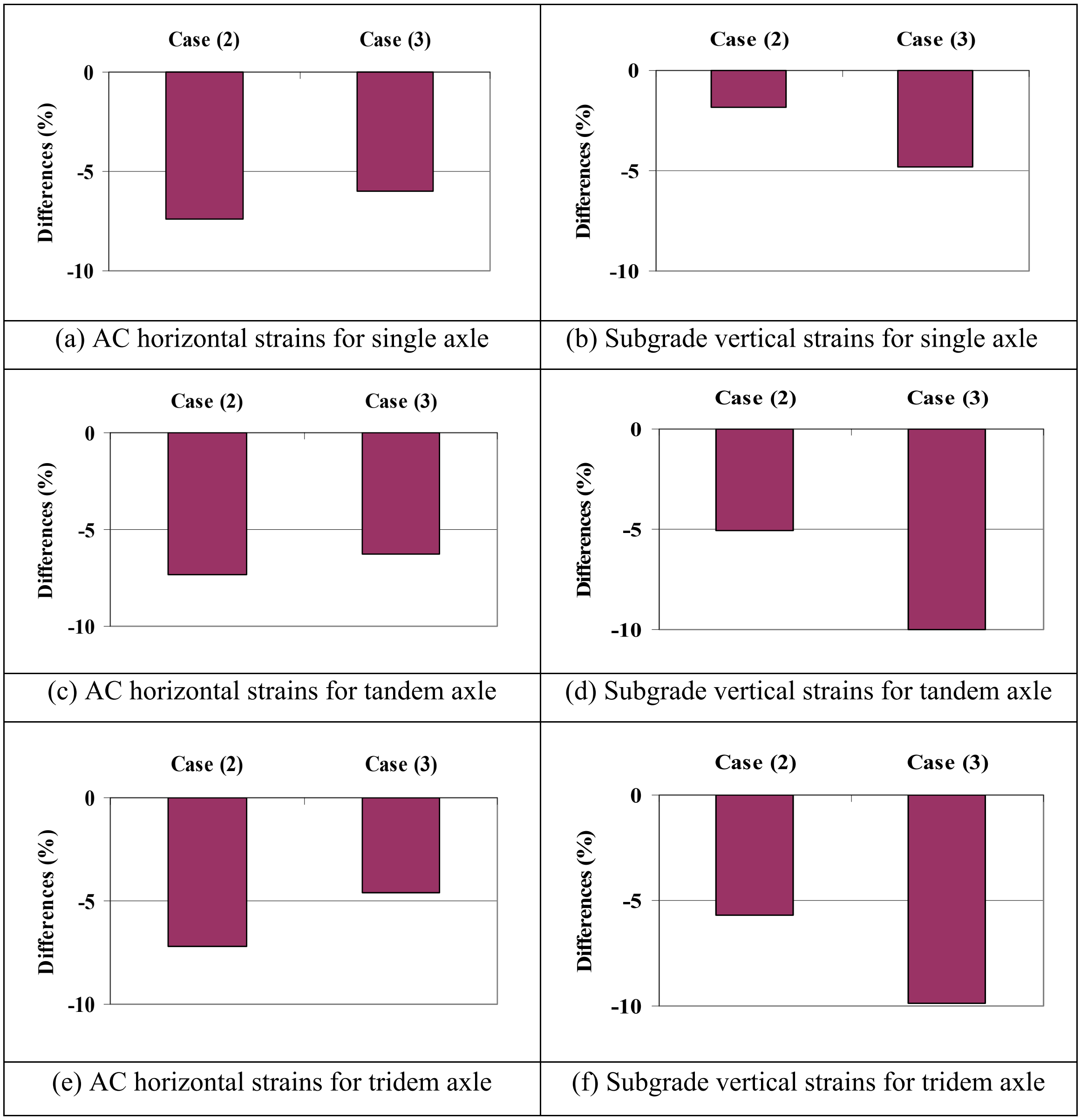


(a) AC horizontal strains for single axle

(b) Subgrade vertical strains for single axle

(c) AC horizontal strains for tandem axle

(d) Subgrade vertical strains for tandem axle

(e) AC horizontal strains for tridem axle

(f) Subgrade vertical strains for tridem axle

Figure 8-9 Differences in Superposed Pavement Responses from Nonlinear Base Analyses

Figure 8-10 gives for all five pavement case studies the differences of critical pavement responses, at the most critical locations, between full three-dimensional and superposition results as obtained from the linear AC, nonlinear base, and nonlinear subgrade analyses listed in Table 8-1. In general, the thicker pavements showed larger differences when compared to the thinner ones. Since most pavement responses obtained from single wheel superposition are larger than the full three-dimensional finite element analysis results, the differences show the negative sign implying that the superposition is in general more conservative except for the subgrade vertical strains under thin pavements with only 152 to 254-mm base course thicknesses. Whereas in pavements with substantially thick granular layers (case 5), surface deflections were different from superposition results for up to 30%. Therefore, such results indicate that the superposition from single wheel loading would not capture adequately effects of multiple wheel load interaction on nonlinear pavement responses. Especially when a high level of material nonlinearity exists and a thick granular layer is considered, large differences will be expected between the results from full three-dimensional and superposition solutions.

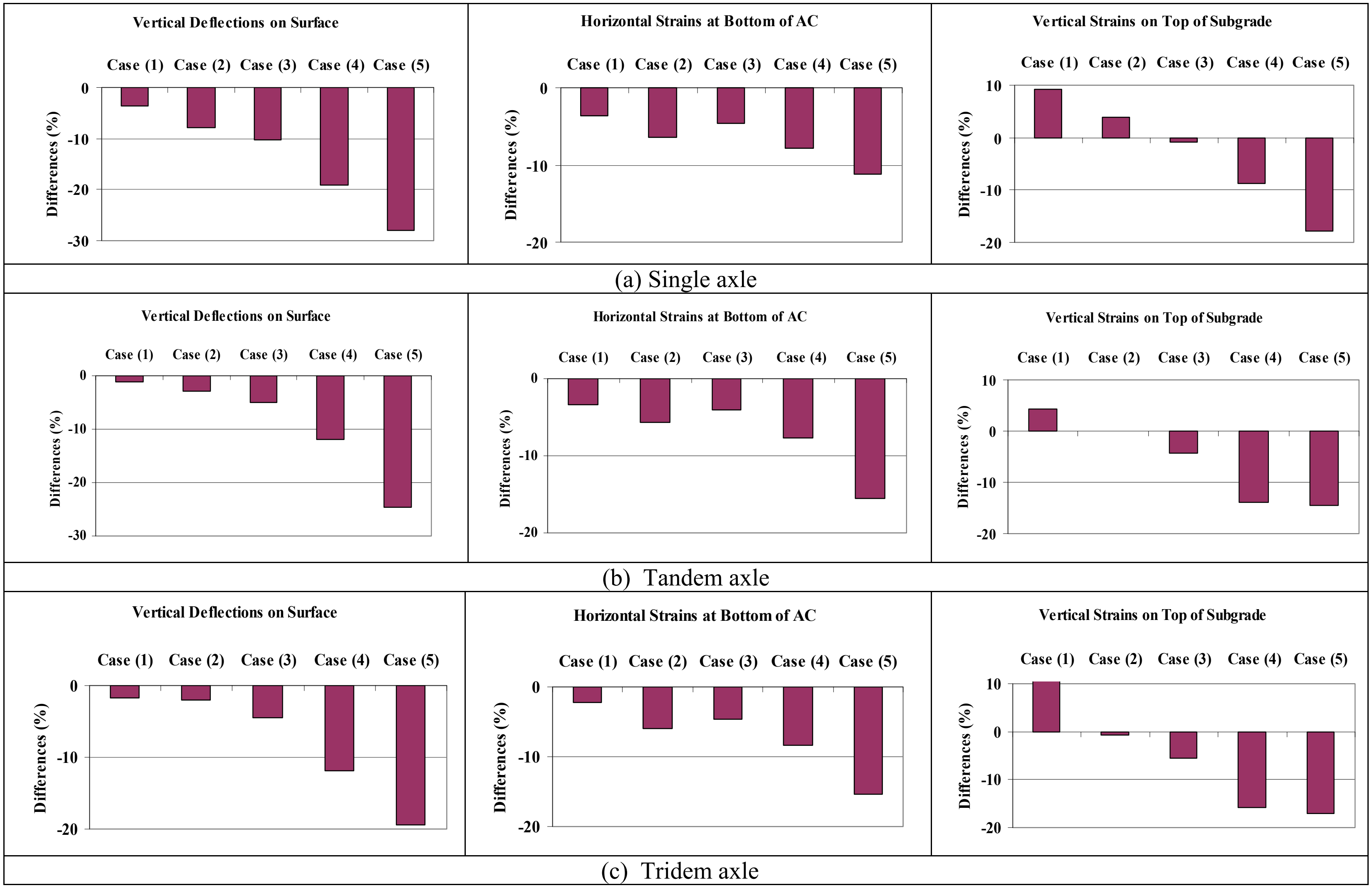


Figure 8-10 Differences in Critical Pavement Responses from Three-dimensional and Superposition Nonlinear Analyses

## 8.3 Summary

From the three-dimensional nonlinear finite element analyses of different conventional pavement geometries, critical pavement responses and their locations in the pavement structure were computed and shown to be significantly influenced by multiple wheel loads coming from single-, tandem-, and tridem-axle type highway vehicle axle/wheel arrangements and/or aircraft gear configurations. From the multiple wheel analysis results, load spreading and nonlinear modulus distributions of the granular base/subbase layers were found to significantly impact the maximum surface deflections. Although three-dimensional pavement structural analysis is known to be limited due to its high cost associated with the complex mesh generation and long analysis time, the findings from this modeling study have clearly established the need and importance of three-dimensional finite element nonlinear analyses of flexible pavements to properly consider both the stress-dependent geomaterial modulus behavior and the implications of multiple wheel loads and their interaction.

One of the main goals of this chapter was to also address applicability of the commonly used single wheel response superposition in nonlinear analyses of pavements subjected to loadings from multiple wheel truck axle arrangements and aircraft gear configurations. The principle of superposition recently proposed as a practical approach was also studied for computing multiple wheel responses from single wheel loading. When superposed responses obtained from this approach were compared to the full three-dimensional analysis results, significant differences in critical pavement responses were found to indicate that even larger errors could be expected with thicker pavements and highly nonlinear base and subgrade properties.

The findings from this modeling study have clearly established the need and importance of three-dimensional finite element nonlinear analyses of flexible pavements to properly consider both the stress-dependent geomaterial modulus behavior and the implications of multiple wheel loads and their interaction. Most importantly, pavement responses under multiple wheel loads were somewhat different than those obtained from the single wheel load response superposition approach, which suggested the need for three-dimensional nonlinear finite element analyses for improved response predictions.

# Chapter 9 Conclusions and Recommendations

## 9.1 Summary and Conclusions

Many general-purpose finite element programs have been used in the past to predict pavement responses under various traffic loading conditions while not considering accurately material characteristics of the unbound aggregate base/subbase and subgrade soil layers. However, previous laboratory studies have shown that the resilient responses of coarse-grained unbound granular material used in untreated base/subbase courses and fine-grained soils of a prepared subgrade follow nonlinear, stress-dependent behavior under repeated traffic loading. Unbound granular materials exhibit stress-hardening, whereas, fine-grained soils show stress-softening type behavior. Therefore, a finite element type numerical analysis needs to be employed to model such nonlinear resilient behavior and more realistically predict pavement responses for a mechanistic pavement analysis. Moreover, finite element based structural analysis has been the main mechanistic approach for analyzing flexible pavements due to its ability to incorporate advanced material characterization models to predict more accurately the wheel load induced responses, such as deformations, stresses, and strains in the pavement structure.

This thesis research has focused on properly characterizing the resilient response of geomaterials, i.e., coarse-grained unbound aggregates and fine-grained subgrade soils. For this purpose, appropriate stress-dependent modulus characterization models were programmed in a user-defined material model subroutine (UMAT) in the general purpose ABAQUS™ finite element program. This way, stress-dependent characterization of the base/subbase and subgrade layers, was made part of the ABAQUS$^{TM}$ finite element nonlinear solutions.

The work areas have consisted of finite element analyses based on comparative case studies and validation studies with measured pavement responses. All these studies were needed to determine the most critical accurate pavement responses related to pavement structural performances, e.g., tensile strain at the bottom of asphalt concrete (AC) linked to fatigue cracking and vertical stress/strain on the top of subgrade linked to rutting. The research findings were intended to better characterized pavement resilient behavior under repeated wheel loads to advance science and technology for the state-of-the-art structural analysis approach.

The methodologies and significant research findings of this study can be summarized as follows:

1. Findings from various past research studies on resilient behavior models and finite element analyses for pavement structures were reviewed. These comprehensive reviews indicated that the finite element analyses considering stress-dependent resilient behavior were needed to obtain accurate pavement responses.
2. Using closed-form linear elastic solutions, an axisymmetric finite element mesh size was selected for accurately predicting pavement responses, i.e., stress, strain, and deflection.
3. To employ stress-dependent resilient models in base/subbase and subgrade layer, a user material subroutine (UMAT) for ABAQUS$^{TM}$ finite element program was developed. To converge smoothly in each loading, a direct secant stiffness

approach was adopted in nonlinear analysis to work suitably for ABAQUS$^{TM}$ flexible pavement response analyses. The results of the nonlinear UMAT analyses were then verified with the axisymmetric GT-PAVE finite element program pavement analysis results for different layer thicknesses of conventional flexible pavement sections studied. Compared to the linear elastic solutions, i.e., one modulus assigned to the whole subgrade or base layer, considerable impact of critical pavement responses, e.g., horizontal tensile strain at the bottom of asphalt concrete (AC) linked to fatigue cracking and vertical strain on the top of subgrade linked to rutting, were predicted when nonlinear analyses were performed in the aggregate base and fine-grained subgrade soil layers.

4. A three-dimensional pavement finite element model was developed and the comparisons were made. The studies between the results of axisymmetric and three-dimensional ABAQUS$^{TM}$ analyses using the developed material models for nonlinear solutions did not indicate major differences in the predicted pavement responses. However, axisymmetric stress analysis is known to be limited in its capacity especially for modeling different geometries and loading conditions, such as multiple wheel/gear loading, and the needed upgrade to the state-of-the-art three-dimensional finite element analyses of flexible pavements should properly implement the nonlinear, stress-dependent pavement foundation geomaterial behavior.

5. For evaluating the impacts of triaxial and true triaxial testing options in the laboratory on the stress-dependent modulus model characterizations, the most realistic true triaxial test data for unbound aggregate base materials were utilized

as obtained from a previous study. Several comparative analyses were undertaken to study the effects of axisymmetric and three-dimensional finite element analyses for a single wheel loading approximation and the consideration of the intermediate principal stress ($\sigma_2$). In the comparison of axisymmetric and three-dimensional finite element results, the largest and the most drastic differences were obtained when comparing responses predicted from the axisymmetric and three-dimensional nonlinear finite element analyses using just the Uzan model developed from triaxial test data with the triaxial assumption of equal minor and intermediate stresses ($\sigma_2$=$\sigma_3$) and the universal model for three-dimensional analysis employing additional intermediate stress ($\sigma_2$) and the octahedral shear stress ($\tau_{oct}$) instead of the deviator stress ($\sigma_d$) for shear stress effects. This means neglecting $\sigma_2$ in the axisymmetric solutions may result in large difference in pavement structural performances.

6. The validation of nonlinear stress-dependent geomaterial model was conducted for multiple wheel loading of pavements. Computed three-dimensional finite element analysis predictions were validated by comparing the field measured responses of the National Airport Pavement Test Facility (NAPTF) pavement test sections. To compare the structural responses, Multi-Depth Deflectometers (MDD) and Pressure Cells were installed and measured for the NAPTF structural response. In general, the nonlinear finite element mechanistic model predictions were in reasonably good agreement with the measured responses of the test sections and the predictions from nonlinear analyses. The predicted values of subgrade vertical stress, subgrade displacement, and surface deflection compared

reasonably well with the order of magnitudes of the measured responses in both sections.

7. The investigations with the developed UMAT for the general purpose finite element programs proved that three-dimensional nonlinear flexible pavement analyses could be accurately performed for multiple wheel/gear loading. From the multiple wheel analysis results, load spreading and nonlinear modulus distributions of the granular base layers were found to significantly impact the maximum surface deflections. When the responses obtained from the principle of superposition were compared to the full three-dimensional analysis results, significant differences in critical pavement responses were found to indicate that even larger errors could be expected with thicker pavements and highly nonlinear base and subgrade properties.

## 9.2 Recommendations for Future Research

1. The mechanistic model can be further enhanced by including appropriate asphalt concrete characterization to model the viscoelastic behavior of AC and address the effects of wheel loads, i.e., dynamic nature of moving wheel, shape of tire imprint, etc. Such enhancements will no doubt come at the expense of much longer analysis times for the convergence of various nonlinear, iterative solutions related to nonlinear modulus characterization, viscoelastic asphalt concrete modeling, contact interface contact modeling, etc. This future consideration will be an invaluable finite element modeling approach and a challenging task.
2. The developed mechanistic model used primarily the isotropic material behavior assuming the same resilient properties in all directions. Several researchers

observed from instrumented test sections that a linear cross-anisotropic model of an unstabilized aggregate base was at least equal to, and perhaps better for predicting general pavement response (Barksdale et al. 1989, Tutumluer 1995). Cross-anisotropy or transverse isotropy is often suitable for the special type of anisotropy observed in geomaterials such as unbound aggregates. Cross-anisotropic unbound aggregate base/subbase modeling can further enhance the mechanistic modeling approach adopted here for nonlinear geomaterial characterization and three-dimensional finite element analyses.

3. To investigate failure mechanisms, large displacement and elastoplastic analysis can be included and permanent deformations can also be modeled for damage analysis due to trafficking of the pavements.
4. More results of several response variables need to be obtained from other well-instrumented field pavement test sections for further validation and improvement of the mechanistic response model. Future research is also needed to utilize the accelerated full scale test results for a detailed analysis and better understanding of the complicated pavement behavior due to various combinations of the effects of speed, load, tire pressure, and tire type.

## References


Australian Standards (1977), AS 1289: Methods of Testing Soils for Engineering Purposes, Standard Association of Australia

Barker, W. R., and Gonzales, C. R. (1991) Pavement Design by Elastic Layer Theory, In Proceedings of Airfield Pavement Specialty Conference, Kansas City, MO

Barksdale, R. D., Robnett, Q., Lai, J., and Zeevaert, A. E. (1982). "Experimental and Theoretical Behavior of Geotextile Reinforced Aggregate Soil Systems." 2nd International Conference of Geotextiles, Vol. 2, Las Vegas, pp. 375-380.

Bettess, P. (1977). "Infinite Elements." International Journal for Numerical Methods in Engineering, Vol. 11, pp. 53-64.

Boateng-Poku, Y., and Drumm, E. C. (1989). "Hyperbolic Model for the Resilient Modulus Response of Fine Grained Subgrade Soil." ASCE Geotechnical Special Publication No.24, Resilient Moduli of Soils: Laboratory Conditions, ASCE, NY

Boussinesq, J. (1885). Application des potentials a l'etude de l'equilibre et du Mouvement des Solids Elastiques, Gauthier-Villars, Paris, France

Boyce, J. R. (1980). "A Nonlinear Model for Elastic Behavior of Granular Materials under Repeated Loading." International Symposium on Soil under Cyclic and Transient Loading, Swansea

Brown, S. F. (1979). "The Characterization of Cohesive Soils for Flexible Pavement Design." 7th European Conference on Soil Mechanics and Foundation Engineering, Vol. 2, pp. 15-22.

Brown, S. F., and Pappin, J. W. (1981). "Analysis of Pavements with Granular Bases." Transportation Research Record 810, TRB, National Research Council, Washington, D.C., pp. 17-23.

Brown, S. F., Loach, S. C., and O'Reilly, M. P. (1987). Repeated Loading of Fine Grained Soils, U.K. Transport and Road Research Laboratory, U.K.

Brunton, J. M., and De Almeida, J. R. (1992). "Modeling Material Nonlinearity in a Pavement Backcalculation Procedure." Transportation Research Record 1377, TRB, National Research Council, Washington, D.C., pp. 99-106.

Burmister, D. M. (1943). "The Theory of Stresses and Displacements in Layered Systems and Applications to the Design of Airport Runways." Highway Research Record 23, TRB, National Research Council, Washington, D.C., pp. 126-144.

Chen, D. H., Zaman, M., Laguros, J., and Soltani, A. (1995). "Assessment of Computer Programs for Analysis of Flexible Pavement Structures." Transportation Research Record 1482, TRB, National Research Council, Washington, D.C., pp. 123-133.

Cho, Y., Mccullough, B. F., and Weissmann, J. (1996). "Considerations on Finite-Element Mothod Application in Pavement Structural Analysis." Transportation Research Record 1539, TRB, National Research Council, Washington, D.C., pp. 96-101.

Chou, Y.T., and Ledbetter, R. H. (1973). The Behavior of Flexible Airfield Pavements under Loads - Theory and Experiments. M.P. S-73-66, U.S. Army Engineer Waterways Experiment Station, Vicksburg, MS

Crockford, W. W. (1993). "Role of Principal Stress Rotation in Flexible Pavement Deformation." Journal of Engineering Mechanics, ASCE, Vol. 119, No. 1, pp. 124-141.

Crockford, W. W., Bendana, L. J. Yang, W. S., Rhee, S. K., and Senadheera, S. P. (1990). Modeling Stress and Strain States in Pavement Structures Incorporating Thick Granular Layers, Final Report, The Texas Transportation Institute, College Station, TX, pp. 57-71.

CTL (1998). National Airport Pavement Test Machine – Instrumentation/Data Acquisition. A Report Prepared for US Army Corps of Engineers. Construction Technology Laboratories, Inc., Skokie, IL

Dawson, A. R., and Gomes Correia, A. (1996). The effects of subgrade clay condition on the structural behavior of road pavement, Flexible Pavements, ed. Gomes Correia, Balkema, pp. 113-119.

Dehlen, G. L. (1969). The effect of Nonlinear Material Response on the Behavior of Pavements Subjected to Traffic Loads, Ph.D. Dissertation, University of California, Berkeley, CA

De Jong. D. L., Peatz, M. G. F., and Korswagen, A. R. (1973). Computer Program Bisar, Layered Systems under Normal and Tangential Loads, Konin Klijke Shell-Laboratorium, Amsterdam, External Report, AMSR.0006.73.

Donovan, P. and Tutumluer, E. (2007). Analysis of NAPTF Trafficking Response Data for Pavement Foundation Deformation Behavior, In Proceedings of the FAA Worldwide Airport Technology Transfer Conference, Atlantic City, NJ

Duncan, J. M., Monismith, C. L., and Wilson, E. L. (1968). "Finite Element Analyses of Pavements." Highway Research Record 228, TRB, National Research Council, Washington, D.C., pp. 18-33.

Erlingsson, S. (2002). "3-D FE Analyses of HVS Tested Low Volume Road Strucutres-Comparison with Measurements." Proceeding of the Third International Symposium on 3D Finite Element for Pavement Analysis, Amsterdam, The Netherlands, pp. 339-350.

Federal Aviation Administration (2004). Advisor Circular (AC) No:150/5320-6D, U.S. Department of Transportation

Foster, C. R., and Ahlvin, R. G. (1958). "Development of Multiple-Wheel CBR Design Criteria." Journal of the Soil Mechanics and Foundations Division, ASCE, Vol. 84, No. SM2, pp. 1647-1 – 1647-12.

Fredlund, D. G., Bergan, A. T., and Wong, P. K. (1979). "Relation between Resilient Modulus and Stress Conditions for Cohesive Subgrade Soils." Transportation Research Record 642, TRB, National Research Council, Washington, D.C., pp. 73-81.

Garg, N. (2003). "Permanent deformation behavior of the granular layers tested at the National Airport Pavement Test Facility." Presented at the 82nd Annual Transportation Research Board Meeting, Washington, D.C., January

Gomez-Ramirez, F. (2002). Characterizing Aircraft Multiple Wheel Load Interaction for Airport Flexible Pavement Design, Ph.D. Dissertation, University of Illinois, Urbana, IL

Gopalakrishnan, K. (2004). Performance Analysis of Airport Flexible Pavements Subjected to New Generation Aircraft, Ph.D. Dissertation, University of Illinois, Urbana, IL

Green, J. L., and Hall, J. W. (1975) Nondestructive Vibratory Testing of Airport Pavements. Vol I: Esperimental Test Results and Development of Evaluation Methodology and Procedure. Technical Report S-75-14, U.S. Army Engineer Waterways Experiment Station, Vicksburg, MS

Harichandran, R. S., Yeh, M. S., and Baladi, G. Y. (1989). "MICH-PAVE: A Nonlinear Finite Element Program for Analysis of Pavements." Transportation Research Record 1286, TRB, National Research Council, Washington, D.C., pp. 123-131.

Hayhoe, G.F. and Garg, N. (2002) Subgrade Strains Measured in Full-Scale Traffic Tests with Four- and six-Wheel Landing Gears, In Proceedings of the Federal Aviation Administration Airport Technology Transfer Conference, Atlantic City, NJ

Hayhoe, G. (2004) Traffic Testing Results from the FAA's National Airport Pavement Test Facility, In Proceedings of 2nd International Conference on Accelerated Pavement Testing, University of Minnesota, Minneapolis, MN

Helwany, S., Dyer, J., and Leidy, J. (1998). "Finite-Element Analyses of Flexible Pavements." Journal of Transportation Engineering, ASCE, Vol. 124, No. 5, pp. 491-499.

Heukelom, W., and Foster, C. R. (1960) "Dynamic Testing of Pavements." Journal of Soil Mechanics and Foundation, ASCE, Vol. 86, No. 1, pp. 1-28.

Hibbit, Karlsson & Sorensen, Inc. (2005). ABAQUS/standard User's Manual, Version 6.5. Hibbit, Karlsson & Sorensen, Inc., Pawtucket, R.I.

Hicks, R. G. (1970). Factors Influencing the Resilient Response of Granular Materials, Ph.D. Dissertation, University of California, Berkeley, CA

Hicks, R. G., and Monismith, C. L. (1971). "Factors Influencing the Resilient Response of Granular Materials," Highway Research Record 345, Washington, D.C., pp. 15-31.

Hjelmstad, K. D., Kim, J., and Zuo, Q. H. (1996). "Finite Element Procedures for Three Dimensional Pavement Analysis." Transportation Research Record 1539, TRB, National Research Council, Washington, D.C., pp. 66-71.

Hjelmstad, K. D., and Taciroglu, E. (2000). "Analysis and Implementation of Resilient Modulus Models for Granular Solids." Journal of Engineering Mechanics, ASCE, Vol. 126, No. 8, pp. 821-830.

Huang, Y. H. (1968). Stresses and Displacements in Nonlinear Soil Media, Journal of the Soil Mechanics and Foundations Division, ASCE, Vol. 94, No. SM1, pp. 1-19.

Huang, Y. H. (1993). Pavement Analysis and Design, 1st Ed., Pearson Prentice Hall, NJ

Hwang, D., and Witczak, M. W. (1979). Program DAMA User's Manual, Department of Civil Engineering, University of Maryland, MD

Itani, S. Y. (1990). Behavior of Base Materials Containing Large-Sized Particles, Ph.D. Dissertation, Department of Civil Engineering, Georgia Institute of Technology, GA

Kasianchuk, D. A. (1968). Fatigue Considerations in the Design of Asphalt Concrete Pavements, Ph.D. Dissertation, University of California, Berkeley, CA

Kim, Y. R. (2000). Assessing Pavement Layer Condition Using Deflection Data, NCHRP project 10-48 Final Report, National Cooperative Highway Research Program

Kirwan, R. W., and Glynn, T. E. (1969). Experimental and Theoretical Investigation of Pavement Deflections, Technical Report to the European Office, US Army, Trinity College, Dublin

Kirwan, R. W., and Snaith, M. S. (1975). Further Investigations towards a Rational Method of Design for Flexible Pavements: Part II, Final Technical Report to the European Office, US Army, Trinity College, Dublin

Kjellman, W. (1936). "Report on an Apparatus for Consummate Investigation of the Mechanical Properties of Soils", Proceeding of 1st International Conference of SMFE, Vol. 2, pp. 16-20.

Kopperman, S., Tiller, G., and Tseng, M. (1986). ELSYM5, Interactive Microcomputer Version: User's Manual, Federal Highway Administration, Washington, D.C.

Kuo, C., Hall, K., and Darter, M. (1995), "Three-Dimensional Finite Element Model for Analysis of Concrete Pavement Support." Transportation Research Record 1505, TRB, National Research Council, Washington, D.C., pp. 119-127.

Lade, P. V., and Nelson (1987). "Modeling the Elastic Behavior of Granular Materials." International Journal for Numerical and Analytical Methods in Geomechanics. Vol. 11, pp. 521-542.

Lekarp, F., Isacsson, U., and Dawson, A. (2000) "State of the Art. I: Resilient Response of Unbound Aggregates." Journal of Transportation Engineering, Vol. 126, No. 1, pp. 66-75.

Lister, N. W., and Powell, W. D. (1987), "Design Practice for Bituminous Pavement in the United Kingdom", Proceeding of 6th International Conference of Structural Design of Asphalt Pavement, Vol. 1, Ann Arbor, MI, pp. 220-231.

Loach, S. C. (1987). Repeated Loading of Fine Grained Soils for Pavement Design, Ph.D. Dissertation, University of Nottingham, Department of Civil Engineering, Nottingham, U.K.

Lytton, R.L., Uzan, J., Fernando, E.G., Roque, R., Hiltunen, D., and S.M. Stoffels. (1993). Development and Validation of Permanent Prediction Models and Specifications for Asphalt Binders and Paving Mixes, SHRP Report A-357, Strategic Highway Research Program, National Research Council, Washington, D.C.

Lytton, R. L. (1995). "Foundations and Pavements on Unsaturated Soils." 1st International Conference on Unsaturated Soils, Paris, France

Mayhew, H. C. (1983). Resilient Properties of Unbounde Roadbase under Repeated Triaxial Loading, Transport and Road Research Laboratory, LR 1088.

Nataatmadja, A. (1989). Variability of Pavement Material Parameters under Repeated Loading, Ph.D. Dissertation, Monash University, Australia

National Cooperative Highway Research Program (2004). Guide for Mechanistic-Empirical Design of New and Rehabilitated Pavement Structures (Final Report), TRB, National Research Council, Washington, D.C.

Nesnas, K., Ellis, S., Schiavi, I., Nunn, M., and Lloyd, W. (2002). "A 3-Dimensional Finite Element Model for the Prediction of Surface Crack Opening due to Temperature Variations." Proceeding of the Third International Symposium on 3D Finite Element for Pavement Analysis, Amsterdam, The Netherlands, pp. 269-282.

Pappin, J. W. (1979). Characteristics of a Granular Material for Pavement Analysis, Ph.D. Dissertation, University of Nottingham, Nottingham, U.K.

Park, S., and Lytton, R. L. (2004). "Effect of Stress-Dependent Modulus and Poisson's Ratio on Structural Responses in Thin Asphalt Pavements." Journal of Transportation Engineering, Vol. 130, No. 3, pp. 387-394.

Perkins, S. W. (2004). Development of Design Methods for Geosynthetic Reinforced Flexible Pavements, Final Report, Montana State University, MT

Pezo, R. F. (1993). "A General Method of Reporting Resilient Modulus Tests of Soils. A Pavement Engineer's Point of View." 72nd Annual Meeting, Record No.93082, TRB, Washington D.C.

Rada, G., and Witczak, M. W. (1981). "Comprehensive Evaluation of Laboratory Resilient Moduli Results for Granular Material." Transportation Research Record 810, TRB, National Research Council, Washington, DC, pp. 22-33.

Raad, L. and Figueroa, J. L. (1980). "Load Response of Transportation Support Systems." Journal of Transportation Engineering, ASCE, Vol. 16, No. TE1, pp. 111-128.

Rowshanzamir, M.A. (1995). Resilient Cross-Anisotropic Behavior of Granular Base Materials under Repetitive Loading, Ph.D. Dissertation, School of Civil Engineering, The University of New South Wales, Sydney, Australia

Saad, B., Mitri, H., and Poorooshasb, H. (2005). "Three-Dimensional Dynamic Analysis of Flexible Conventional Pavement Foundation." Journal of Transportation Engineering, ASCE, Vol. 131, No. 6, pp. 460-469.

Schwartz, C. W. (2002). “Effect of Stress-Dependent Base Layer on the Superposition of Flexible Pavement Solutions.” The International Journal of Geomechanics, Vol. 2, No. 3, pp. 331-352.

Seed, H. B., Mitry, F. G., Monismith, C. L., and Chan, C. K. (1967). “Factors Influencing the Resilient Deformation of Untreated Aggregate Base in Two Layer Pavements Subjected to Repeated Loading,” Highway Research Record 190, Washington, D.C.

Shifley, L. H. (1967). The Influence of Subgrade Characteristics on the Transient Deflections of Asphalt Concrete Pavements, Ph.D. Dissertation, University of California, Berkeley, CA

Shoukry, S. N., and Gergis, W. W. (1999). “Performance Evaluation of Backcalculation Algorithm through Three-Dimensional Finite-Element Modeling of Pavement Structures.” Transportation Research Record 1655, TRB, National Research Council, Washington, D.C., pp. 152-160.

Sousa, J. B., and Monismith, C. L. (1987). “Dynamic Response of Paving Materials.” Transportation Research Record 1136, TRB, National Research Council, Washington, D.C., pp. 57-68.

Standard Method of Test for Resilient Modulus of Subgrade Soils and Untreated Base/Subbase Materials AASHTO Designation T 307 (2002), Standard Specifications for Transportation Materials and Methods of Sampling and Testing, PART II Tests.

Stock, A. F., Brown, S. F., and Pell, P. S. (1979). Analysis of Structural Performance of Flexible Pavements, Report No. AFS/3, Asphalt and Coated Macadam Association, University of Nottingham, Nottingham, U.K.

Sukumaran, B. (2004). "Three Dimensional Finite Element Modeling of Flexible Pavements." The 2004 FAA Worldwide Airport Technology Transfer Conference, Atlantic City, NJ

Sweere, G. T., Penning, A., and Vos, E. (1987). "Development of a Structural Design Procedure for Asphalt Pavements with Crushed Rubble Base Courses." Sixth International Conference on the Structural Design of Asphalt Pavements, Ann Arbor, MI

Taciroglu, E. (1998). Constitutive Modeling of the Resilient Response of Granular Solids, Ph.D. Dissertation, University of Illinois at Urbana-Champaign, Urbana, IL

Thompson, M.R., and Elliott, R.P. (1985). "ILLI-PAVE Based Response Algorithms for Design of Conventional Flexible Pavements." Transportation Research Record 1043, TRB, National Research Council, Washington, D.C., 50-57.

Thompson, M.R., and Garg, N. (1999). Wheel Load Interaction: Critical Airport Pavement Responses, In Proceedings of the Federal Aviation Administration Airport Technology Transfer Conference, Atlantic City, NJ

Thompson, M. R. and Robnett, Q. L. (1979). "Resilient Properites of Subgrade Soils." Journal of Transportation Engineering, ASCE, Vol. 105, No.TE1.

Tutumluer, E. (1995). Predicting Behavior of Flexible Pavements with Granular Bases, Ph.D. Dissertation, Georgia Institute of Technology, GA

Tutumluer, E., and Thompson, M. R. (1997). “Anisotropic Modeling of Granular Bases in Flexible Pavements.” Transportation Research Record 1577, TRB, National Research Council, Washington D.C., pp. 18-26.

Tutumluer, E., and Thompson, M. R. (1997). “Granular Base Moduli for Mechanistic Pavement Design.” In Proceedings of the ASCE Airfield Pavement Conference, ASCE, Seattle, Washington, pp. 33-47.

Uddin, W., Zhang, D., and Fernandez, F. (1994). “Finite Element Simulation of Pavement Discontinuities and Dynamic Load Response.” Transportation Research Record 1448, TRB, National Research Council, Washington, D.C., pp. 100-106.

Uddin, W., and Ricalde, L. (2000). “Nonlinear Material Modeling and Dynamic Finite Element Simulation of Asphalt Pavement.” $14^{th}$ Engineering Mechanics Conference, ASCE, Austin, TX

Ungless, R. L., (1977), “Infinite Finite Element.” International Symposium on Innovative Numerical Analysis in Applied Engineering Science, Versailes, France, pp. 13-16.

Uzan, J. (1985). “Characterization of Granular Material.” Transportation Research Record 1022, TRB, National Research Council, Washington D.C., pp. 52-59.

Wang, J. (2001). Three-Dimensional Finite Element Analysis of Flexible Pavements. Master Thesis, The University of Maine, ME

Warren, H., and Dieckman, W. L. (1963). “Numerical Computation of Stresses and Strains in a Multiple-Layer Asphalt Pavement System.” International Report, Chevron Research Corporation, Richmond, CA

Witczak, M. W., and Uzan, J. (1988). The Universal Airport Pavement Design System: Granular Material Characterization, University of Maryland, Department of Civil Engineering, MD

Zaghloul, S. M., and White, T. D. (1993). "Use of a Three-Dimensional, Dynamic Finite Element Program for Analysis of Flexible Pavement." Transportation Research Record 1388, TRB, National Research Council, Washington, D.C., pp. 60-69.

Zeevaert, A. E. (1980). Finite Element Formulation for the Analysis of Interfaces, Nonlinear and Large Displacement Problems in Geotechnical Engineering, Ph.D. Dissertation, Georgia Institute of Technology, GA

## Author's Biography

Minkwan Kim was born in Gwangju, Korea on November 5, 1973. He graduated from Inha University, Korea in 1998 with a Bachelor of Engineering degree in Civil Engineering. He completed a Master of Engineering in Civil Engineering with emphasis in Structural Engineering from Inha University in 2000. In 2001, he began his Doctor of Philosophy study at the University of Illinois at Urbana-Champaign. He has studied the finite element analyses of flexible pavements considering nonlinear pavement foundation behavior. In the meantime, he obtained a Master of Science degree with specializing in Transportation Engineering in 2005 and worked as a student structural analyst in Champaign Simulation Center of Caterpillar, Inc. for 2 years. He completed his Doctor of Philosophy degree in December 2007.